NASA Contractor Report 158349

NASA-CR-158349
19790010746

ANALYSIS OF SOME AERODYNAMIC CHARACTERISTICS DUE TO WING-JET INTERACTION

Greg L. Fillman and C. Edward Lan

THE UNIVERSITY OF KANSAS CENTER FOR RESEARCH, INC.
Lawrence, Kansas 66045

NASA Grant NSG-1139
July 1979

National Aeronautics and Space Administration

Langley Research Center
Hampton, Virginia 23665

TABLE OF CONTENTS

LIST OF SYMBOLS

Symbol	Description
AR	Aspect ratio
A_j	Cross sectional area of the jet at the nozzle exit
B, B_w	Wing span
b_j	Jet Span
$C_{D_{i\ Total}}$	Total induced drag coefficient with jet on
$C_{D_{i\ Wing\ Alone}}$	Total induced drag coefficient with jet off
$C_{D_{i\ L.E.\ THRUST}}$	Induced drag coefficient contributed by leading edge thrust
$C_{D_{i\ PRESSURE}}$	Induced drag coefficient contributed by pressure force
ΔC_{D_i}	Incremental induced drag coefficient due to the jet effects
$\Delta C_{D_{i\ L.E.\ THRUST}}$	Incremental change in the leading-edge-thrust component of induced drag coefficient
$\Delta C_{D_{i\ PRESSURE}}$	Incremental change in the pressure drag coefficient due to the jet
c_{d_i}	Sectional induced drag coefficient
C_{L_W}, $C_{L_{Wing\ Alone}}$	Lift coefficient for the wing alone
c_{ℓ_W}	Sectional lift coefficient for the wing alone
ΔC_L, ΔC_{L_J}	Incremental change in lift coefficient due to the jet effects
Δc_ℓ, Δc_{ℓ_j}	Incremental change in sectional life coefficient due to the jet

Symbol	Description
C_{L_α}	Lift-curve slope
C_N	Normal force coefficient of the net pressure distribution
C_p	Lifting pressure coefficient
ΔC_p	Incremental change in pressure coefficient due to jet effects
c_r	Root chord
c_t	Tip chord
C_t	Coefficient of leading edge thrust
C_μ, C_T	Jet thrust coefficient
M_∞	Mach number of the freestream
M_j	Mach number of the jet
q	Dynamic pressure
r_j	Radius of round OWB jets at the nozzle
S, S_w	Wing area
T_∞	Freestream absolute static temperature
T_j	Absolute static temperature of the jet
V_j	Velocity of the jet
V_∞	Velocity of the freestream
x_j	Longitudinal coordinate of the jet exit center
y_j	Lateral coordinate of the jet centerline
Y	Wing spanwise station
$\frac{2Y}{B}$	Spanwise fraction of halfspan
z_j	Distance of the jet center (OWB) above the wing plane
α	Angle of attack

Symbol	Description
Δ	Incremental quantity difference between jet on conditions and wing alone conditions
λ	Wing taper ratio = c_t/c_r
μ	Ratio of freestream/jet velocities = V_∞/V_j
ρ_j	Density of the jet flow
ρ_∞	Density of freestream
Λ_{LE}	Sweep angle of the leading edge
∞	Freestream conditions
j	Jet condition, jet on
W.A.	Wing alone, or jet off
Entrainment Alone	Effects of wing-jet interaction are not included in the computation
L.E.	Leading edge
T.E.	Trailing edge
OWB	Over wing blowing
USB	Upper surface blowing

Abstract

The following is a presentation of the results of two separate theoretical investigations. Both studies utilize the computer program described in Reference 1. This program is capable of predicting the aerodynamic characteristics of both upper-surface blowing (USB) and over-wing blowing (OWB) configurations.

The first investigation is a theoretical analysis of the effects of over-wing blowing jets on the induced drag of a 50° sweep back wing. Experiments have shown net drag reductions associated with the well known lift enhancement due to over-wing blowing. This study reveals the mechanisms through which this drag reduction is brought about. It is shown that both jet entrainment and the so called wing-jet interaction play important roles in this process and neither effect can be overlooked.

In the second investigation, the effects of a rectangular upper-surface blowing jet are examined for a wide variety of planforms. In all cases the jet characteristics were identical. The isolated effects of wing taper, sweep, and aspect ratio variations on the incremental lift due to blowing are presented. The effects of wing taper ratio and sweep angle were found to be especially important parameters when considering the relative levels of incremental lift produced by an upper-surface blowing configuration.

1. Analysis of the Induced Drag Reduction of an Over-Wing Blowing Configuration at Mach Number of .4.

The following report is a theoretical investigation into the mechanisms through which the induced drag of over-wing-blowing configurations are affected. The analysis was carried out with the computer program of Reference 1. This program utilizes the theory reported in Reference 2 by Lan. The over-wing blowing configuration used for this investigation is identical to that used in an experimental test carried out by Putnam[3]. In that experiment, a jet was exhausted from above and ahead of a 50° swept back wing from four different positions (see Figure 1), and freestream Mach numbers ranging from .4 to .95. In this theoretical study, only the two aft jet locations were investigated (high-aft and low-aft) and a freestream Mach number of .4 was used throughout the analysis.

It is well known that significant increases in lift coefficient can be obtained with over-wing blowing jets and that improvements in take-off and landing performance can be achieved. This is evident in Figure 2 where the predicted incremental lift coefficients of the present theory are compared with the experimental data of Reference 3 and results of a OWB theory of Putnam, reported in Reference 4. The theory by Putnam accounts for the jet entrainment effect only and is limited to jets located rather high above the wing (>1.5 jet diameters) or jets which do not wash the wing. The present theory accounts for both jet entrainment and also wing-jet interaction. The additional lift increment due to wing-jet interaction is shown by the experimental data and the theory of Lan (see Figure 2). This interaction effect becomes much larger as the jet is lowered closer to the wing. Figure 3 shows the incremental drag reduction due to the OWB jet. Again the accuracy of Lan's theory is seen. The theory of Putnam underpredicts the influence of the jet because it accounts for entrainment effects only.

These induced drag reductions associated with over-wing blowing configurations offer a means of improving the cruise performance of jet aircraft. This is verified experimentally and theoretically in Figure 4. This drag reduction associated with a lift enhancement is seen again in Figure 5. Note that in Figure 5 drag reductions seem possible at low angles of attack only, because changes in induced drag are evaluated at a constant alpha rather than at a constant lift coefficient as in Figure 4. Because increases in lift at large alpha are comparatively larger than drag increases, the overall L/D with the jet on is still larger than for the wing alone (see Figure 4).

Comparisons of the present theory with other OWB experiments have also shown good agreement[5,6]. Reference 7 compares experimental results for another OWB configuration with the predictions of the present theory and also the theory of Putnam. Again the improved accuracy of the theory by Lan was shown. The drag reduction associated with additional lift production is one of the least understood phenomena associated with OWB configurations. The main purpose of this investigation is to gain a better understanding of how particular OWB configurations can produce significant increases in lift and reductions in induced drag as compared to a wing alone.

As shown in Figure 6 the sectional induced drag is the sum of two components of opposite sign. The drag component of the pressure distribution is partially nullified by the thrusting component of the leading edge thrust. Figure 7 shows the increased pressure distribution induced by the high-aft jet configuration of Figure 1. Because the pressure distribution must remain normal to the camber line, any increase in the resultant pressure force must also produce a proportionate increase in

the induced drag component of this force, see Figure 6. More insight into the nature of the incremental pressure coefficient can be gained from Figure 8. Note that in Figures 7 and 8 the coefficient Cp is the coefficient of the net pressure force acting on the airfoil section, (usually referred to as Δ Cp). Also in Figure 8 the Δ Cp term is the coefficient of the additional pressure distribution induced by the jet, above what the wing alone is capable of producing. Examination of the pitching moment data for the configuration of Figure 8 reveals that the center of pressure is unaltered by the jet, however significant forward movement of aerodynamic centers have been shown both experimentally[8] and theoretically[9] for upper-surface-blowing configurations with large thrust coefficients. One mechanism through which the OWB jet can increase the wing pressure distribution is the jet entrainment. The jet entrainment produces upwash on the wing which not only increases the wing pressure distribution but also induces larger normal velocities around the leading edge and hence more leading edge thrust. Figure 9 shows that the entrainment effect induces larger increments of leading edge thrust as compared to the incremental pressure drag. Thus a net decrease in total drag is achieved. Figure 10 reflects this property of the jet entrainment, showing all increments of drag to be negative and showing the powerful influence of jet velocity ratio. Figure 11 again shows that when jet entrainment alone is considered, that in every instance the increment of leading edge thrust is larger than the entrainment induced increment of pressure drag. Figures 12 and 13 show that the spanwise increments of pressure drag and leading edge thrust coefficient due to the entrainment of the high-aft jet. As might be expected, the effect that entrainment has on a given portion of the wing is a function

of distance from the jet, the most powerful influences being exerted on the blown portion of the wing where the jet entrainment is strongest. Figure 14 shows the entrainment effect on the incremental leading edge thrust coefficient for varying angles of attack. Again maximum leading edge thrust increments are seen to be generated near the blown portion of the wing but not exactly on the jet centerline as expected, but closer to the outboard edge of the jet. Also the portion of the wing outboard of the jet is more strongly influenced than the inboard portion. This might be explained by re-examining the wing geometry, Figure 1. The jet is entraining air along its entire length. The portion of the jet above the wing is shielded from below by the wing. If the portion of the jet downstream of the leading edge is entraining air around the leading edge it will affect the outboard portion of the leading edge most because the wing is highly swept and the outboard edge is closer to the downstream portion of the jet. See sketch A.

So far, only the effect of the jet entrainment of the high-aft jet configuration has been analyzed. However, it has been shown by Lan[2] and Putnam[4] that accounting for the jet entrainment alone results in an underprediction of the jet induced lift. The presence of the jet near the wing will modify the wing flow field and in the same way the wing will alter the jet flow. This wing-jet interaction process must be accounted for. Details of how this is done in this theory can be found in Reference 9. When the wing-jet interaction is also taken into account as in Figures 15 and 16 it is seen that the incremental pressure drag (and lift) coefficients are increased above what entrainment alone is capable of. (Compare to Figures 11 and 12.) It is also seen that wing-jet interaction also has a detrimental effect upon the leading edge thrust. Thus only at high blowing rates and low angles of attack can net

reductions in drag be achieved, see Figure 15. By comparing Figure 17 to Figure 13 and Figure 18 to Figure 14, it can be observed that this deterioration of the incremental leading edge thrust occurs near the wing panel blown by the jet, which is exactly where the entrainment exerted its most powerful effects. Figure 19 shows that at low blowing rates the leading edge thrust in the jet region can be reduced to less than that produced by the wing alone. The reason will be explained later.

It is known that the vertical height of the jet relative to the wing has a powerful effect on how much the jet can increase the lift coefficient of the wing. All of the data discussed previously have been for the high-aft jet location. To better understand the effects of the jet vertical height on the induced drag, the low-aft configuration of Reference 3 was also analyzed. The program predicted that the jet would wash the wing in this configuration and so an equivalent upper-surface-blowing jet was used for the interaction computation[2]. Figure 20 shows that this prediction was verified experimentally. Figure 21 shows that indeed, two or three times the incremental lift coefficient of the high-aft jet can be obtained with the low-aft jet but a much larger induced drag penalty must be paid. Figure 22 shows why this is so. Not only is a large increment of pressure drag (and lift) being generated on the blown portion of the wing but the leading edge thrust in this same vicinity is reduced to a very small proportion of what the wing was producing alone. Figures 23 and 24 show how these two phenomena together produce very large induced drag increments in the jet region. Figure 25 exhibits the large error in the prediction of the incremental induced drag that would be made if wing-jet interaction was not accounted for. Figure 25 also shows that at large thrust coefficients the low-aft jet can produce

net increases in the leading edge thrust even with the large deteriorations in the jet blown region. Figures 26 and 27 clarify how this is possible. However, no matter what the sign of the leading edge thrust increment is, the large decrements of leading edge thrust coefficient in the jet blown region will prevent the low-aft jet configuration from achieving the efficiencies shown for the high-aft jet in which the leading edge thrust is increased along the entire wing span. Thus from a cruise performance point of view, the high-aft jet would be more appealing. Figure 28 shows the large error that would be made in the prediction of the incremental leading edge thrust if the wing-jet interaction is ignored. The interaction effect of a low jet cannot be ignored.

Figure 29 compares the incremental leading edge thrust coefficients for the low-aft and high-aft jet configuratiosn. Curves are also shown for the entrainment alone simplification. It is seen from the dashed lines that lowering the jet close to the wing surface does increase the entrainment effect upon the leading edge thrust as would be expected. However, this change in the entrainment effect is not nearly as dramatic as the effect the jet height has upon the wing-jet interaction. Figure 29 also shows one reason why the simple entrainment alone assumption may be adequate for a jet far above the wing but is not realistic for a low over-wing blowing or upper-surface blowing jet. The integrated values for the two high-aft jet curves are roughly the same. They are not even close for the low-aft jet, see also Figure 28. Figure 30 compares the spanwise distribution of induced drag due to the pressure distribution for the low and high jet. The peaks in the loading at either edge of the jet are explained in detail in Reference 10 but briefly are due to the side surfaces of the equivalent rectangular USB jet used in the computation. Figure 31 shows the total induced drag coefficients and leading edge thrust contributions for the low-aft and high-aft jets. The data

in the corner of the plot show that the integrated spanwise leading edge thrust for the high-aft jet is larger than that of the low-aft jet, even though sectional coefficients on either side of the jet region are larger for the low jet, it is seen that the large deterioration in leading edge thrust in the jet blown region is the major cause of the large induced drag associated with this configuration. The question arises as to what is causing this. One of the boundary conditions of the interaction theory is that the jet surface is a stream surface and that the flow on either side (inside or outside) of this surface must be parallel to that surface. The jet is assumed to be flowing parallel to the local chord which in this case is also the local camber line. If the jet is near the wing and parallel to it and the outer flow near the jet is constrained to be parallel to the jet then this flow must also be parallel to the wing chord. Becuase the jet is slightly above the wing small normal velocities may be possible at the leading edge, but not as large as would occur with the wing alone. If the jet were lowered all the way down to the wing surface the normal velocities and hence leading edge thrust should go to zero in the region close to the jet.

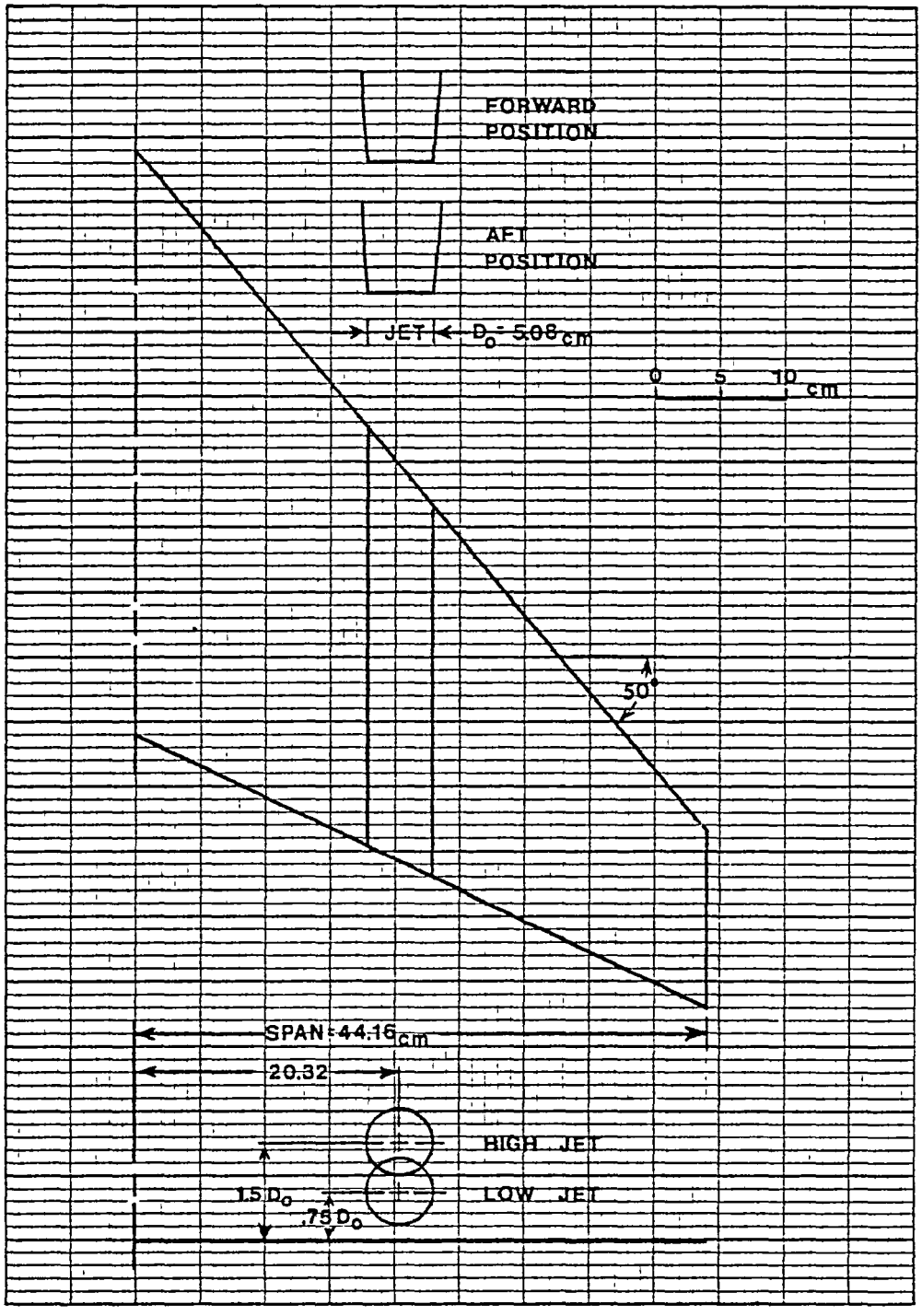

Figure 1. Idealized geometry of the OWB wind tunnel model used in Putnam's investigation, see NASA TN D-7367

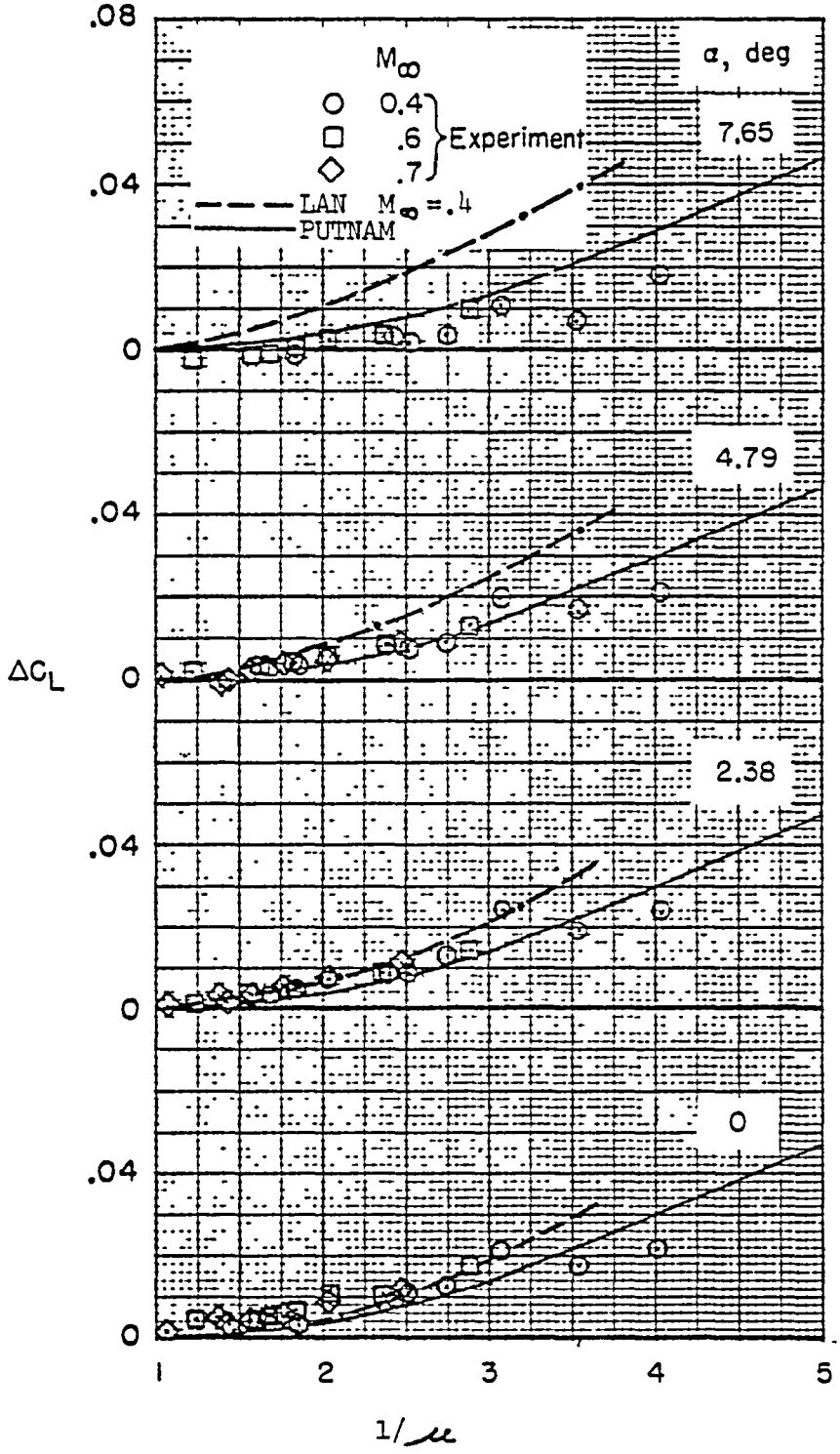

Figure 2. Comparison of the predicted incremental lift coefficient with the experimental data of reference 3 and the theory of reference 4, for the high-aft jet configuration.

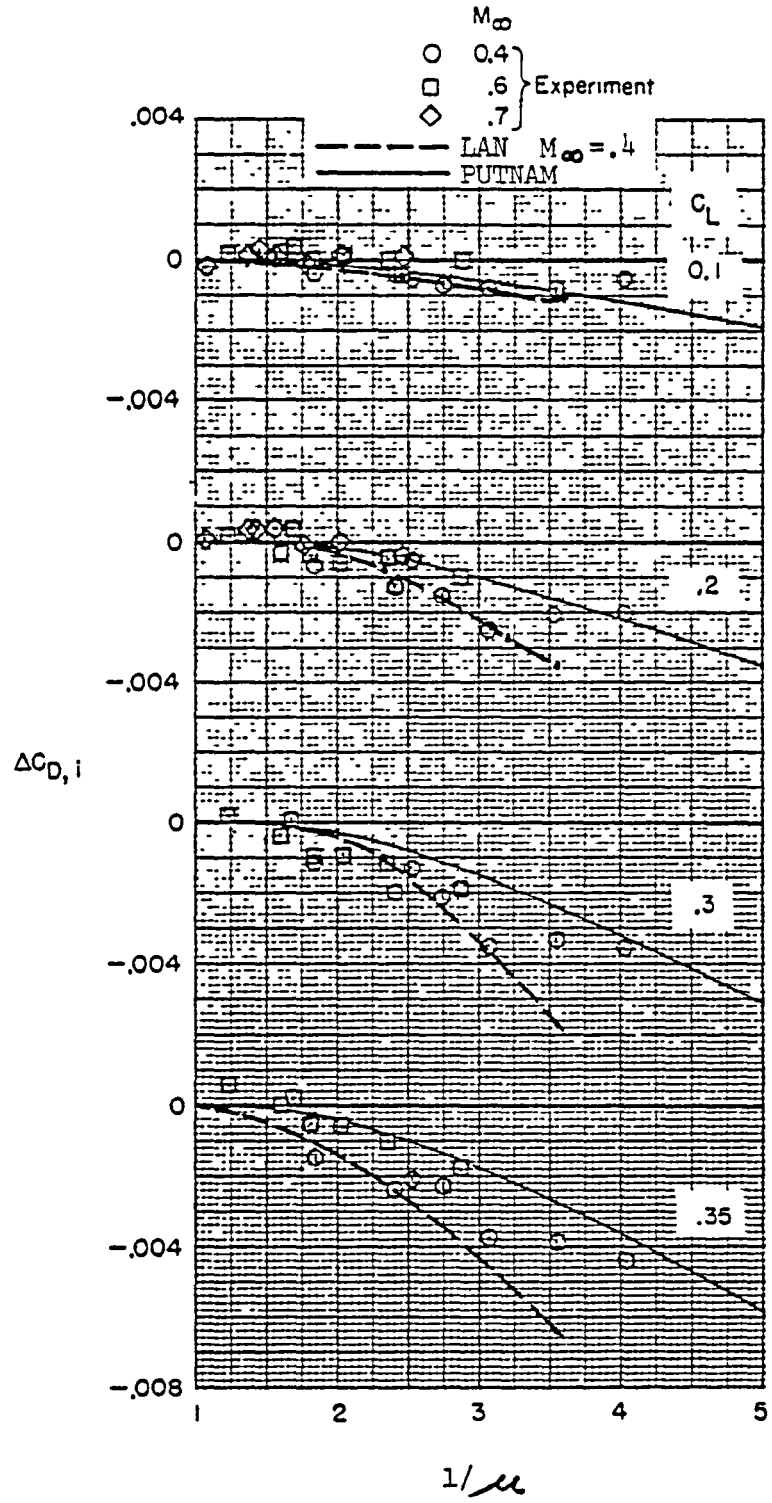

Figure 3. Comparison of the predicted incremental induced drag with the experimental data of reference 3 and the theory of reference 4, for the high-aft jet configuration.

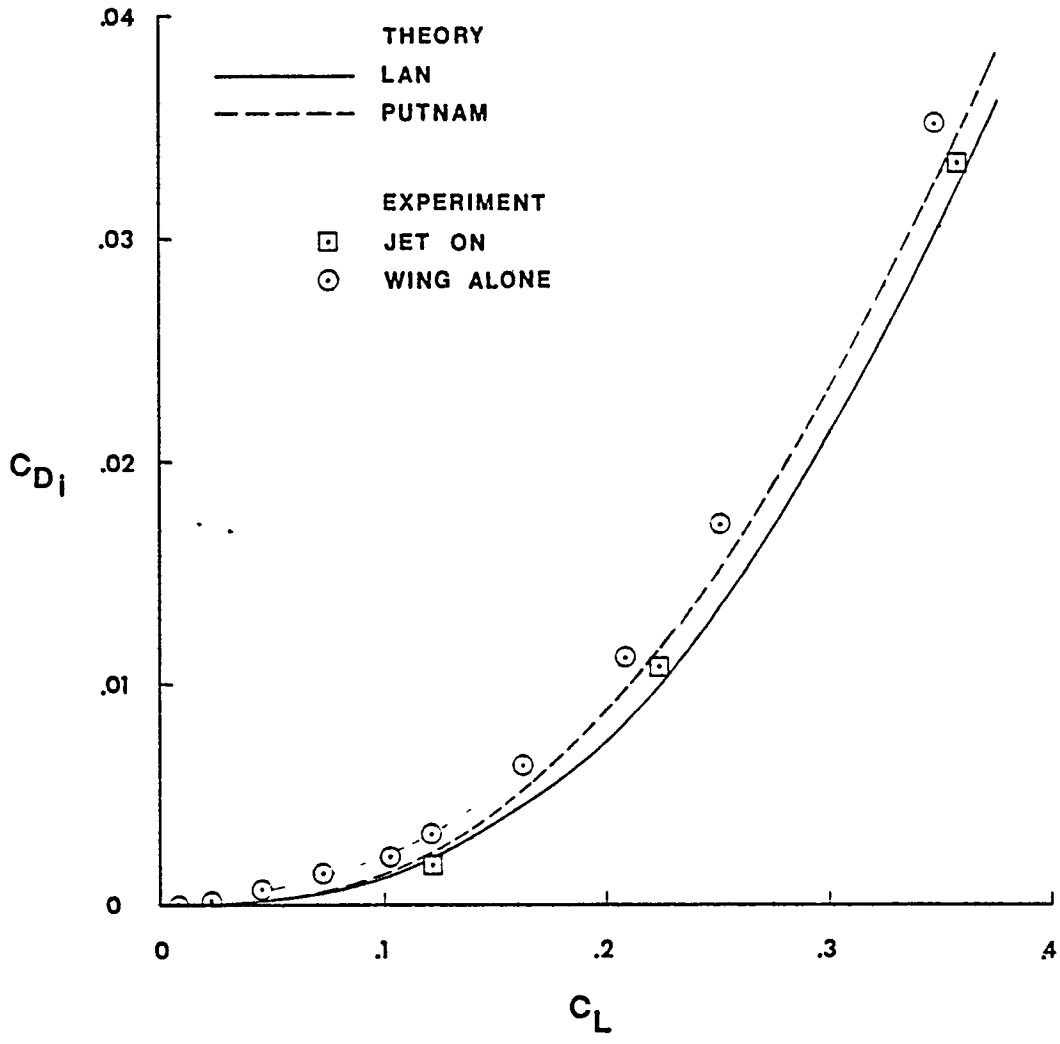

Figure 4. Comparison of the present theory with the theory of reference 4 and the experimental data of reference 3. high-aft jet, α =.31, M_∞ =.4

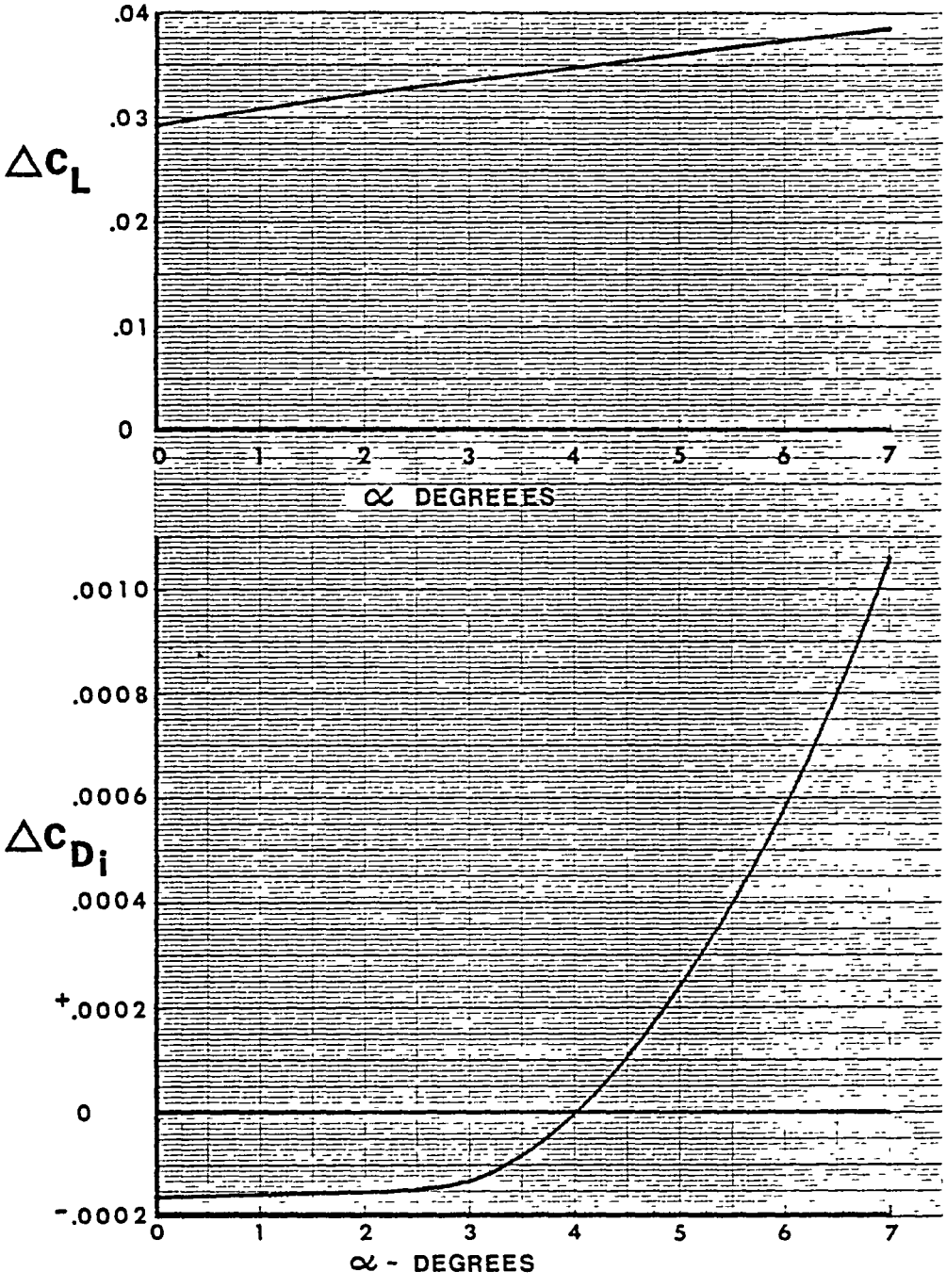

Figure 5. Incremental lift and drag coefficients for the high-aft jet configuration. Entrainment and interaction effects included in the calculations. μ=.28

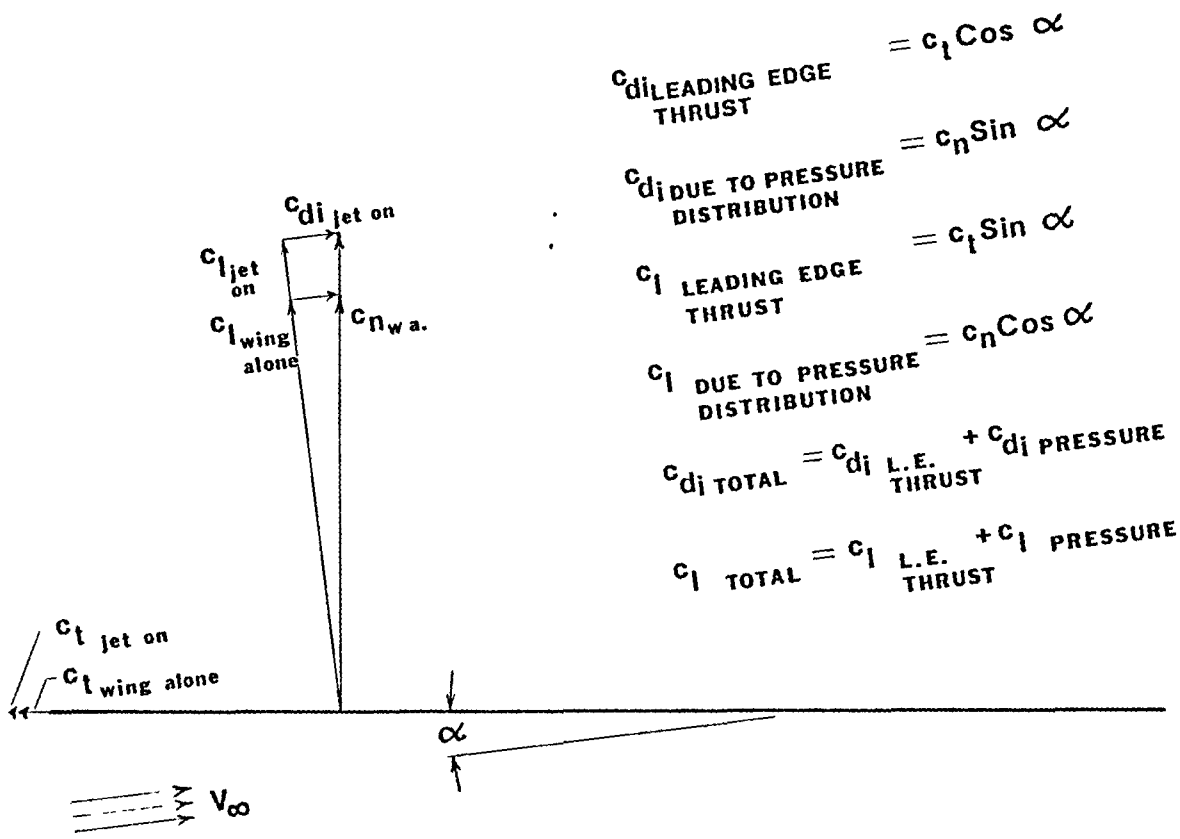

Figure 6.

Definition of the components of the total lift and induced drag coefficients. Drawn to scale for the High-aft jet $\alpha = 7^o$, $\mu = .28$, Y/B/2=.384

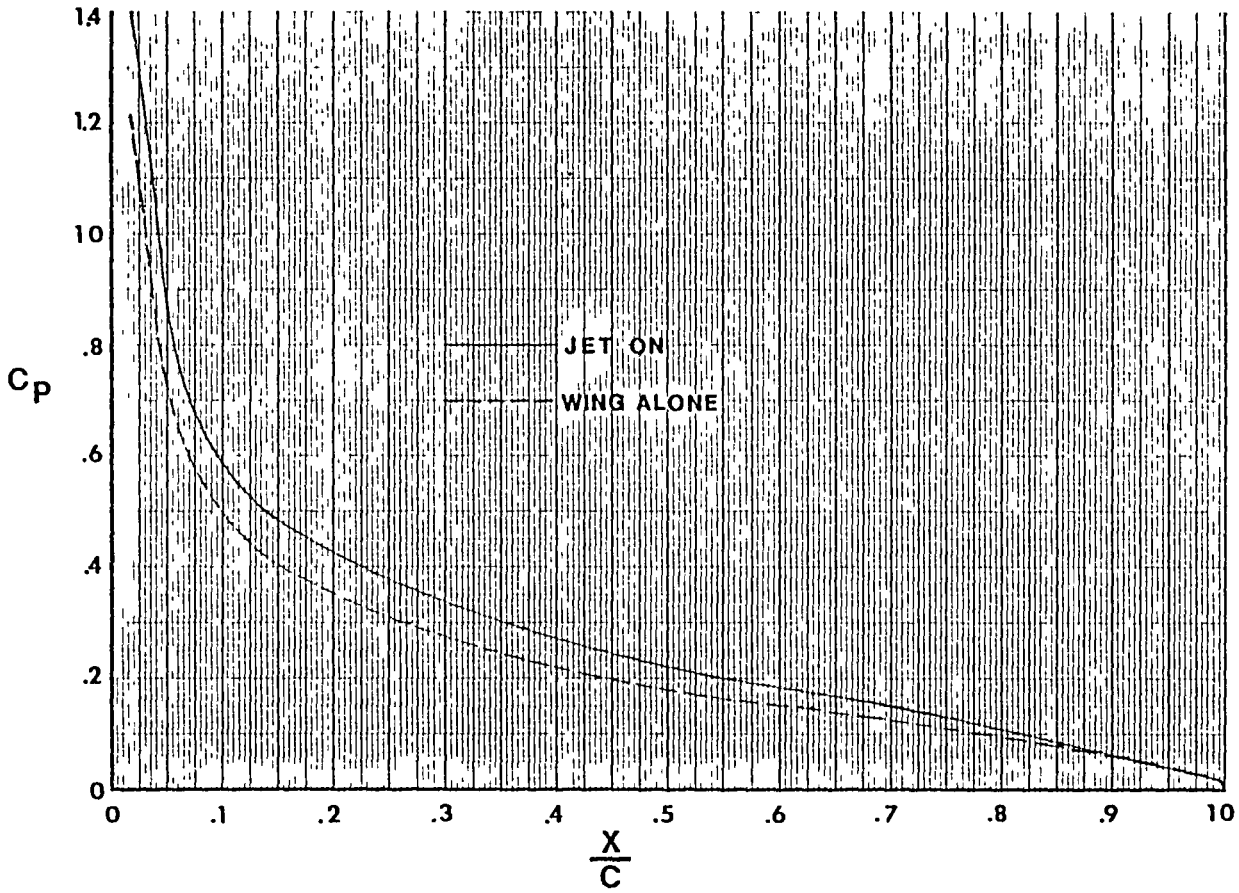

Figure 7. Pressure distributions for the wing alone and due to a high-aft jet. $\alpha=5^{o}$, $\mu=.28$, Y/B/2=.384

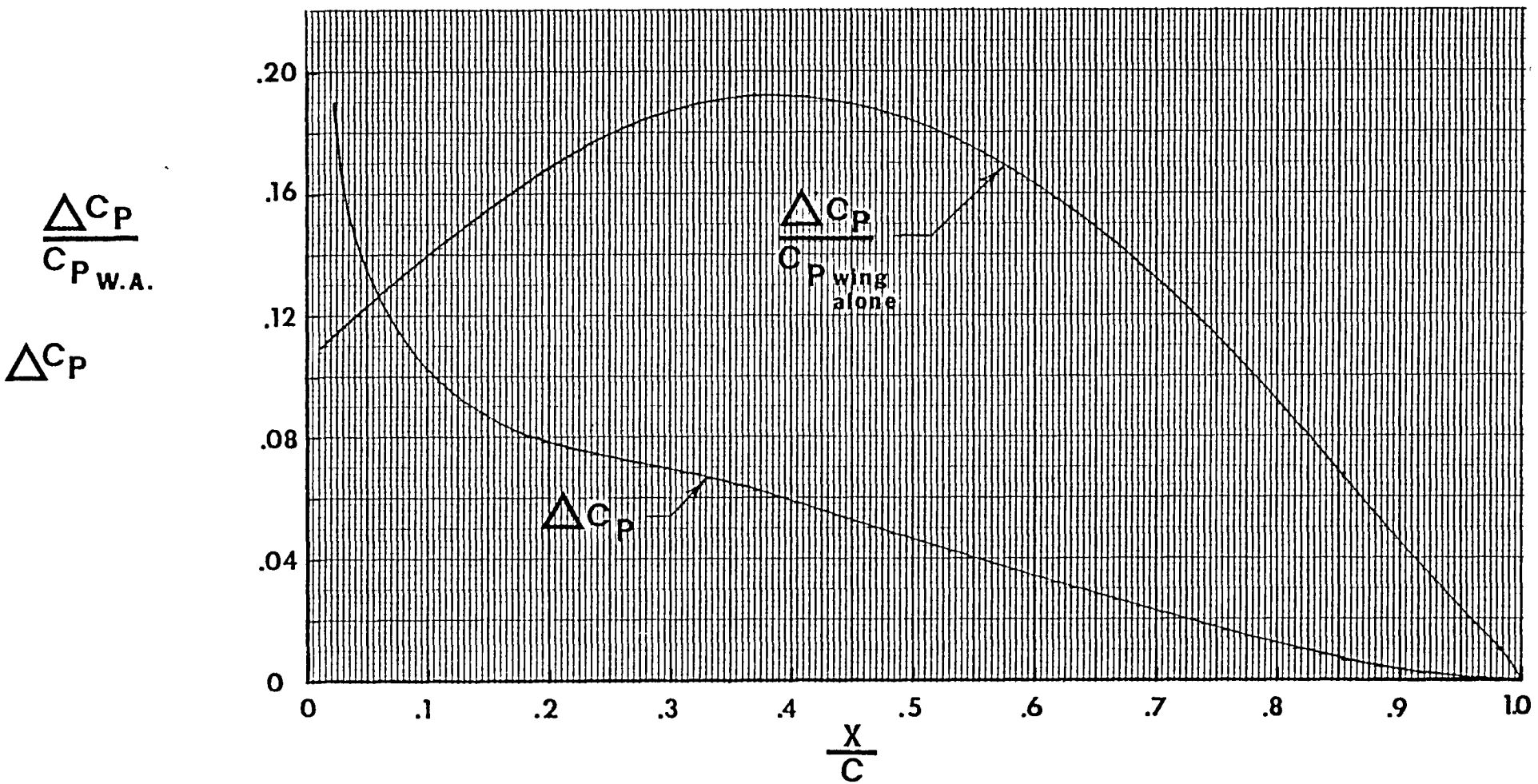

Figure 8. Chordwise distribution of incremental pressure coefficient due to a high-aft jet. $\alpha = 7^{\circ}$, $\mu = .28$, Y/B/2=.384

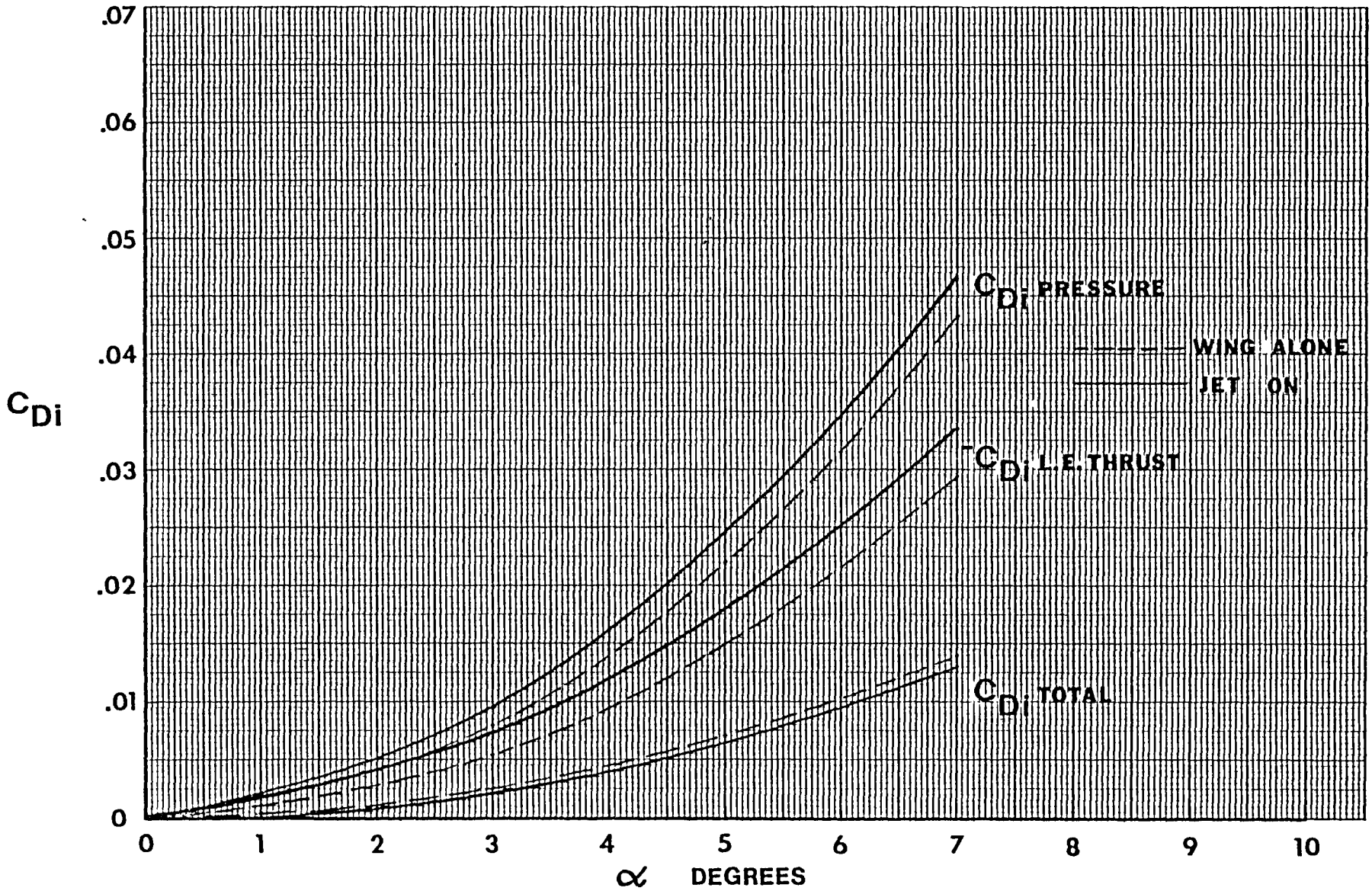

Figure 9. The change in induced drag components due to a high-aft jet. Entrainment effects only μ =.28

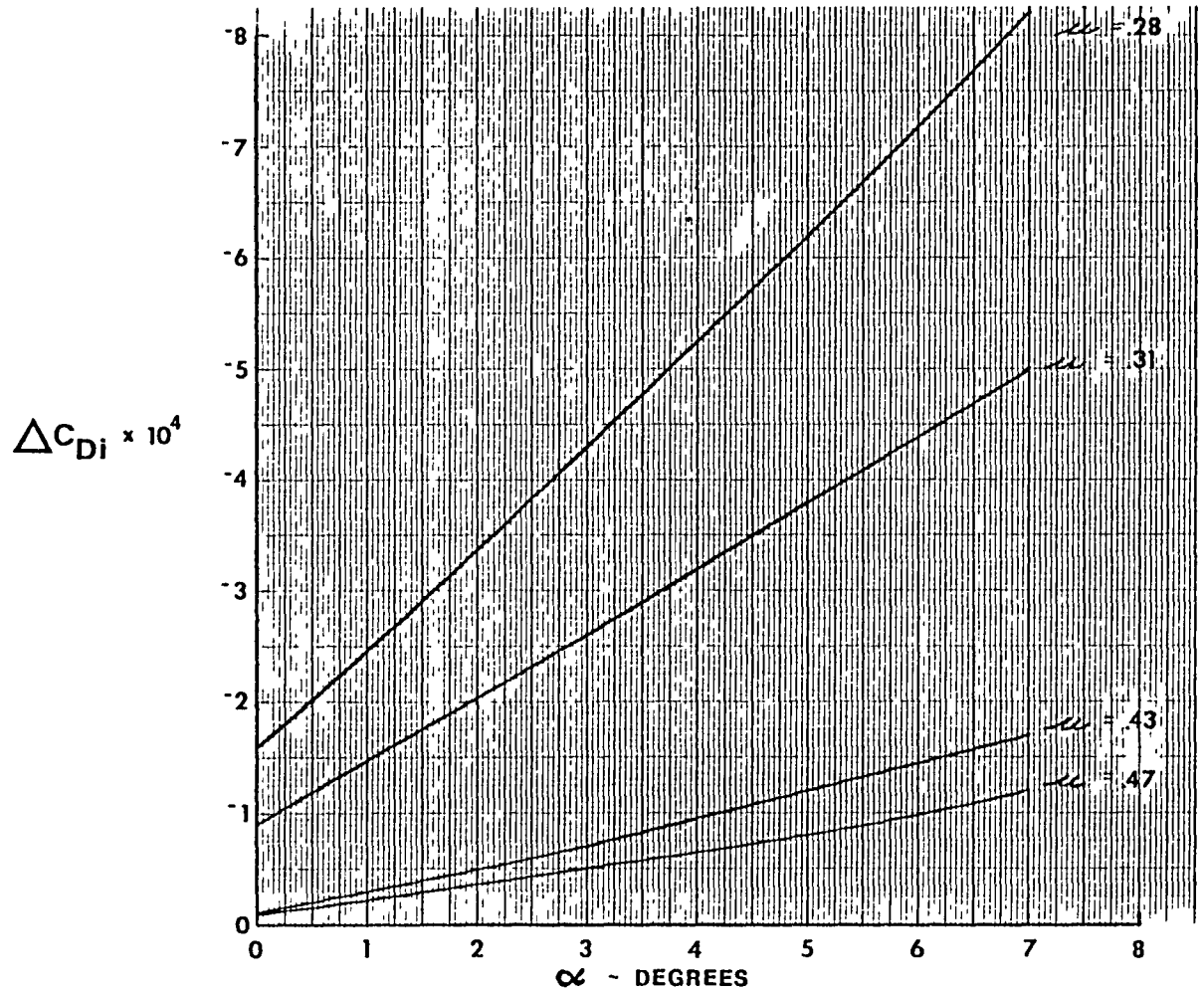

Figure 10. Effect of jet velocity ratio on incremental drag coefficient for a high-aft jet with entrainment only.

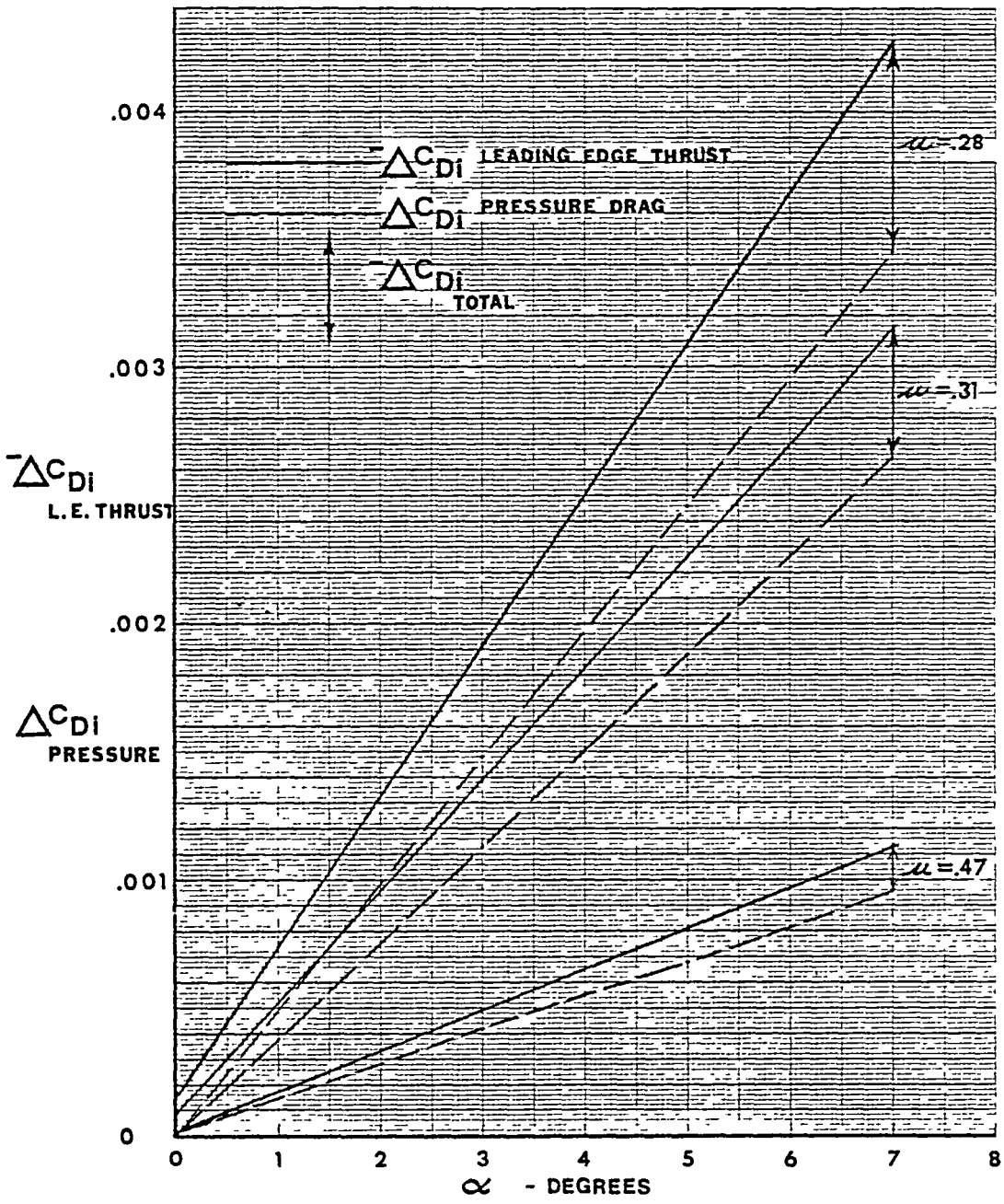

Figure 11. Increments of leading edge thrust and pressure drag due to a high-aft jet at three different velocity ratios. Entrainment effects only.

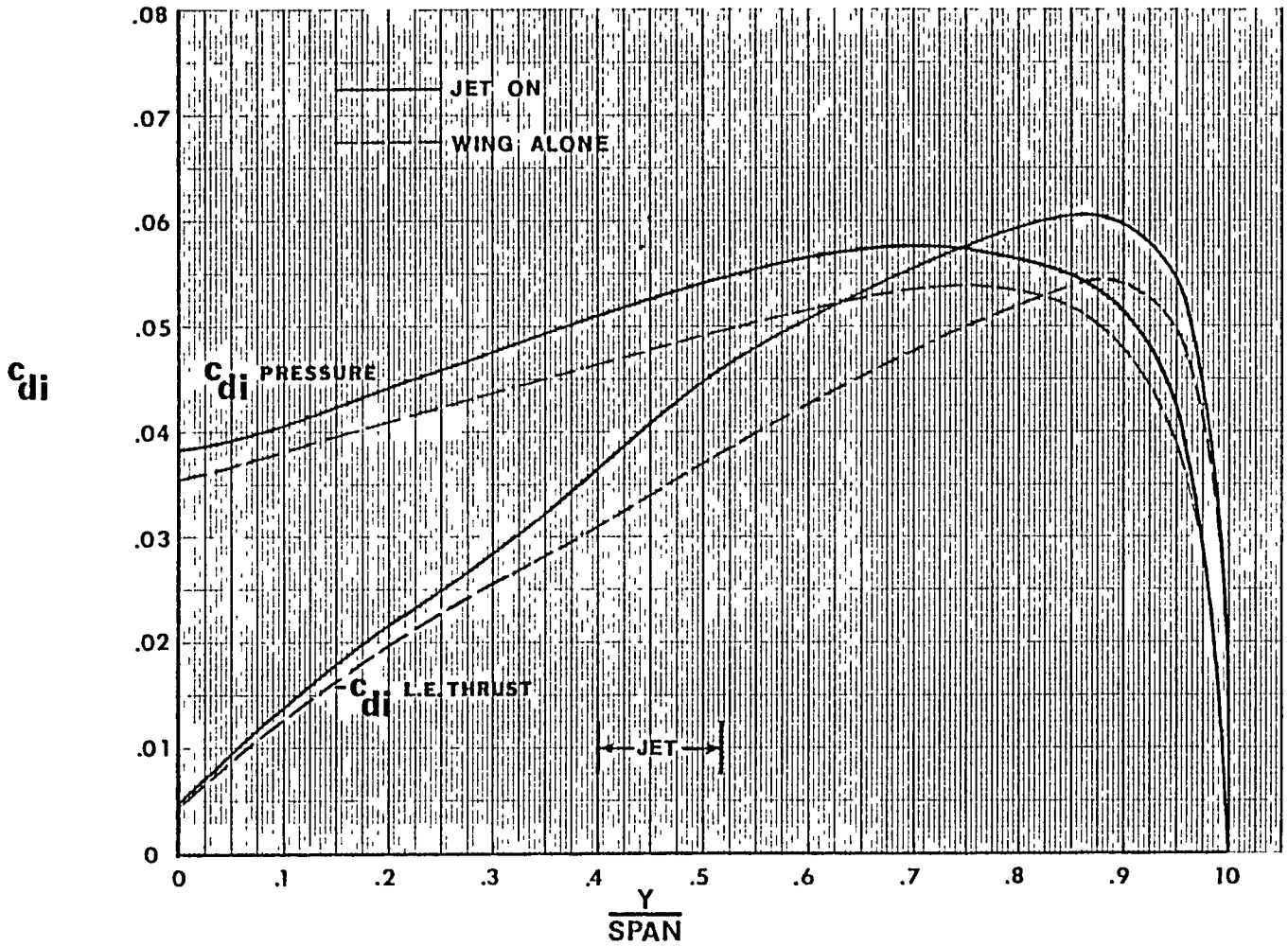

Figure 12. Spanwise distribution of pressure drag and leading edge thrust for the wing alone and due to a high-aft jet. Intrainment effects only $\mathcal{M}$ = 28, α =7°

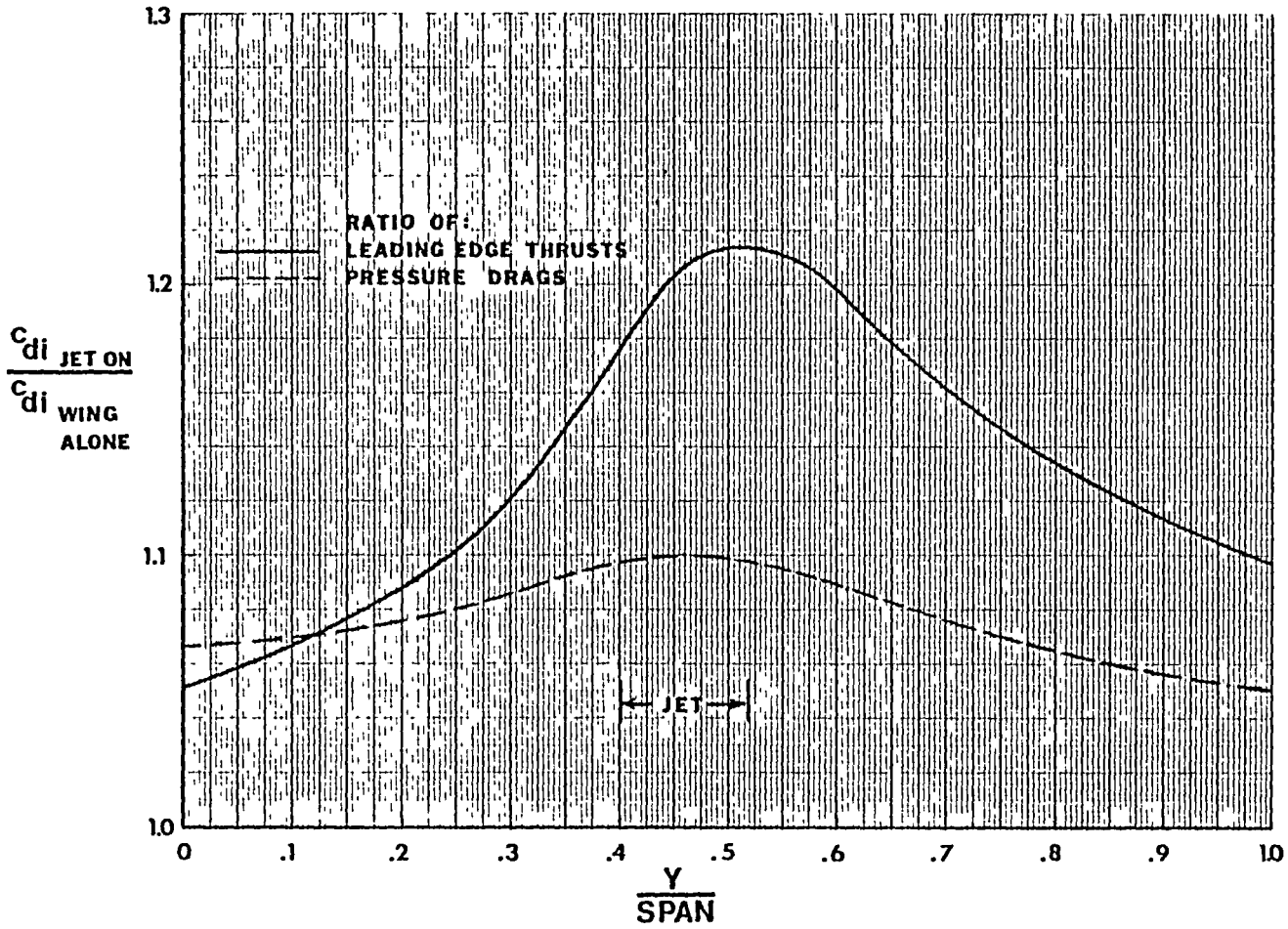

Figure 13 Spanwise distribution of pressure drag and leading edge thrust due to a high-aft jet, normalized with wing alone data. Entrainment alone μ=.28, α =7°

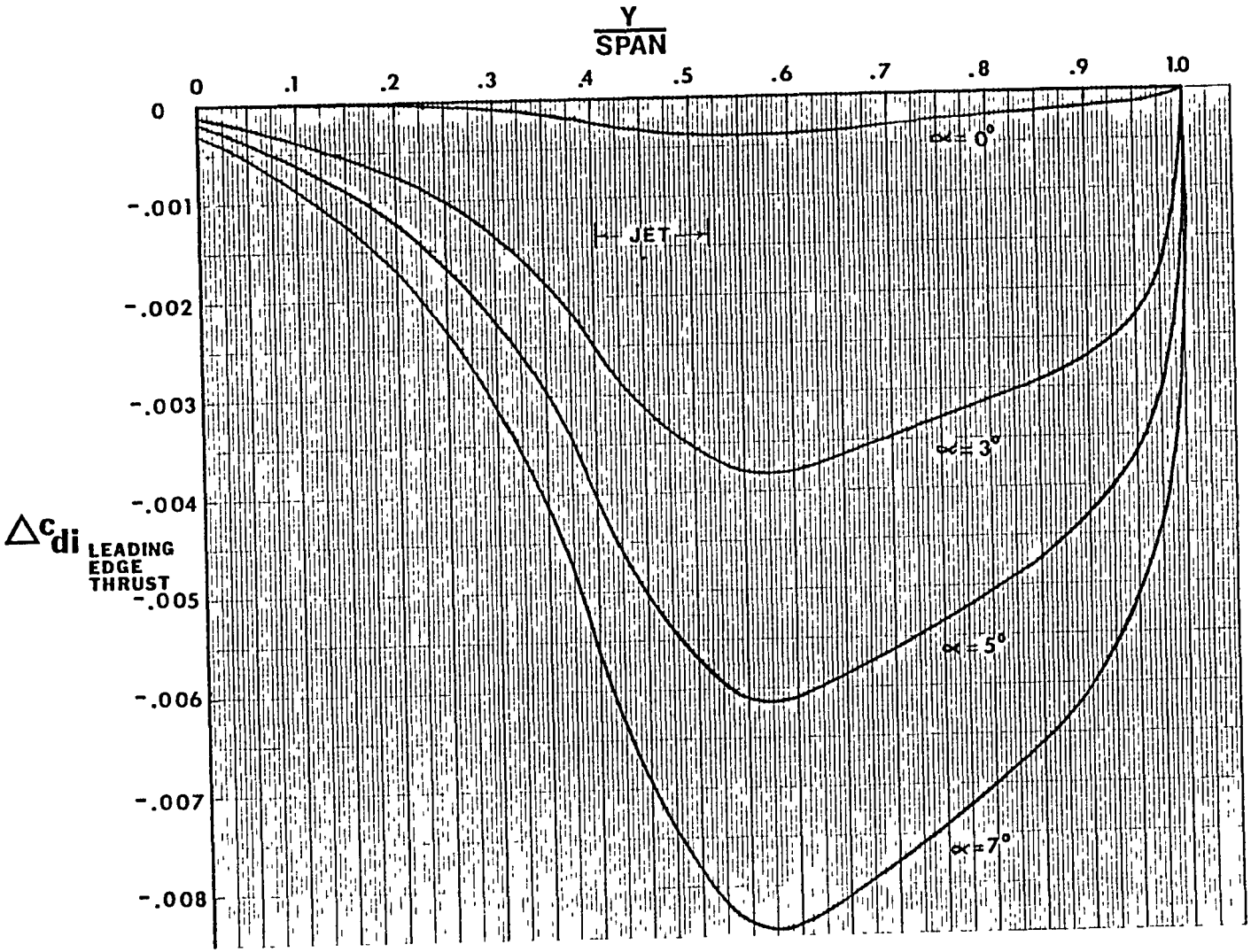

Figure 14. Effect of alpha on the spanwise distribution of incremental leading edge thrust due to a high-aft Jet. Entrainment effects only $\mu = .08$, $\alpha = 1^{\circ}$

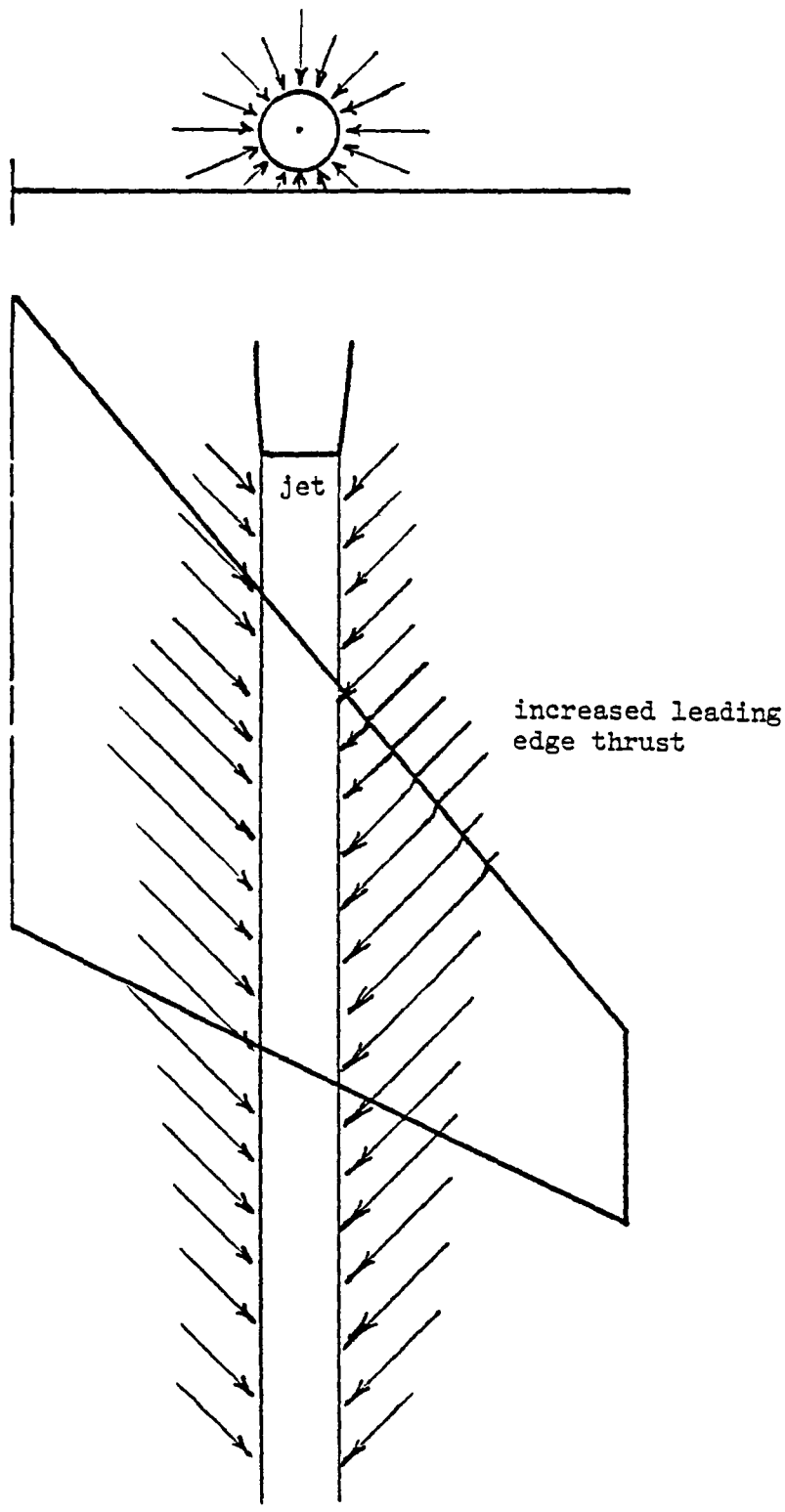

Sketch A. Effect of jet entrainment upon the leading edge thrust of the outboard wing portion.

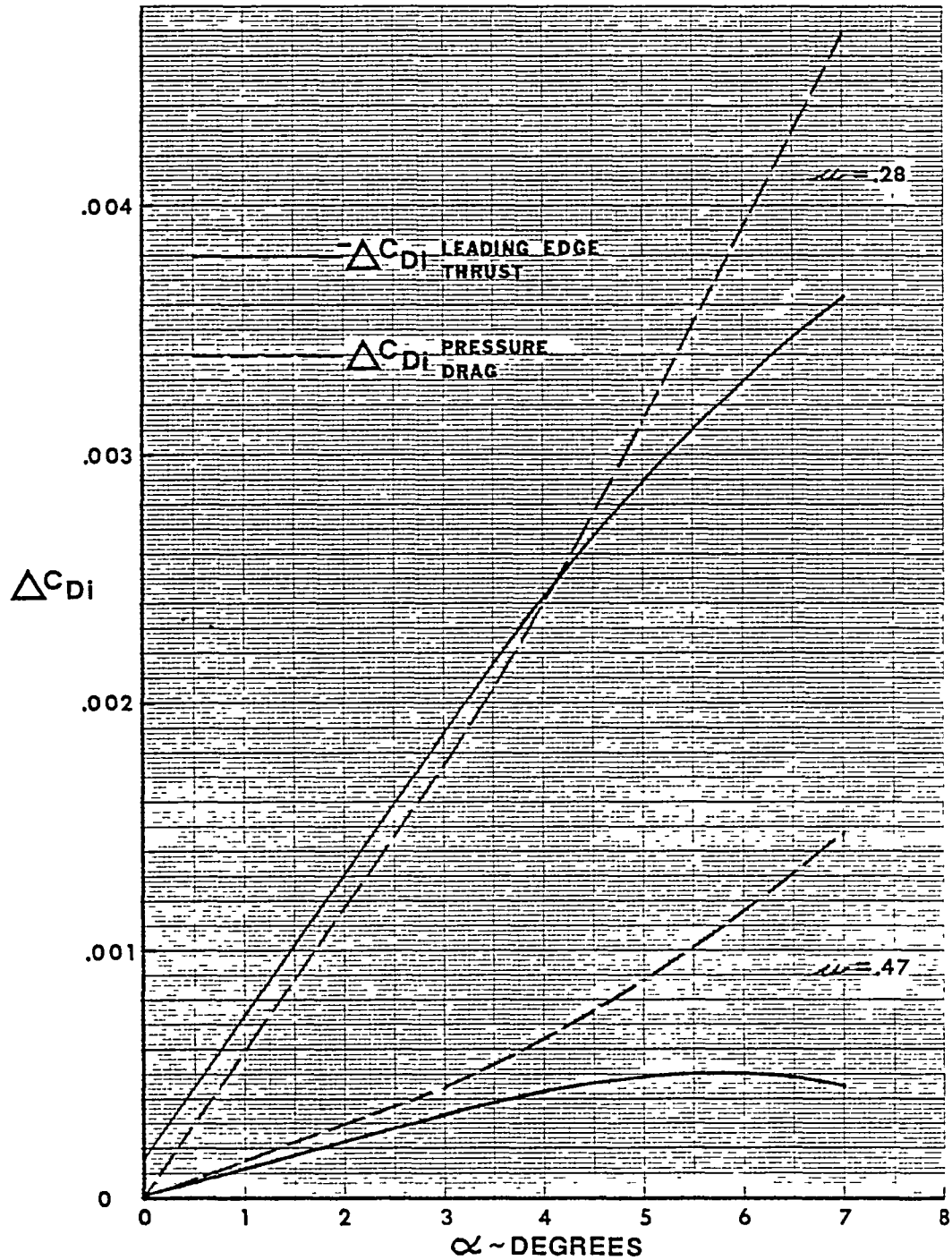

Figure 15. Increments of leading edge thrust and pressure drag due to a high-aft jet at two different velocity ratios. Entrainment and interaction

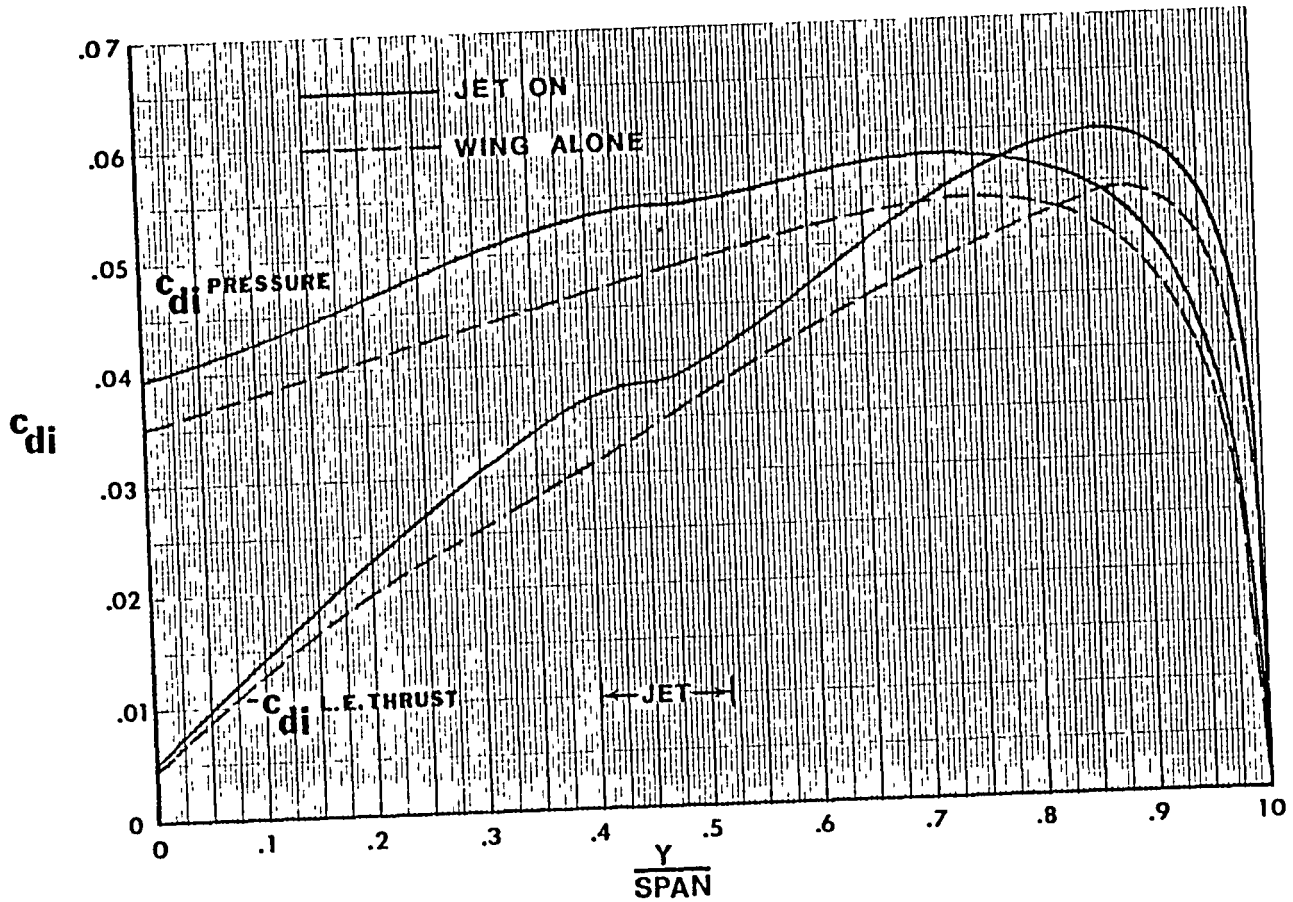

Figure 16. Spanwise distribution of pressure drag and leading edge thrust for the wing alone and due to a high-aft jet. Entrainment and interaction effects $\mu = .28$, $\alpha = 1^{0}$

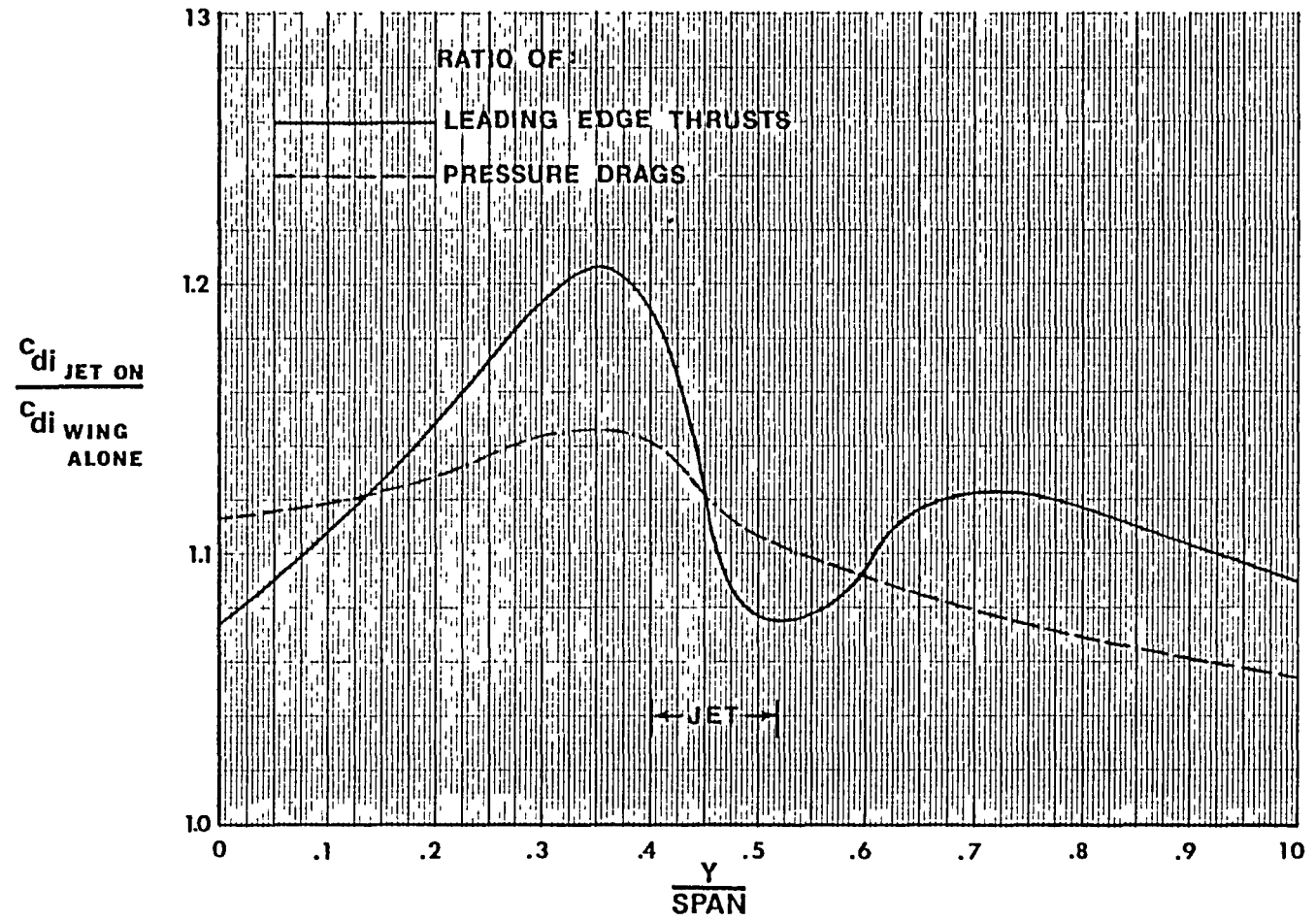

Figure 17. Spanwise distribution of pressure drag and leading edge thrust due to a high-aft jet, normalized with wing alone data. Entrainment and interaction effects $\mu = .28$, $\alpha = 1^{o}$

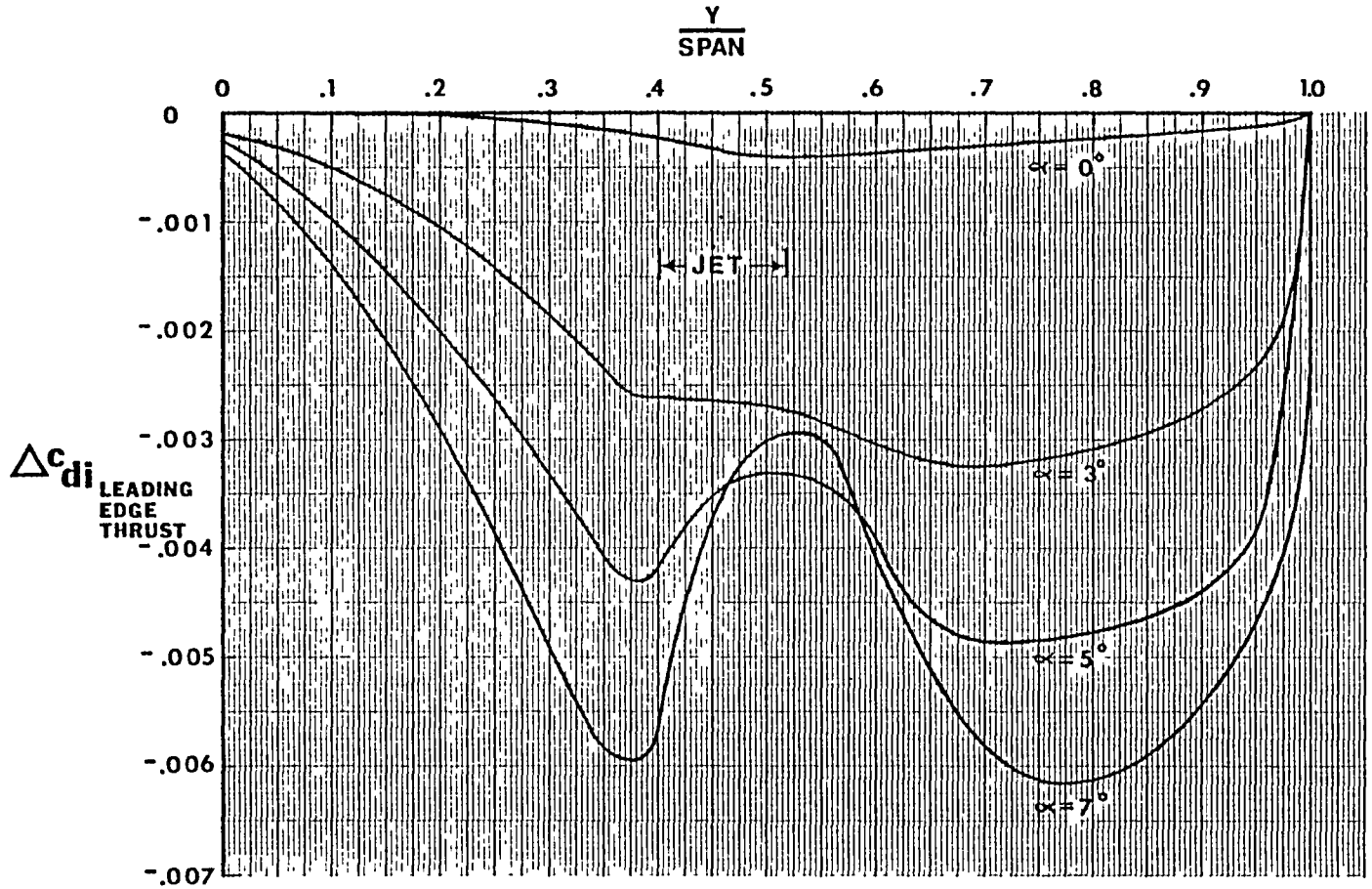

Figure 18. Effect of alpha on the spanwise distribution of incremental leading edge thrust due to a high-aft jet. Entrainment and interaction effects $\mu = .28$

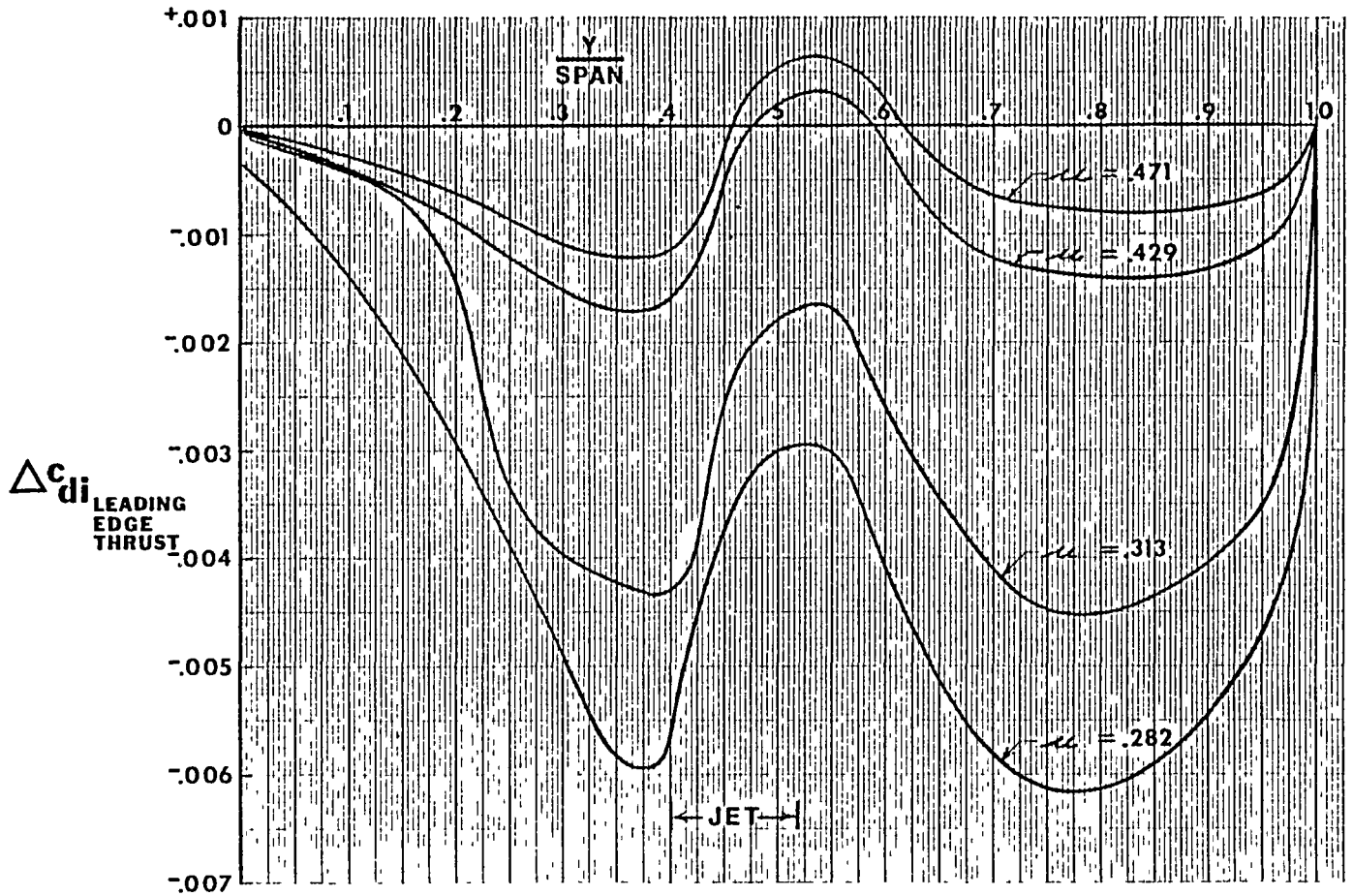

Figure 19. Effect of jet velocity ratio on the spanwise distribution of incremental leading edge thrust due to a high-aft jet. Entrainment and interaction effects $\alpha = 7^0$

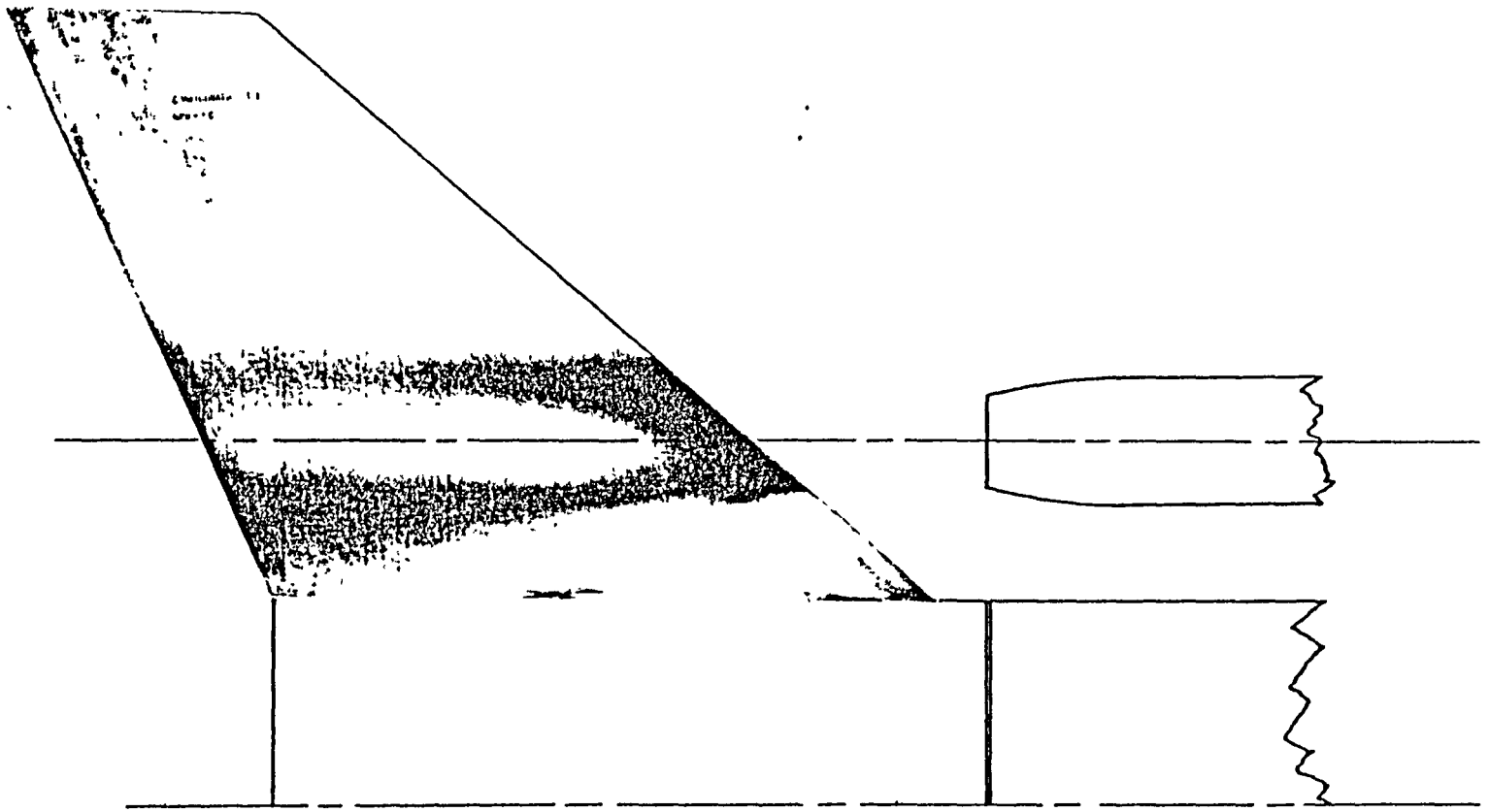

L-73-6825

Figure 20. Photograph taken from reference 1 showing the portion of the wing washed by a low-aft jet.
$\mu = .43$

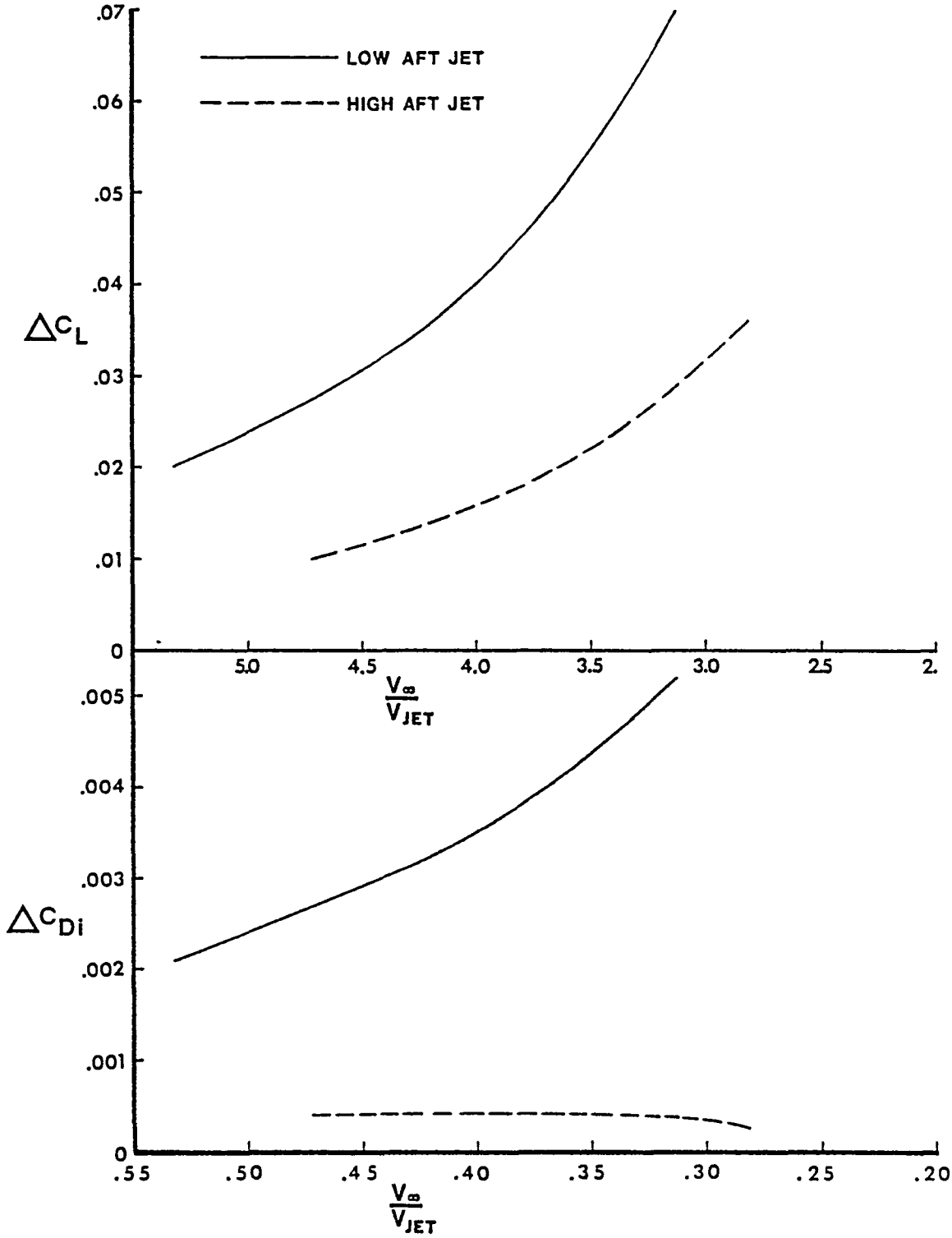

Figure 21. Comparison of the incremental lift and drag coefficients due to a low-aft and high-aft jet. $\alpha = 5^{\circ}$

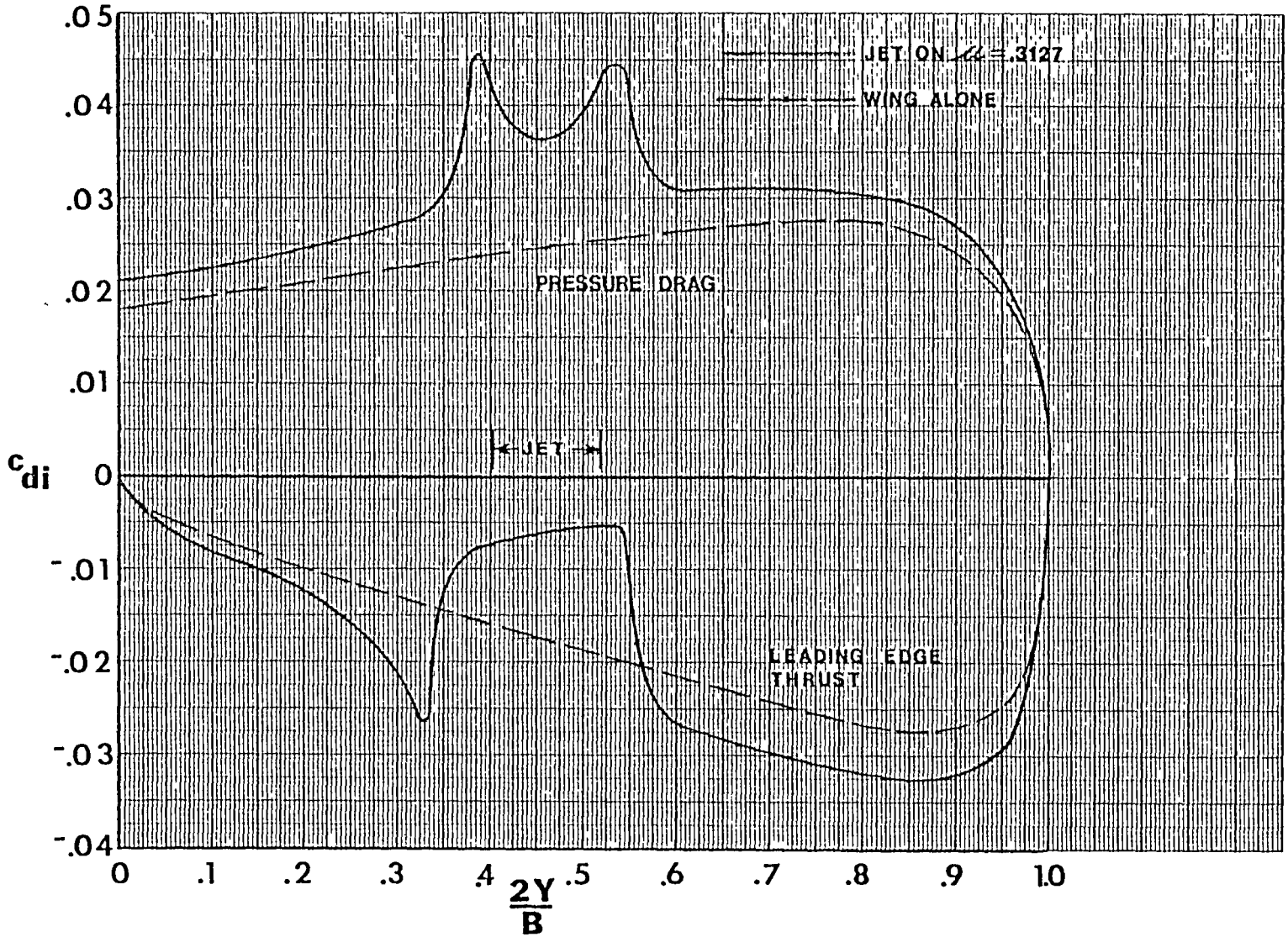

Figure 22. Comparison of the spanwise distribution of pressure drag and leading edge thrust coefficient for the wing alone and a low aft jet. μ = .31, $\alpha = 5^0$ Entrainment and Interaction effects

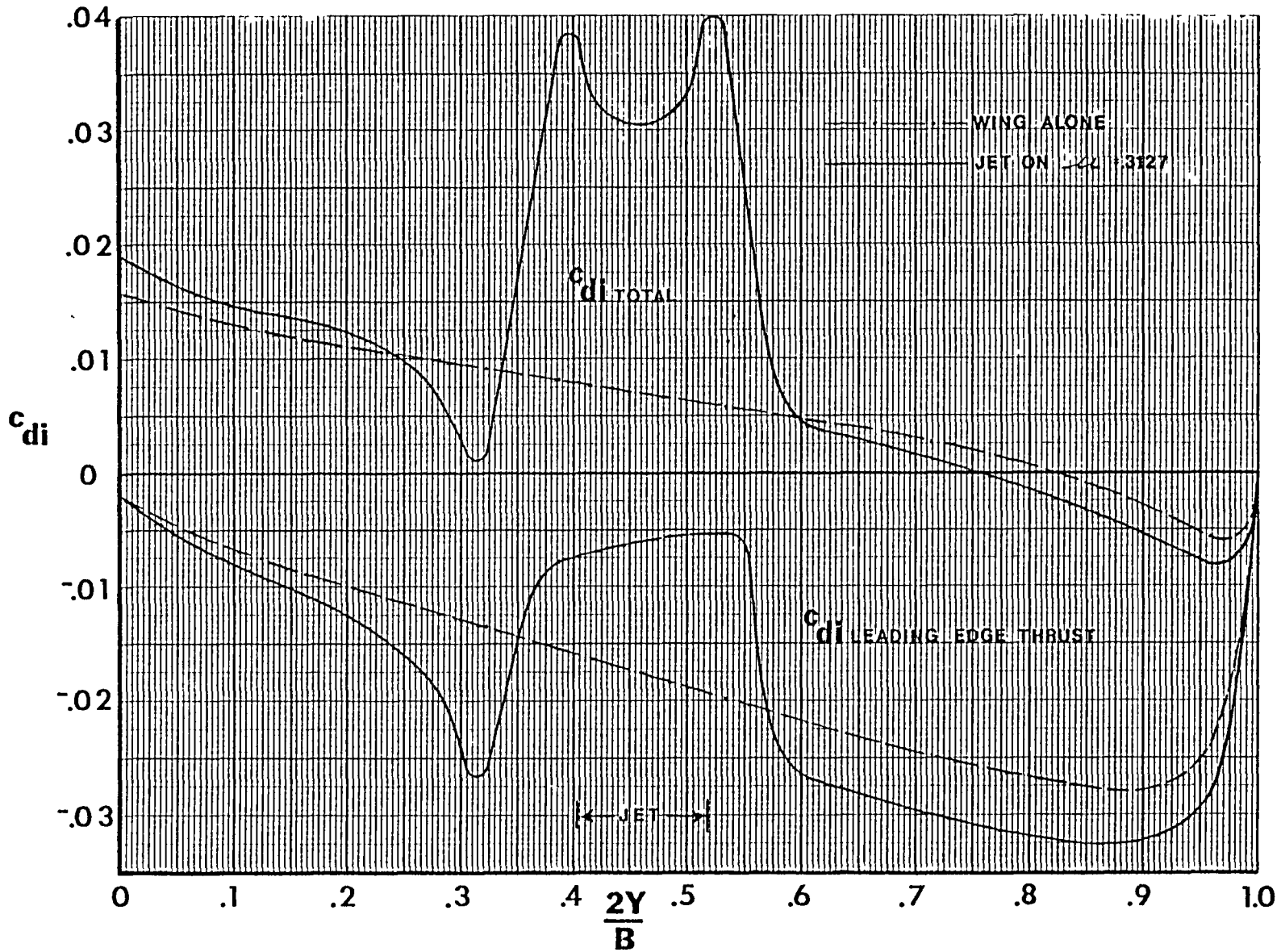

Figure 23. Effect of a low-aft jet on the spanwise distribution of total drag coefficient and also the leading edge thrust contribution. Entrainment and interaction $\mu = .31$, $\alpha = 5^0$

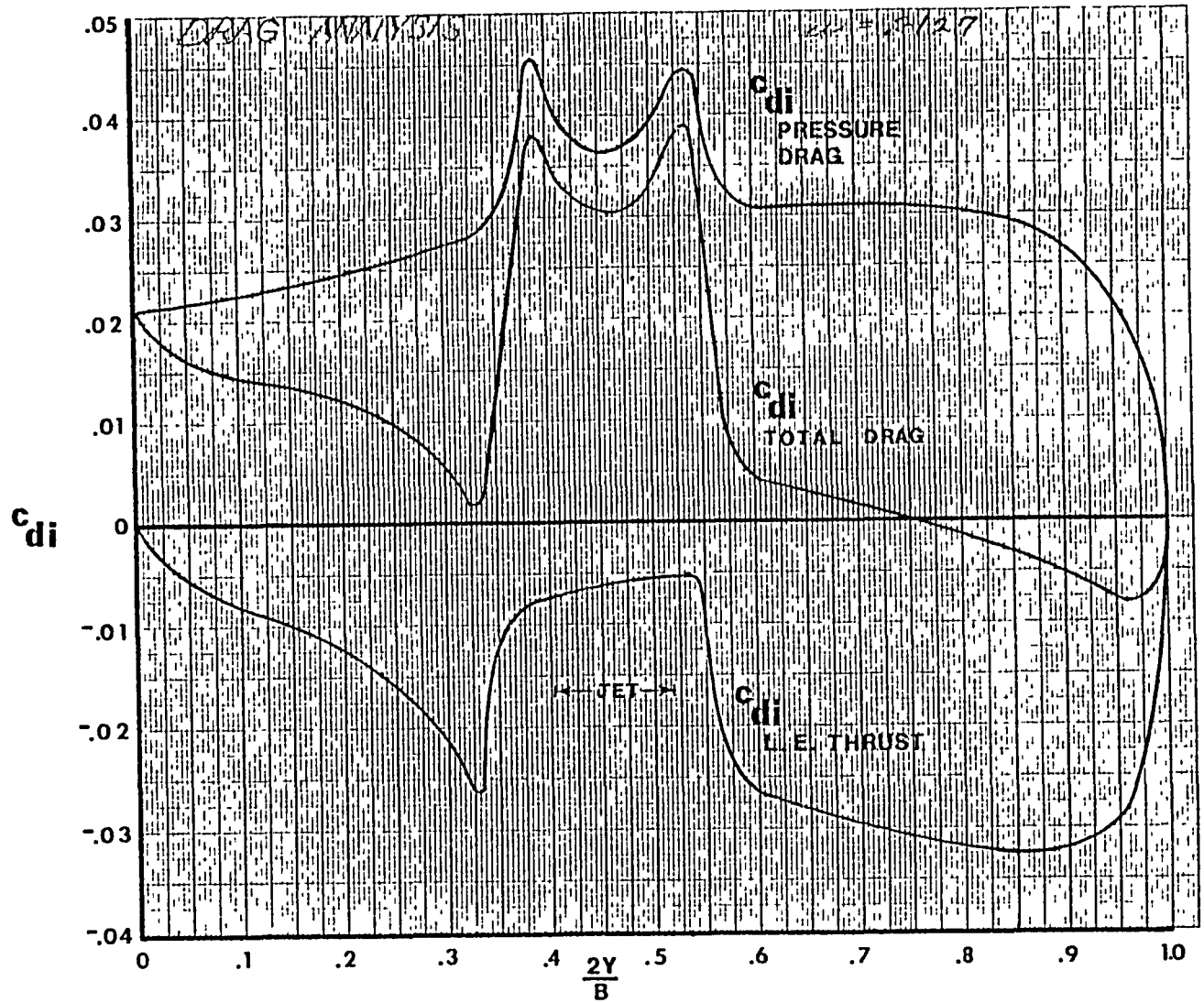

Figure 24. Spanwise distribution of the two components of the induced drag coefficient for the low-aft jet. Entrainment and interaction effects $\mu = .31$, $\alpha = 5^0$

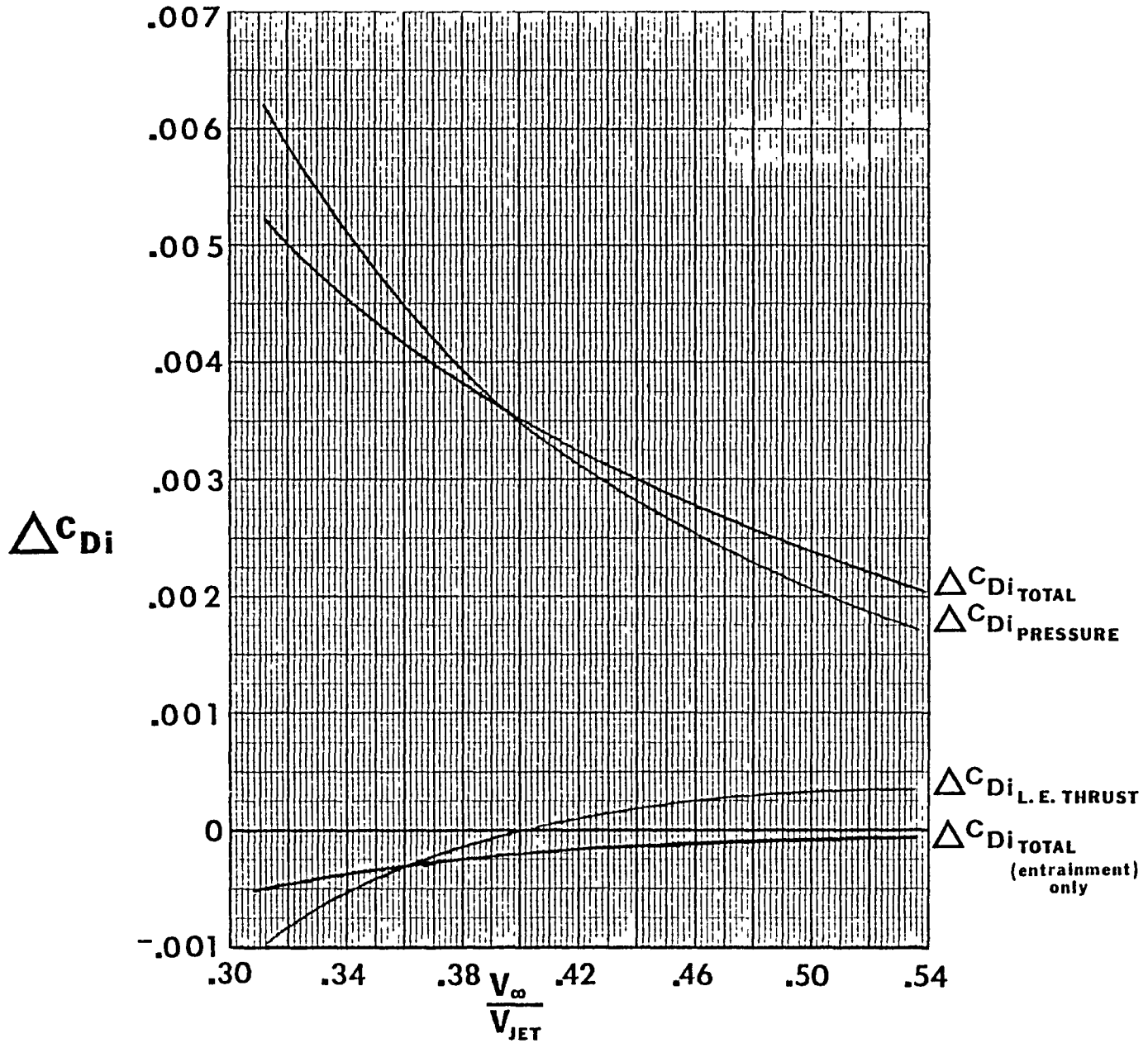

Figure 25. Incremental drag coefficient and it's two components, all for the interaction and entrainment of a low-aft jet. Also shown: The incremental drag due to entrainment only. $\alpha = 5^0$

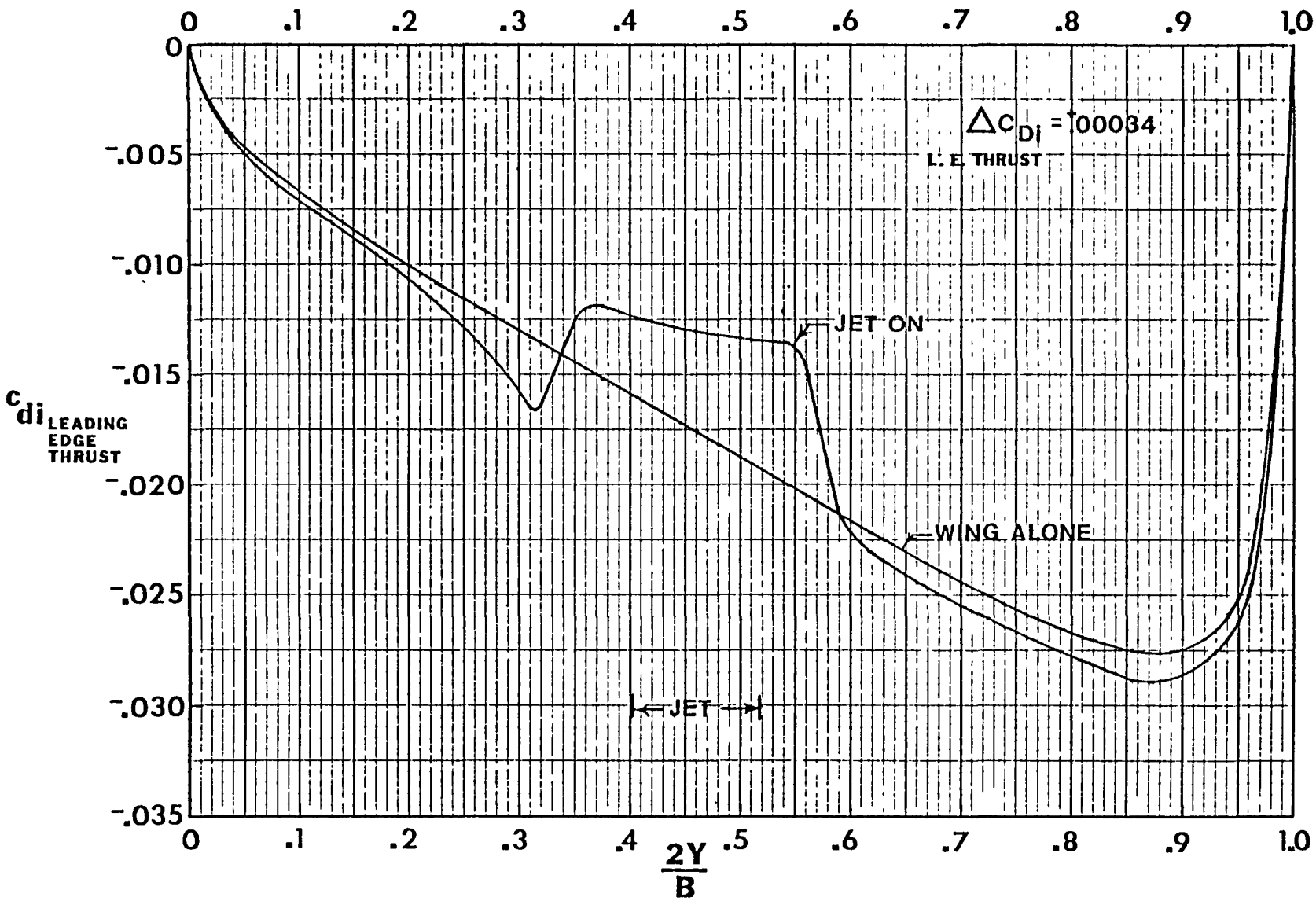

Figure 26 Comparison of the spanwise distribution of leading edge thrust coefficient for a low-aft jet and the wing alone. $\mu = .532$, $\alpha = 5^0$

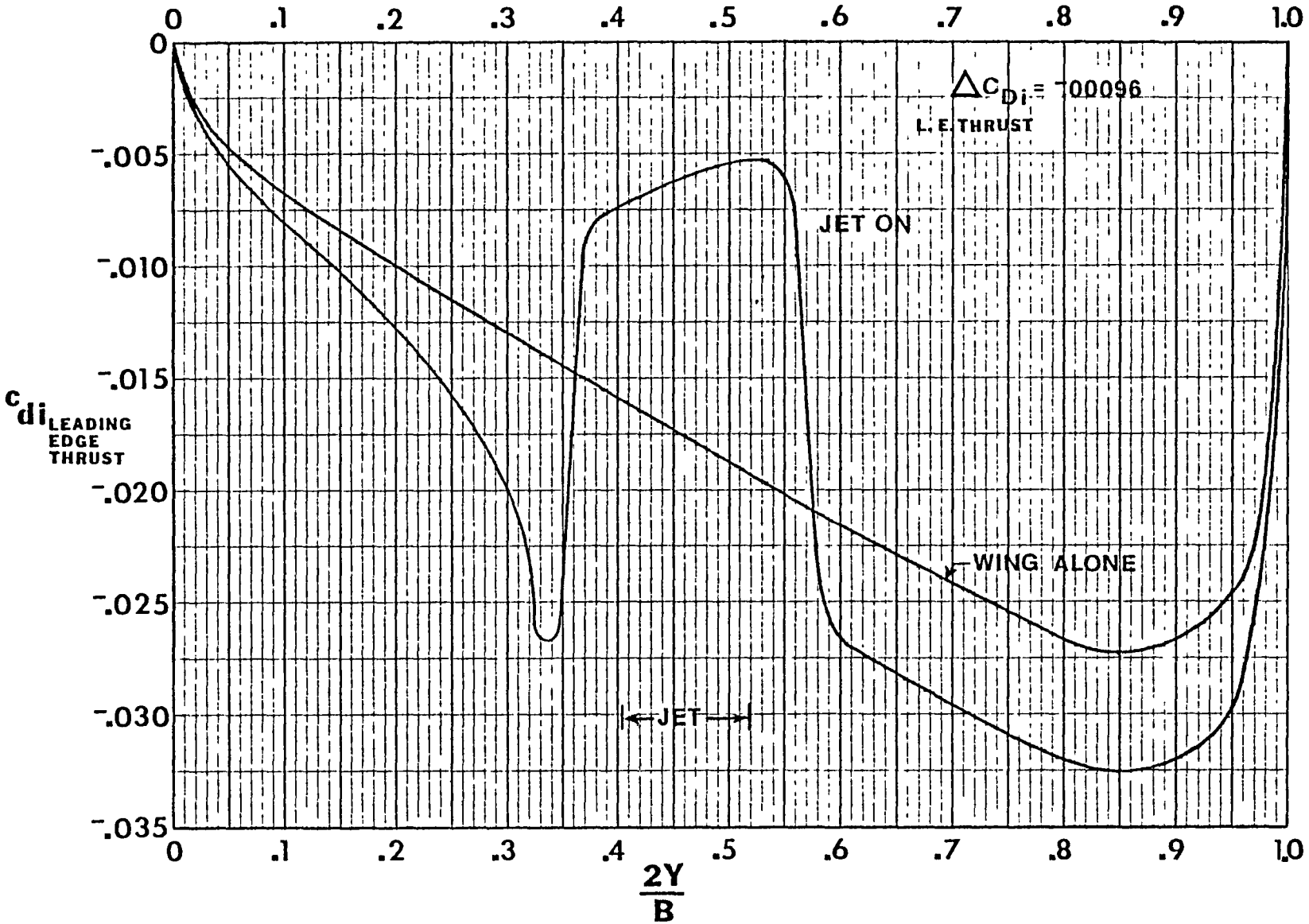

Figure 27. Comparison of the spanwise distribution of leading edge thrust coefficient for a low-aft jet and the wing alone. μ = .31, $\alpha = 5^0$

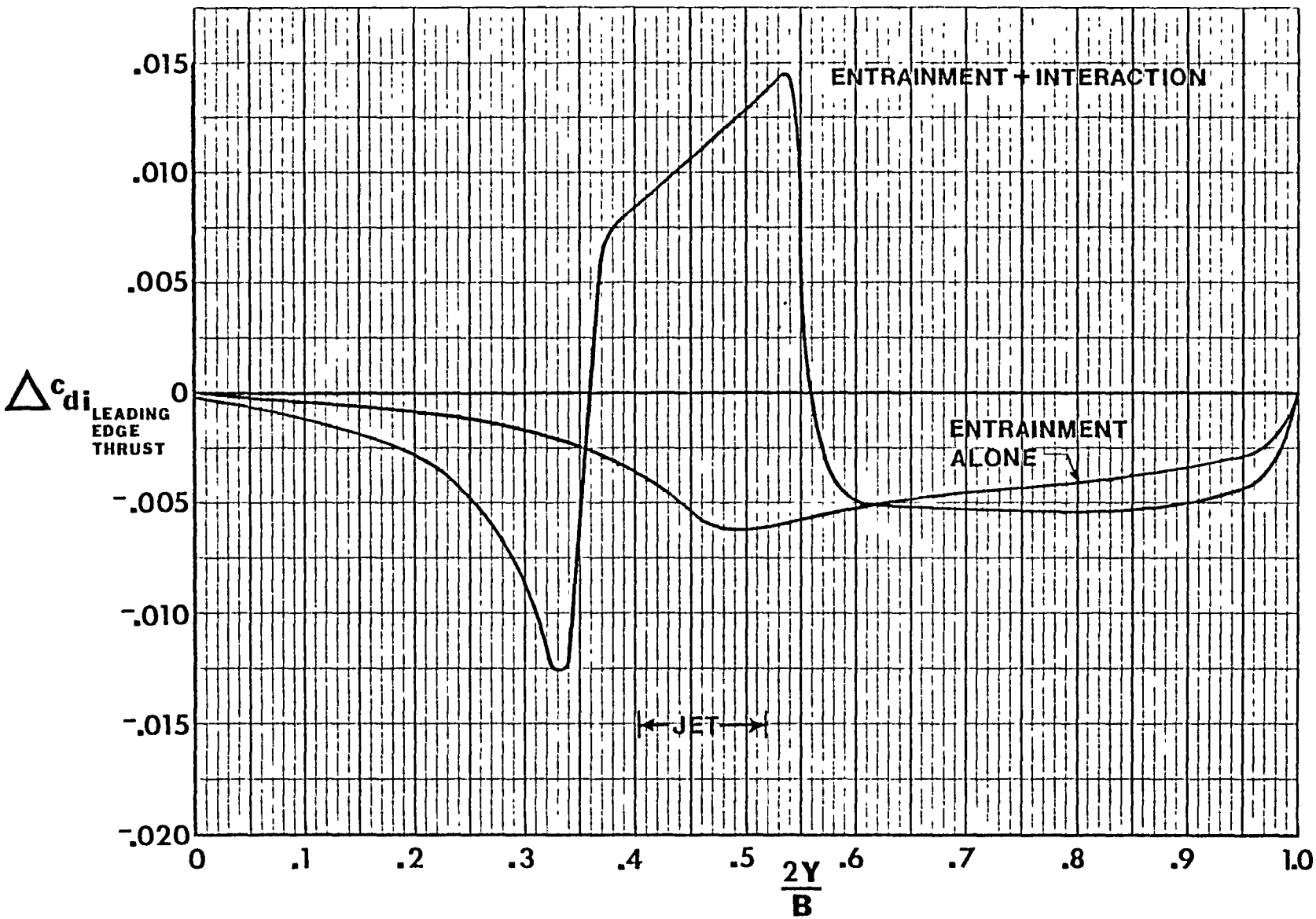

Figure 28. Comparison of the spanwise distribution of incremental leading edge thrust coefficient for entrainment alone and entrainment plus interaction effects. Jet in the low-aft configuration. $\mu = .31$, $\alpha = 5^0$

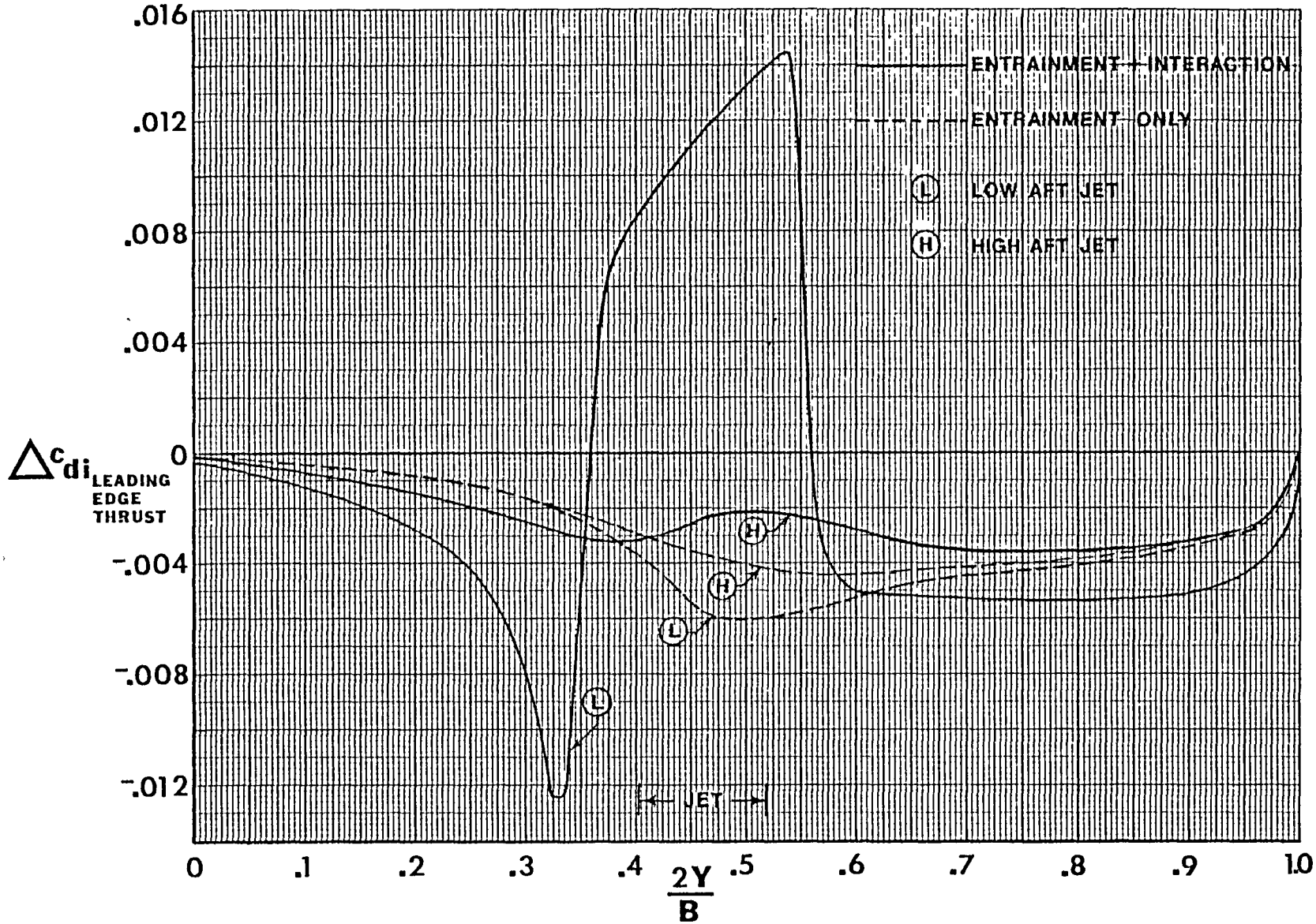

Figure 29 Spanwise distribution of incremental leading edge thrust coefficient for a high-aft and low-aft jet, shown with entrainment alone and for entrainment plus interaction effects. $\mu = .31$, $\alpha = 5^{o}$

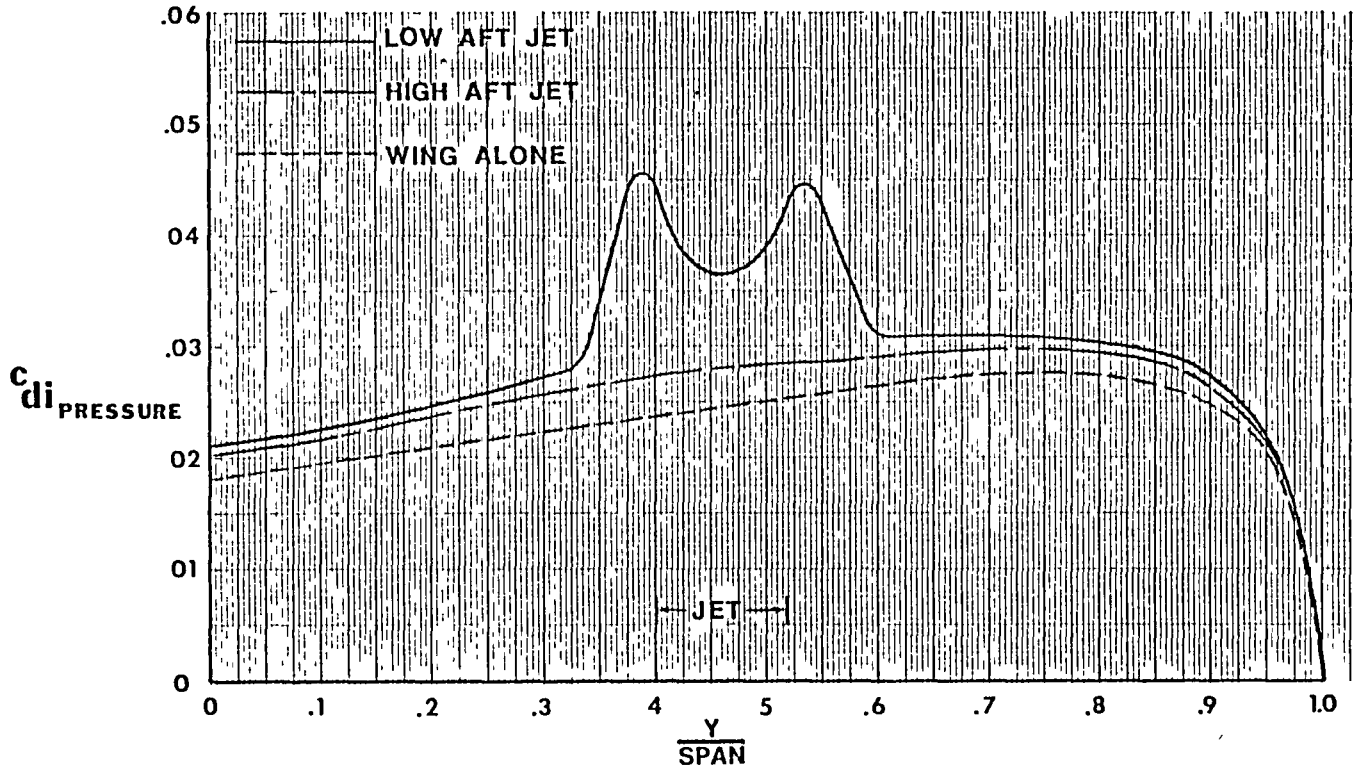

Figure 30 Comparison of the spanwise distribution of induced drag coefficient due to the pressure distribution with a low-aft jet and a high-aft jet. Entrainment plus interaction $\mu = .31$, $\alpha = 5^{\circ}$

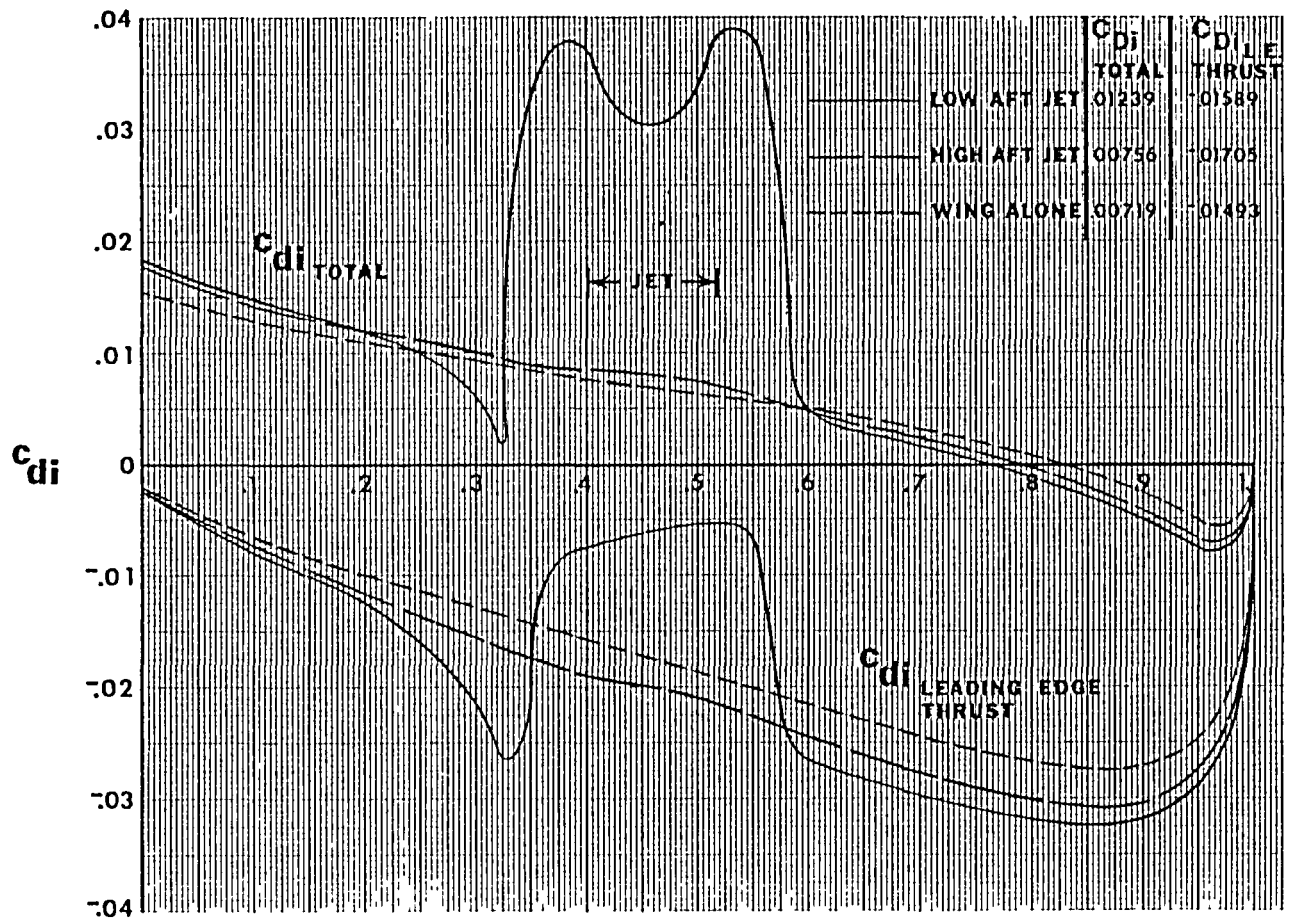

Figure 31 Comparison of the induced drag coefficient and leading edge thrust coefficient for a low-aft jet, a high-aft jet, and the wing alone. Entrainment plus interaction $\mu = .31$, $\alpha = 5^{\circ}$

2. Analysis of Planform Effects on Upper-Surface Blowing Lift Augmentation

2.1 INTRODUCTION

It is a well-known fact that an upper-surface blowing jet induces large increments of lift beyond the potential flow limit of a wing without blowing. This increment of additional lift has been shown to be strongly dependent upon the amount of blowing (thrust coefficient). This additional lift has also been shown to be very sensitive to the location of the jet exit relative to the wing. One of the major reasons the aerodynamic characteristics of an upper-surface blowing configuration are sensitive to the characteristics of the jet is the so called wing-jet interaction effect[9]. The wing flow field is modified by the presence of the jet and conversely the jet flow field is altered by the presence of the wing. Thus the wing characteristics as well as the jet characteristics are important in the over-all performance of the wing-jet system. The effects of jet location and jet thrust coefficient have been studied in numerous wind tunnel investigations, the trend being to pick a particular wing planform of interest and vary the jet location and nozzle geometry in an effort to optimize a particular wing jet combination.

In this computer analysis the opposite approach was taken in that the characteristics and geometry of the jet were fixed beforehand and the wing planform was varied, in order to determine what particular wing parameters are important in optimizing a wing which utilizes upper-surface blowing (USB). A wide range of planforms were examined in hopes of finding a wing parameter to which incremental lift is a direct function of. This parameter could thus be used to predict the incremental lift of any general wing planform for a given amount of jet blowing. A family of such relations for varying levels of blowing could be used in the design process for an upper-surface blowing (USB) configured aircraft. Partial

success was made in this direction, however, the problem is complex. It was found that any alteration of the wing flow field also disturbs the way the wing and jet interact and the incremental lift produced by the interaction process. No one wing parameter was found to be dominant but rather all three parameter variations undertaken (sweep, aspect ratio, taper ratio) effected important changes in the incremental lift due to blowing. By the same reasoning, any major modification of the jet flow field should disturb the interaction process and resulting additional lift. Thus all of the data shown, apply only to the particular jet characteristics and geometry used for this test, although the trends of the results are probably very general.

The wing-jet interaction effect was calculated according to the theory reported in Reference 9, using the computer program of Reference 1. The theoretical predictions of this program have been compared extensively with experimental results and the theoretical results were in good agreement with the USB experiments[9,11].

2.2 GEOMETRY OF THE JET

As was stated earlier, the major emphasis of this investigation was the effect of wing planform variations on upper surface blowing performance. The same jet was used for all wings tested to insure that any variations in incremental lift were due solely to planform changes. Because only one jet configuration was used throughout the analysis, it is important that it be as realistic as possible so that subsequent findings lend themselves to real world situations. Much of the jet characteristics used (see Table 1) are similar to data taken from Reference 12 and jet parameters of the Boeing YC-14 advanced medium STOL transport. The

Table 1

Description of the Jet

Used Throughout this Investigation

Geometry: rectangular USB exit

Aspect Ratio $(\frac{\text{width}}{\text{thickness}}) = 5.0$

$\frac{A_{jet}}{S_w/2} = .038088$

$\frac{V_\infty}{V_j} = .16$

$C_u = 2.0$

$\frac{T_j}{T_\infty} = 1.25$

$M_j = .838$

$M_\infty = .15$

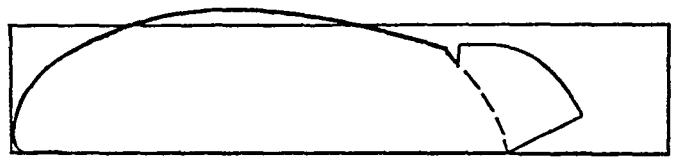

Comparison of the USB jet exit with the YC-14 exit based on fraction of wing area.

input data used models conditions during low-speed flight. A rather high aspect ratio rectangular jet exit was used because wide thin jets have been shown to exhibit the highest lift augmentation at low speed and superior flow turning around flaps. However, it should be noted that severe cruise drag penalties can result from the large boattail angles necessary for such nozzles[13]. This problem was overlooked because, from a cruise drag point of view, the jet scrubbing of any upper-surface blowing (USB) configuration is not favorable when compared to an over-wing blowing (OWB) configuration.

In all cases, the jet exit was placed directly on the leading edge of the wing. Although the lateral extent of the jet was held constant, the sweep angle of the exit varied with the planforms such that the inboard and outboard edges of the jet exit always remained directly on the leading edge. The exit was placed on the leading edge because many unrelated wind tunnel investigations have shown that this longitudinal location relative to the wing yields the largest increments of additional lift. In all cases the jet was located as far inboard as possible, its inboard edge lying on the root chord. This is the probable location for most USB configurations because of the problem of lateral trim with one engine out.

2.3 DESCRIPTION OF WING GEOMETRIES

In this investigation the effects of planform variations were explored through the variation of three important planform parameters: aspect ratio, leading edge sweep angle, and taper ratio. Only plain unflapped wings were investigated. Hopefully this investigation can serve as a data base for subsequent studies of the effects of flap geometry variations

or other wing parameters of a more secondary nature. For example the wing camber distribution has been shown to be important to the drag of OWB configurations[6].

The original set of wing planforms used in this study can be seen in Figures 32 through 35. These wings shapes were chosen to represent a wide range of aircraft now in service. Each wing is code-marked with an alphabetical letter from A to P. The original set seen in Figure 32 is a two dimensional matrix of wings with consistent levels of aspect ratio and leading edge sweep. Seven increments of sweep were used; 0°, 10°, 25°, 38°, 50°, 65°, 70°. Six distinct levels of aspect ratios were used; 1.5, 2.5, 3.75, 5.0, 7.0, 9.5, with an additional set of aspect ratios 12 wings included later. (See Figure 36.) Wing taper ratio was preset in reference to sweep angle. This was done to economize computing time. Allowing a three dimensional matrix of wings with seven levels of sweep, aspect ratio, and taper ratio would generate 343 possible combinations. It was presumed beforehand that wing sweep and aspect ratio would be the two most important parameters in the production of additional lift due to blowing. Wing sets with the same sweep angle such as B, C, D or E, F, G were all given the same taper ratio. More swept sets were given more taper. In this way the effect of aspect ratio can be seen for groups of wings with identical sweep and taper. The sweep-taper combinations were an attempt to model real aircraft planforms with a minimum of wings. This was done through the use of Figures 37 and 38 in which the taper ratios and wing sweeps of a wide range of aircraft are plotted as a function of their aspect ratios. Although the data shown represent jet aircraft ranging from fighters to subsonic transports, a fairly well defined band exists for both sweep and taper relative to

aspect ratio. This is no doubt due to structural and performance constraints. The matrix of wings A through P was laid out across these design bands as shown. As stated earlier, this matrix of wings is conducive to the study of aspect ratio effect for wings of constant sweep and taper. However, the effect of sweep on wings of constant aspect ratio such as groups C, F, I, K or D, G, L is complicated by taper variation as well as sweep variation. This problem was overcome in the following way. Two wings (G and N) were chosen for a taper variation, see Figures 39 and 40. The aspect ratio and leading edge sweep were held constant while the taper ratio was varied. This taper variation was carried out such that many of the wings had the identical taper ratios of other wings in the matrix. For example, the pairs of wings N-3, M or N-2, H both have identical aspect ratios and taper ratios and thus a sweep effect study can be made for these wings. Also the G and N series of wings were used to show the effect of taper ratios on wings with the same leading edge sweep and aspect ratio. In this way the effect of aspect ratio, taper ratio and leading edge sweep were all examined independently with all other variables held constant. All three parameters have important effects on the magnitude of the additional lift due to blowing, as will be shown.

The original matrix of wings (A through P) was enlarged with wings Q, R, S, T (see Fig. 36). The entire set can be seen in Figure 41. An additional wing V (Fig. 42) was input which exhibited a sweep angle change along its leading edge. This was done to discern whether complicated planforms such as variable sweep wings, offer any particular advantage or disadvantage in a USB application.

All of the wings used in this theoretical investigation were flat plates with no camber and no twist. All of the planforms have identical

wing areas. In this way the scale of the wings and the thrust coefficient were held constant in reference to the jet geometry. The wing area was simply rearranged around the jet by planform shape variations with no area variation.

2.4 EFFECT OF WING TAPER RATIO

The effect of wing taper ratio on the incremental lift due to blowing was investigated through the use of the N and G series of wings seen in Figures 40 and 39. The presumption that taper ratio would only have a small effect on incremental lift was totally incorrect as seen in Figure 43. The untapered N-1 configuration produces twice the incremental lift of the highly tapered N-4 configuration. Note also that the ratio of incremental lift to wing alone lift is very consistent for all configurations, with only a slight deterioration at high angles of attack. Thus this ratio of incremental/wing alone lift is independent of the angle of attack or wing lift coefficient, but strongly dependent upon the spanwise lift distribution as will be shown. The relationship between incremental lift and taper ratio is very linear for both the N and G series of wings, (see Fig. 44). It is seen in Figure 44 that for both wing sets, 100% improvement in incremental lift/wing alone lift ratio is achieved by the untapered wing as compared to a highly tapered configuration. Figure 45 shows the untapered wing to have the smallest lift curve slope and yet Figure 46 reveals that the untapered wing produces the largest increments of additional lift. Thus, the ratio of additional lift to wing alone lift is very high for the untapered wing. This is seen in the sectional data of Figure 47.

The key to why the untapered wing is such an efficient producer of additional lift is seen in Figure 48. The tapered wings are highly loaded near the wing tip where the influence of the jet is smallest. However,

the spanwise loading of the untapered wing is concentrated farther inboard where the jet influence is most powerful. Figure 47 shows that the wing-jet interaction process does not confine itself to inboard modifications of wing lift coefficient, but rather, it is distributed along the entire wing span. Figure 48 suggests that the tapered wings offer an "uphill gradient" to this process whereby the jet tries to modify already large lift coefficients near the tip where its influence is the smallest. Thus for a jet of finite strength, this is not a conducive environment for the production of additional lift. Figure 48 shows that the magnitude of the sectional lift coefficients are almost the same in the inboard third of the wings and yet Figure 47 shows the incremental lift in this same vicinity to vary widely. Because the lift of the outboard portion of the untapered wing is more easily modified by the jet, the inboard portion can be modified to a greater extent, as seen in Figure 47. This phenomena is further illustrated in Figures 49 and 50. Figure 49 compares the spanwise distributions of wing alone lift and total jet-on lift for the untapered G-2 configuration and the highly tapered planform, G-4 (refer to Fig. 39). As always, the incremental lift due to blowing is distributed along the entire wing span. Examining the outboard halves of each wing it is seen that the incremental lifts are of the same order of magnitude but the ratio of incremental to wing alone lift is not. Also the incremental lift of the untapered wing goes to zero at the tip as does the wing alone lift. It is obvious that the elliptical lift distribution of the untapered wing is more easily enhanced by the jet. The inboard lift distributions show that although the wing alone sectional lift coefficients are higher for the untapered wing, the incremental lift there is also very

much larger and thus the relative improvement is much better as shown in Figure 50.

The above discussion has revealed that the spanwise lift distribution of the wing alone plays an important role in determining the efficiency of the wing-jet interaction. Wings that are highly loaded in the near field of the jet are seen to be the best producers of additional lift. These results imply that the spanwise distribution of camber or twist could be very important in the production of additional lift due to jet blowing.

2.5 THE EFFECT OF LEADING EDGE SWEEP ANGLE

It was shown that the taper ratio of a given planform has an important effect on the additional jet-induced lift the wing is capable of producing. The sweep of the wing was also found to be important. Figure 51 compares three pairs of wings. Each wing pair have identical aspect ratios and taper ratios. It can be seen in all three instances that increased sweep of the wing has a very beneficial effect on the capability of a wing to produce additional lift with blowing. Figures such as Figure 51 can be misleading. This figure shows the ratios of the incremental lift coefficient to the wing alone lift coefficient, at an angle of attack of 20°. It is true that the more highly swept wings have a smaller lift-curve slope for the wing alone. Therefore, if two wings of different sweep were generating equal levels of incremental lift, the ratio of incremental to wing alone lift would be higher for the more swept wing because its wing alone lift coefficient would be smaller. This, however, is not the case. Figure 52 is included to show that indeed the levels of incremental lift are higher for the more swept wings. This results in the much improved ratios of incremental to wing alone lift as indicated in Figure 51.

The reader may also question the unusually high angle of attack (20^{o}) used for these calculations. Solutions were found also at angles of attack of 2 degrees and 10 degrees for all wings. As mentioned in the previous section, the ratio of incremental to wing alone lift is a constant for all angles of attack. (see Fig. 43). The theory does not account for flow separation or vortex lift effects at large angles of attack.

The sweep effect is so pronounced that even wing sets of constant aspect ratio but non-constant taper ratio can be used to show the effects of sweep. Figure 53 shows the ratio of incremental lift to wing alone lift for all of the wings at $\alpha = 20^{o}$. Referring back to Figure 32 it can be seen that all wings sets of constant aspect ratio such as C, F, I, K have increased taper with increased sweep angle. The detrimental effect of taper can be reviewed by examining the N and G series of wings in Figure 53. Wings N-1 and G-2 are untapered. Wings N-4 and G-4 are highly tapered. On the basis of taper alone one would expect wing K to be inferior to wing C, for example. This is not the case, however, the sweep effect is so powerfully beneficial that in examining wings of constant aspect ratio, (Fig. 53), it is seen that increased sweep angle still yields increased increments of additional lift. One reason this is true is because the taper variation within any aspect ratio set is not too large. For example, set C, F, I, K all have tapers ranging from 1/2 to 1/6.5. If wing K were given the large taper of wings O or P it could not be expected to remain superior to wings C, F or I. If this so-called taper effect and sweep effect are consistent and independent phenomena, one would expect a planform with a large degree of sweep and no taper to have the largest incremental lift due to blowing. Wing N-1 embodies both of these qualities

and Figure 53 reveals it to be an excellent producer of additional lift. Conversely, a wing with only small sweep and a large taper ratio would be expected to be a poor choice for lift augmentation by blowing. Wing H (Fig. 53) is such a planform and only a 6% lift gain was achieved with the upper-surface blowing of this wing. Planforms H and N-2 each have an aspect ratio of 2.5 and a taper ratio of .25. Planform H has a leading edge sweep of 25 degrees while the N-2 configuration has a 65 degree leading edge sweep. The improvement due to increased sweep can be seen in Figures 53 and 54. Figure 54 shows the additional lift due to blowing to be very uniform throughout a wide angle of attack range. Only a slight deterioration of incremental lift is evident at high angles of attack. This is the case for all of the configurations studied here. Wings L and G-3 both have an aspect ratio of 5 and a taper ratio of 1/6.5. Again the more swept wing is seen to produce the higher levels of incremental lift, (see Fig. 54). Figure 54 shows this lift augmentation to be invarient throughout a wide range of angles of attack.

The question arises as to why the lift of a highly swept wing would be influenced to a greater extent by an upper-surface blowing jet. A clue is found in comparing the spanwise lift distributions of planforms H and N-2 (see Fig. 56,57). The planforms being identical except for sweep angle have similar spanwise lift distributions with no blowing. However, with blowing the highly swept N-2 configuration shows an incremental lift distribution which increases from root to tip, with the largest gains being made in the mid-span region. The incremental lift of wing H starts at the root chord with roughly the same magnitude as N-2 but from there deteriorates in the outboard regions of the wing. This is seen

more clearly in Figure 58 where the ratio of incremental lift to wing alone lift is plotted for both wings, along the span. It can be seen from this figure that the ratio of incremental lift to wing alone lift is the same for both wings near the root section but the swept wing produces more lift in the outboard areas of the wing. Comparing the geometry of the two planforms relative to the jet exit and the jet itself, (Figure 32) several things can be observed. If the N-2 wing is sliced streamwise into many strips, each strip is increasingly farther downstream from the jet exit in comparison to its equivalent strip on the H planform. Evidently the jet, which is emanating at the leading edge, can effect larger disturbances on wing panels which are farther downstream of the jet exit. This would explain the increased lift augmentation of the outboard portion of the highly swept wing. Also the outboard portion of the swept N-2 wing is geometrically closer to the trailing jet section. This can be seen in Figure 32 by connecting two imaginary lines from the tip chords of wing H and N to the trailing jet section. In fact, much of the outboard portion of N-2 is actually downstream of the frontal boundary of the trailing jet section. The entire planform H lies upstream of this boundary. More interaction could exist between the swept wing and the trailing jet vortices by virtue of their close proximity.

The same situation is seen to exist for the two equivalent wings G-3 and L; see Fig. 59. Figure 59 clearly depicts the spanwise incremental lift distribution that is typical of all the wings tested in this USB investigation. There are three distinct zones along the span. A large "bubble" of incremental lift is generated by the portion of the wing which is being blown by the jet. The magnitude of this "bubble" determines

the incremental lift that will be generated outboard of the jet section. The incremental lift deteriorates at the same rate (Fig. 59) from the level at the jet section, for all wings. If the incremental lift is large in the blown region of the wing, it will carry over all the way toward the wing tip. In other words, the incremental lift deterioration never exhibits drastic changes from regions of peak lift but rather always deteriorates in the same gradual fashion (see Fig. 59). Between the blown portion of the wing and the outboard deterioration zone a sharp peak of incremental lift is produced. This peak is due to the side surface of the equivalent rectangular USB jet used in the computations.[10]

A conveniently simple parameter was found to account for the sweep effect upon wings of equal aspect ratio. A polar plot was created as shown in Figure 60. A single point was plotted for each wing. The radial coordinate was the ratio of incremental lift to wing alone lift produced by the wing in question at α = 20 degrees. The angular coordinate of each wing point was simply the sweep angle of the leading edge. This was done to produce a sort of contour map with which the efficiency of unswept wings could be compared to that of swept wings. All wings with equal aspect ratios were connected by the curves shown. If, for example, the sweep of the wings was irrelevant and all wings of common aspect ratio developed the same ratio of incremental lift, then these curves would be concentric, like the rings of a tree stump. However, a much more interesting result was found. Although the curves represent wings with taper variation as well as sweep variation; wings which share only a common aspect ratio, all of the curves are very linear and all parallel to the chord or stream direction. The lines connecting H to N-2 and M to N-3

are special cases with no taper variation amongst the pairs, and the lines are seen to be very close to parallel with the center line. With the aid of Figure 61 it can be seen that the data of Figure 60 is implicating that the parameter, $(\Delta C_L/C_{LW})\cos\Lambda_{LE}$, is a constant for any group of wings with a common aspect ratio and taper ratios which are close or equal.* Plotting this parameter as a function of wing aspect ratio results in a condensation of the scattered data of Figure 53 into a single curve or band of data; see Fig. 62. This parameter does nothing to constrict the scatter due to taper effect seen in Figure 53 for the N and G series of wings. This problem will be discussed later.

2.6 THE EFFECT OF WING ASPECT RATIO

There are five sets of wing planforms within the matrix that share a common taper ratio and leading edge sweep angle. No two sets have the same sweep or taper ratio (Fig. 32). The effect of increasing aspect ratio on each of these five wings sets can be seen by following the five curves in Figures 53 and 63. Each plot shows the ratio of incremental lift to wing alone lift at angles of attack of 20 degrees and 10 degrees respectively. An aspect ratio variation from 2.5 to 12.0 has a very small effect on four of the five wing groups. The only exception is the most highly swept group O, N, T. This group shows a marked improvement between wing O of aspect ratio 1.5 and wing N with an aspect ratio of 2.5. This is the only wing group with a constituent wing of aspect ratio 1.5. If the other wing groups had been extended to such a low aspect ratio they would probably also show the same deterioration of incremental lift. The ratio of incremental lift to wing alone lift is fairly stable for wings of

*This data applies only to flat plate planforms with no camber or twist.

aspect ratio 5 or larger. The level of additional lift produced by each wing group is mainly a function of the group's sweep angle and also the taper ratio. Below an aspect ratio of 5 the level of lift augmentation begins to drop off. This is an unexpected result when one considers the fact that as aspect ratio is decreased, the ratio of jet span to wing span increases. The entire inboard halves of wings O and P are blown by the jet while the jet span represents only 18 percent of the wing span of wings Q, R, S with aspect ratios of 12.

Figure 64 shows the spanwise distribution of wing alone lift for the wing set O, N, T. All three wings have a taper ratio of 1/9.214 and a leading edge sweep of 65 degrees. All three wings generate similar lift distributions, (see Fig. 64), with high loading of the wing tips. Figure 65 shows the spanwise distribution of the incremental lift/wing alone lift ratio for wings O, N, T. As mentioned previously in the section on sweep effects, it can be seen that the incremental lift extends over the entire span. The relative level of incremental lift always deteriorates to a small level at the wing tips and this deterioration takes place at a gradual rate for all three wings. Comparing wings O and T in Figure 65 it is seen that planform T is able to generate very large increments of additional lift inboard because this planform has a large unblown portion of its span along which this large lift increment may decay. Wing O, however, has a much smaller portion of wing span along which this gradual decay can take place and thus the level of incremental lift inboard is limited. This trend is again illustrated in Figure 66 which shows the ratio of incremental lift to wing alone lift, as it is distributed along the spans of wings E, F, G, H. All four wings exhibit the same trend of

deterioration of incremental lift outboard of the jet span. The more span that is available for this deterioration, the higher the level of incremental lift from which this decay begins.

Although Figure 63 shows that the wings of a given set generate almost constant ratios of incremental lift to wing alone lift, this result is deceiving. Each incremental increase in aspect ratio within a given set of wings causes a proportionate increase in the lift-curve slope as seen in Figure 67. An equivalent increase in incremental lift occurs also, as seen in Figure 68, and thus the ratio of incremental and wing alone lift remain constant. This is the case with all of the wing sets as shown in Figures 69 through 72. Figure 73 compares the relative levels of lift with the jet on and for the wing alone. Note the large gains of incremental lift for aspect ratio increases from 1.5 to 5 and the rather gradual increases from 5 to 12. Note also amongst wings of aspect ratio 5 that the highly swept wing T can produce the largest increments of additional lift while operating at the smallest lift coefficient. Figure 73 also shows clearly that wings which have the largest ratio of jet span to wing span, such as wings O, N, M do not necessarily produce the largest increments of additional lift due to blowing. In fact, a specific portion of unblown span seems to be needed for decay of the large increments of lift generated under the jet. For this jet, the aspect ratio 5 wings seem to have the optimum level of unblown span. This gives a jet span to wing span ratio of .28.

2.7 SUPPLEMENTAL RESULTS

The original intent of this investigation was to find some wing parameters with which the incremental lift, caused by an USB jet, could

be predicted for any general planform. Once accomplished, a series of design curves could be found for jets of varying size and power.

The incremental lift developed by an upper surface blowing jet is primarily due to the interaction between the jet and the wing. This is referred to here as the interaction effect. This is not the case with over-wing blowing configurations where most of the jet induced lift can be attributed to the entrainment effect. The blowing jet has the tendency to entrain or suck external flow into its own flow thereby creating upwash on the wing and additional lift. The entrainment effect is very small for USB configurations because of the shielding effect of the wing when directly below the jet. Thus, for USB configurations the ratio of incremental lift to wing alone lift is a measure of the efficiency with which the wing and jet interact. A wing-jet combination which exhibits a great deal of interaction is an efficient producer of additional lift.

The relative efficiencies of all the wings investigated can be seen in Figures 53 and 63. Highly tapered wings were shown to be very inefficient producers of additional lift compared to similar but untapered wings. Increased sweep angle was found to have a very beneficial effect on a wing's ability to produce additional lift. The efficiencies of wings with widely varying sweep angles were reduced to a single curve in Figure 62 by use of the multiplying factor ($\cos\Lambda_{LE}$). This does little to account for the taper effect as seen in Figure 74 where the scatter due to taper variations of the N and G series of wings is evident. However, a relatively narrow band encompasses most of the wings. Only wings with extreme taper ratios of .0278 and wings with no taper at all lie outside this band, see Figure 63. Note also in Figure 63 the stability of the

data over a very wide range of aspect ratios. For this particular jet geometry, the incremental lift begins to diminish for planforms with aspect ratios less than 5.0.

Figure 75 shows the ratio of incremental lift to wing alone lift as a function of each wing's taper ratio. The two curves seen in Figure 75 reflect the effects of taper variations on the N and G series of wings. Note the linear increase in incremental lift with decreasing taper ratio. This linear relationship between taper ratio and the efficiency of incremental lift production can be seen also in Figure 76. In Figure 76 the multiplying factor ($\cos\Lambda_{LE}$) was applied to the data which resulted in some shrinking of the data scatter. This occurs because all of the highly tapered wings also have large leading edge sweep angles and the cosine of these angles is smaller than one. This causes a magnitude reduction for the data plotted and shrinkage of the range of scatter. A simple multiplying factor was desired such as ($\cos\Lambda_{LE}$) which could normalize the taper ratio effect and reduce the slope of the linear curves seen in Figures 75 and 76 to zero. For this purpose Figure 77 was constructed. In Figure 77 the incremental lift efficiency of each tapered N and G wing was normalized with the efficiency of the untapered wings, and plotted as a function of taper ratio. Both curves show the highly tapered planforms to be only about 50 percent as effective at producing additional lift compared with the untapered wings. Figure 77 shows that the curves for the cube root and fourth root of the taper ratio to follow closely the efficiency ratio curves. Possibly these parameters could be used as multiplying factors to cancel variations due to taper effect. The inverse relationship is seen in Figure 78. Note also in both Figures 77 and 78 the divergence

of the root curves from the wing curves at large taper ratios. The fourth root of the taper ratio was chosen as a multiplying factor because of its smaller divergence at large taper ratios. This multiplying factor was applied to the data of Figure 74 in hopes of reducing the data spread due to taper variations. The result seen in Figure 79 shows the scatter of data for the N and G wing sets to have been reduced, but the scatter amongst the other wings was increased. The problem of predicting taper ratio effects remains unresolved.

Probably the most straightforward approach to predicting lift increments due to blowing is to examine the effect blowing has upon the lift-curve slope of a wing. It has been shown that the incremental lift coefficient due to blowing is a constant fraction of the lift coefficient produced by the wing alone. A simpler way of stating this is that the net effect of the jet is to increase the lift-curve slope of a wing. This point is illustrated in Figure 80, which shows the effect of the USB jet upon the three untapered wings A, G-2 and N-1. In all cases the lift curve slope was increased to a higher but constant level. Note in Figure 80 that the jet exerts a smaller and smaller influence upon the lift-curve slope of a wing as the magnitude of that slope increases for the wing alone. This trend can be seen also in Figure 81 where it becomes evident that there is more potential for lift augmentation of wings with small lift-curve slopes. The boundary lines drawn in Figure 81 indicate that a jet of finite strength can exert only a minimum effect upon an infinite aspect ratio wing, (2-D wing). The scatter band for the data of Figure 81 can be reduced greatly by using the multiplying factor, $(\cos\Lambda_{LE})$, previously used in Figures 62 and 74, (see Fig. 82). Most of the data points fit

along a single line curve. An upper bound on the incremental lift ratio is created by the untapered wings. The wings with the most extreme taper represent a lower bound for the ratio of additional lift/wing along lift. Most of the wings fit along a linear curve with zero slope. This allows the incremental lift of a wide range of aircraft to be predicted for this jet thrust coefficient. A family of curves such as Figure 82 would facilitate incremental lift predictions at any power setting.

EXAMPLE: (See Fig. 82)

For this jet geometry and this power setting ($C_u = 2.0$)

$$\frac{\Delta C_L}{C_{L_W}} \cos\Lambda_{LE} = f(C_{L_\alpha})$$

for $C_{L_\alpha} \geq 2.6$:

$$\frac{\Delta C_L}{C_{L_W}} = \frac{.076}{\cos\Lambda_{LE}} = .076\ (\sec\Lambda_{LE})$$

$$\Delta C_L = .076(C_{L_W})(\sec\Lambda_{LE})$$

Note: only accurate for ($.1 < \lambda < .75$)

Figure 82 has shown that the planforms with the greatest potential for lift augmentation by upper-surface blowing are highly swept untapered planforms. Upper-surface blowing could be used to enlarge the flight envelope of high speed aircraft and improve their maneuverability. The untapered N-1 configuration with a 65 degree sweep angle showed a 24 percent increase in lift-curve slope due to interaction with the USB jet. This is accomplished without the use of flaps. Upper-surface blowing could represent an alternative to variable sweep concepts with their inherent weight

penalties and structural complications. By use of controlled vortex lift, upper-surface blowing, or spanwise blowing[13] or combination thereof, the low speed performance of planforms with high sweep angles can be improved greatly.

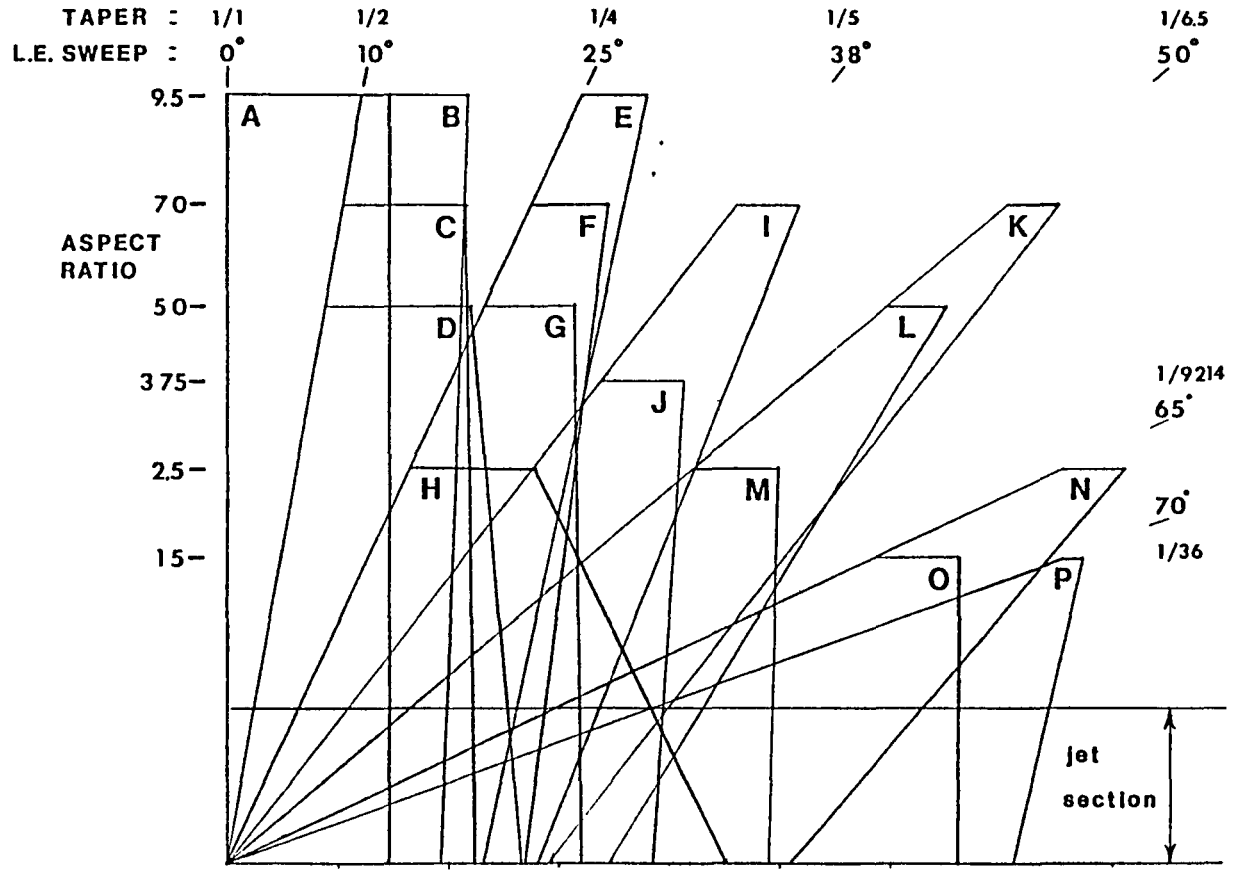

Figure 32. Original matrix of wing planforms A through P All wings are flat plates with no camber or twist.

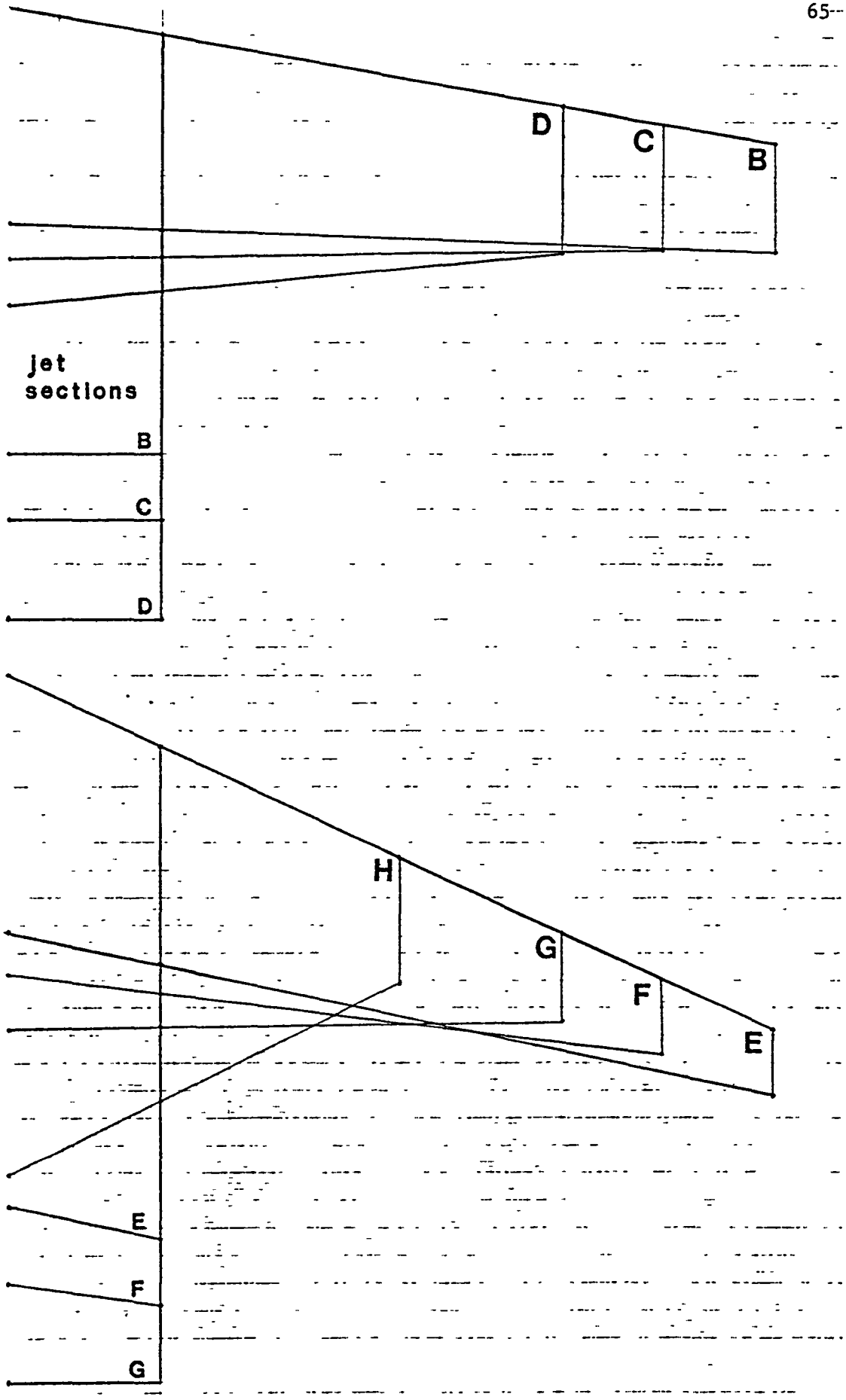

Figure 33. Wing set B, C, D, $\Lambda_{LE} = 10^{\circ}$, $\lambda = .5$. Wing set E, F, G, H, $\Lambda_{LE} = 25^{\circ}$, $\lambda = .25$.

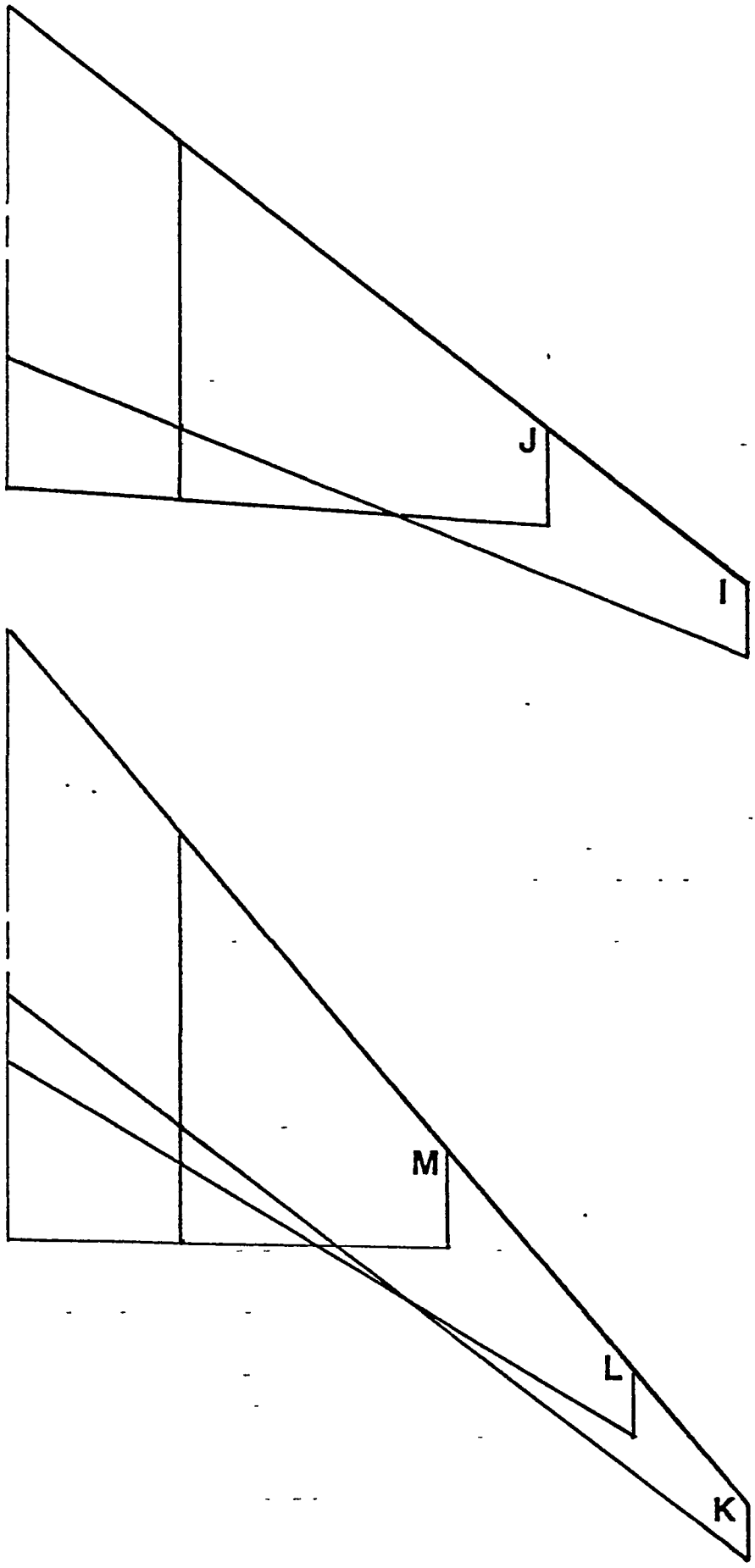

Figure 34. Wing set I, J, $\Lambda_{LE} = 38^{\circ}$, $\lambda = .20$. Wing set K, L, M, $\Lambda_{LE} = 50^{\circ}$, $\lambda = 1/6.5$.

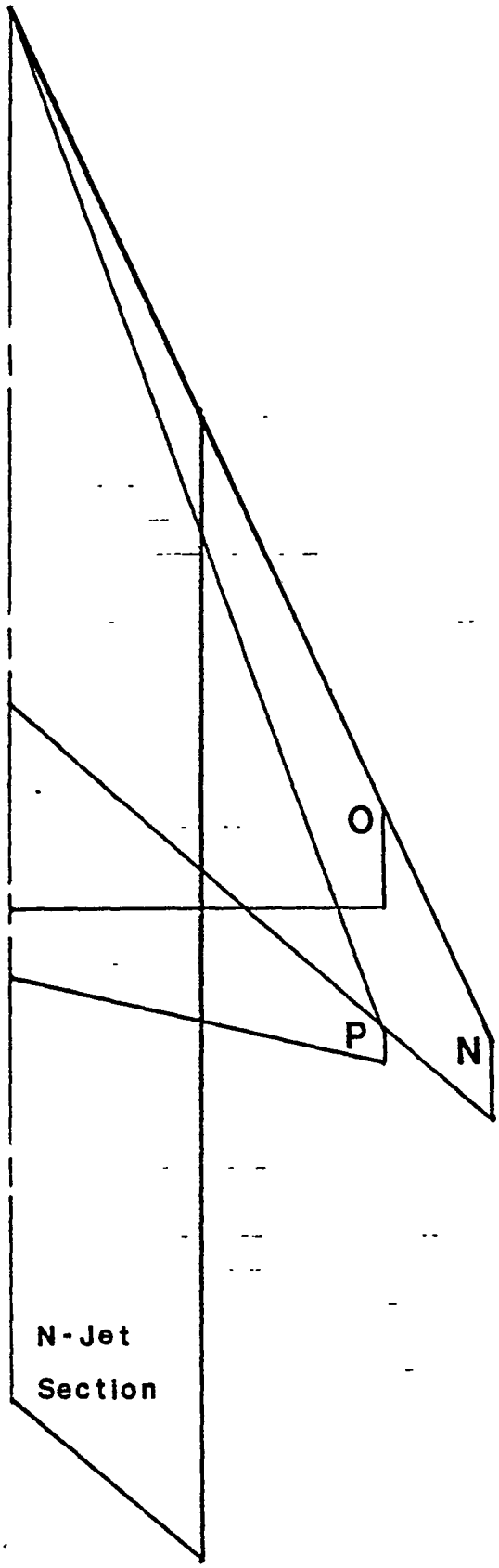

Figure 35. Wing set N, O, $\Lambda_{LE} = 65^{\circ}$, $\lambda = 1/9.214$. Wing P, $\Lambda_{LE} = 70^{\circ}$, $\lambda = 1/36$.

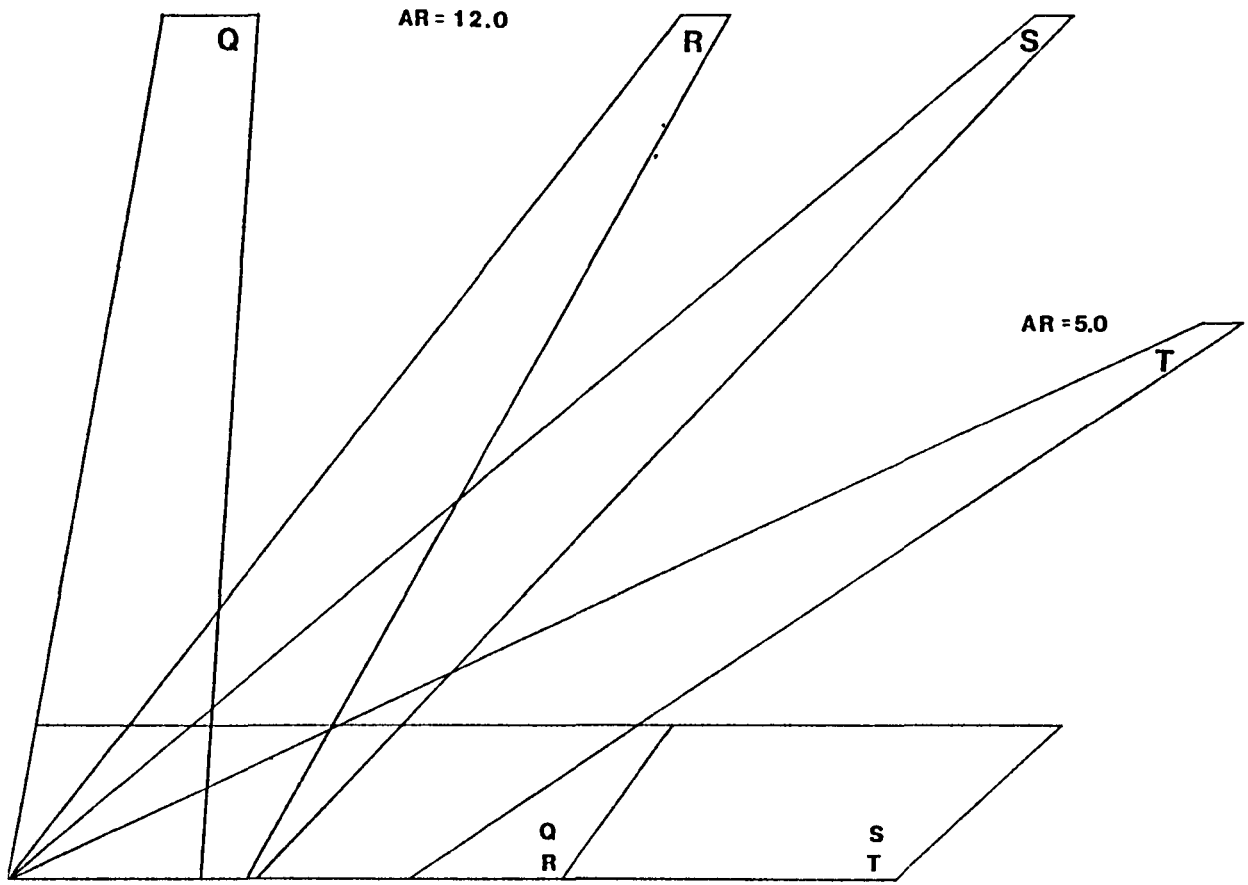

Figure 36. Additional wings Q, R, S, T. Wing Q, $\Lambda_{LE} = 10$, $\lambda = .5$. Wing R, $\Lambda_{LE} = 38^{o}$, $\lambda = .20$. Wing S, $\Lambda_{LE} = 50^{o}$, $\lambda = 1/6.5$. Wing T, $\Lambda_{LE} = 65^{o}$, $\lambda = 1/9.214$.

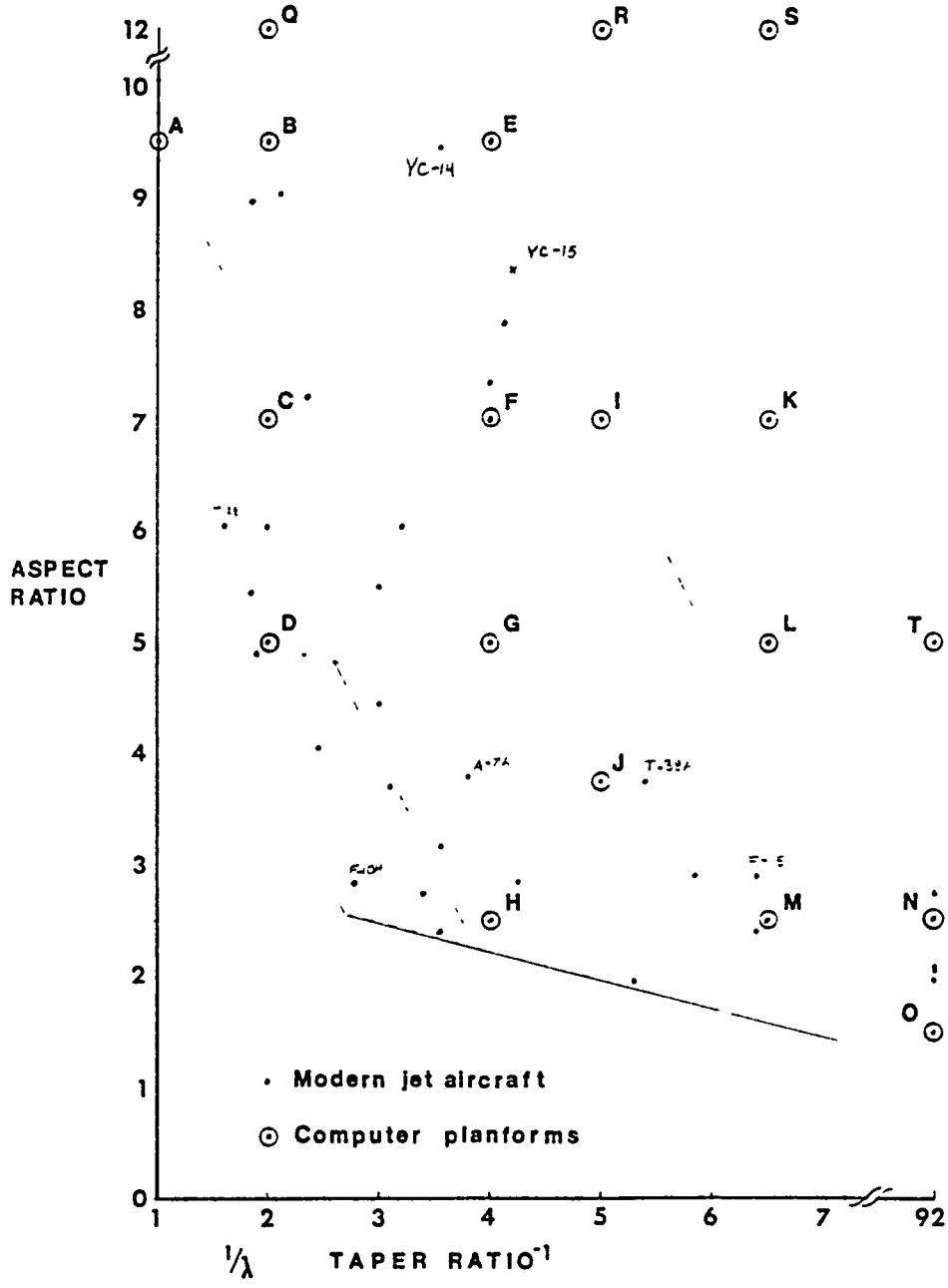

Figure 37. Plot of the aspect ratio, taper ratio combinations for a wide range of modern jet aircraft. Combinations used for computed planforms also shown.

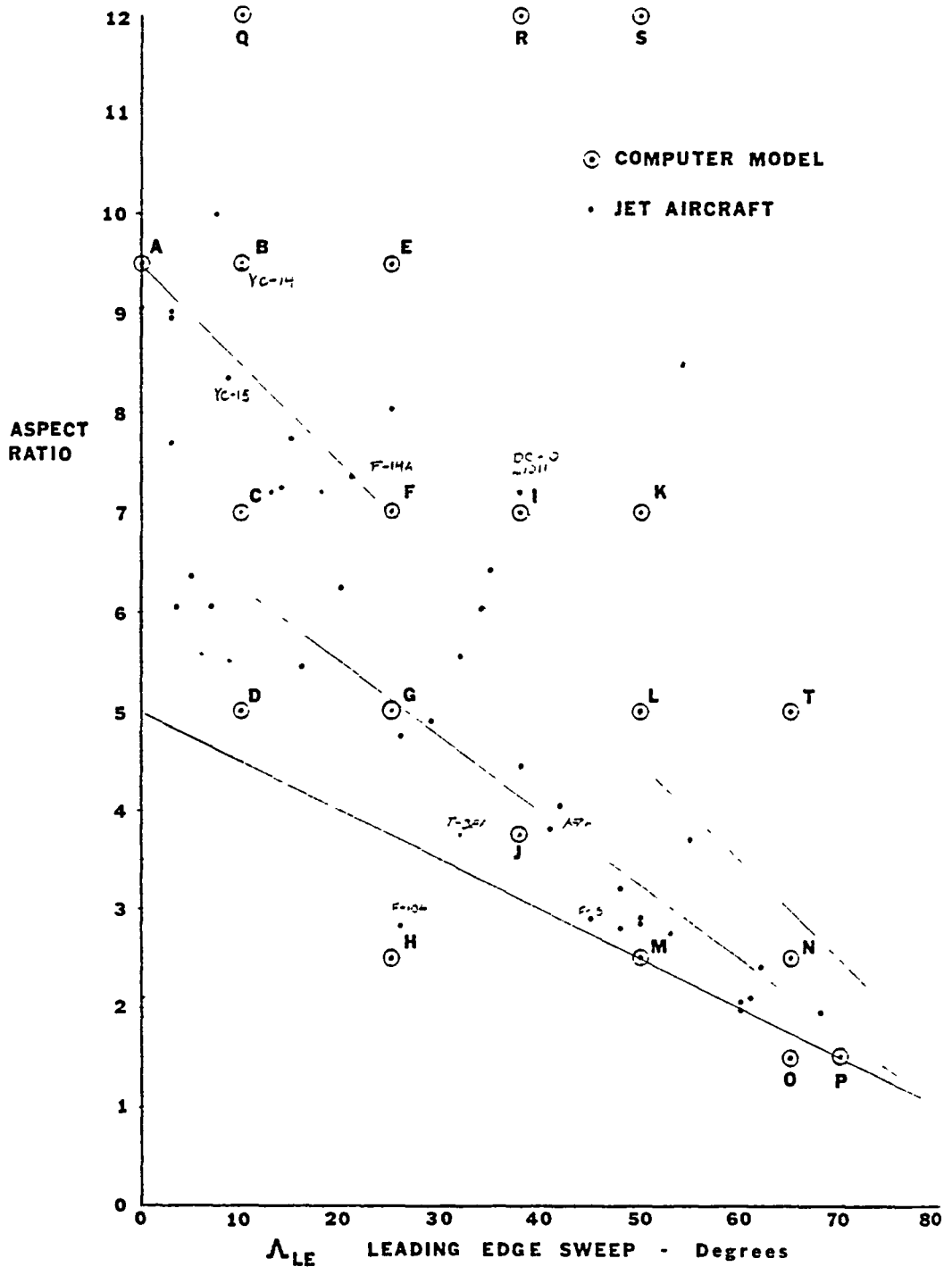

Figure 38. Plot of the aspect ratio, leading edge sweep angle combinations found for a wide range of jet aircraft. Combinations used for computed planforms also shown.

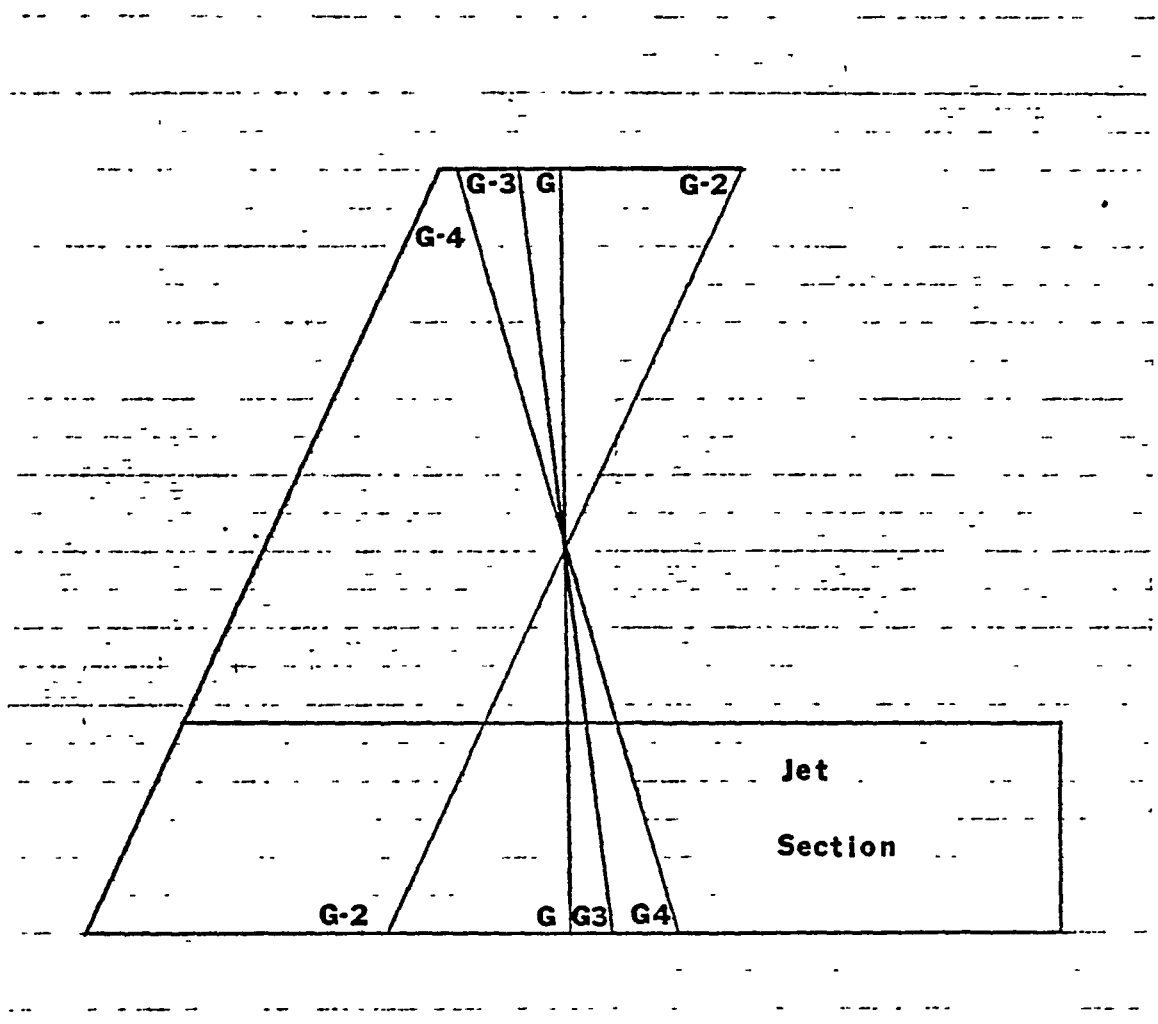

Figure 39. G-series of wing planforms. $\Lambda_{LE} = 25^{\circ}$, AR = 5.0. Taper ratios: G-4 $\lambda = 1/36$, G-3 $\lambda = 1/6.5$, G $\lambda = 1/4$, G-2 $\lambda = 1.0$.

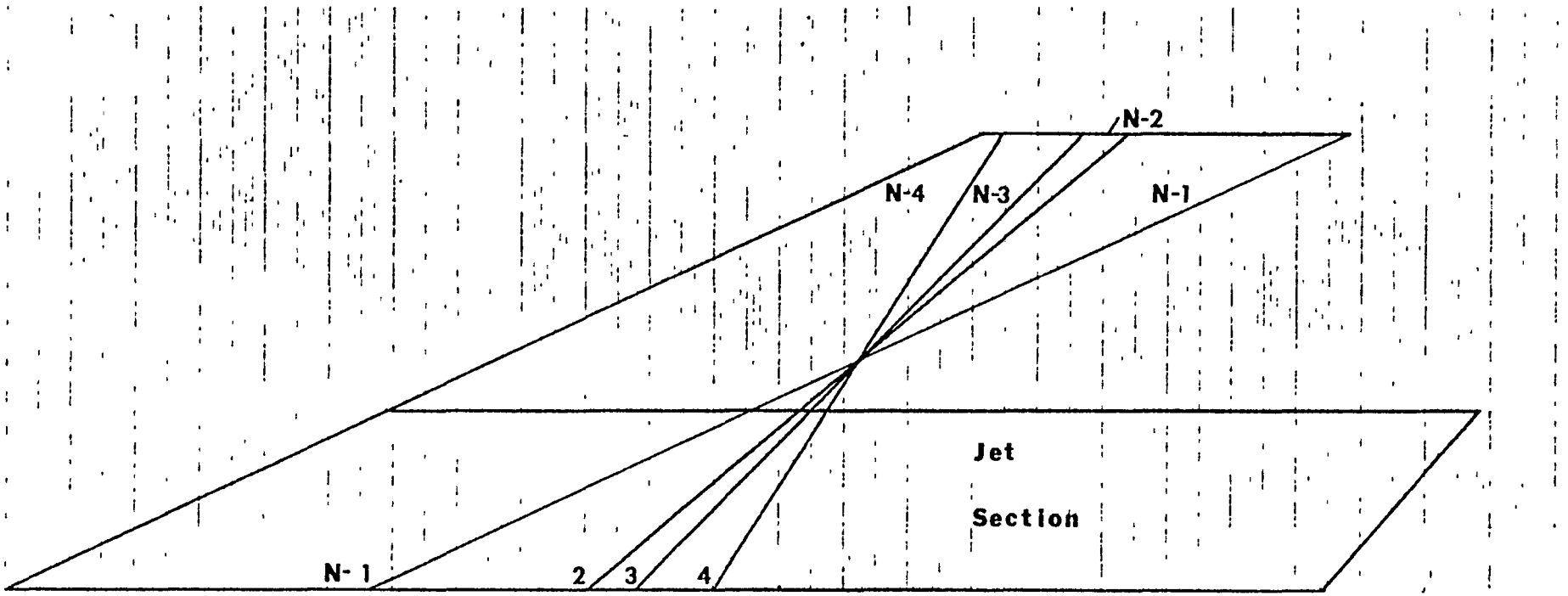

Figure 40. N-series of wing planforms $\Lambda_{LE} = 65^{o}$, AR = 2.5. Taper ratios: N-4 λ = 1/36, N-3 λ = 1/6.5, N-2 λ = 1/4, N-1 λ = 1.0. Wing N not shown, λ = 1/9.214.

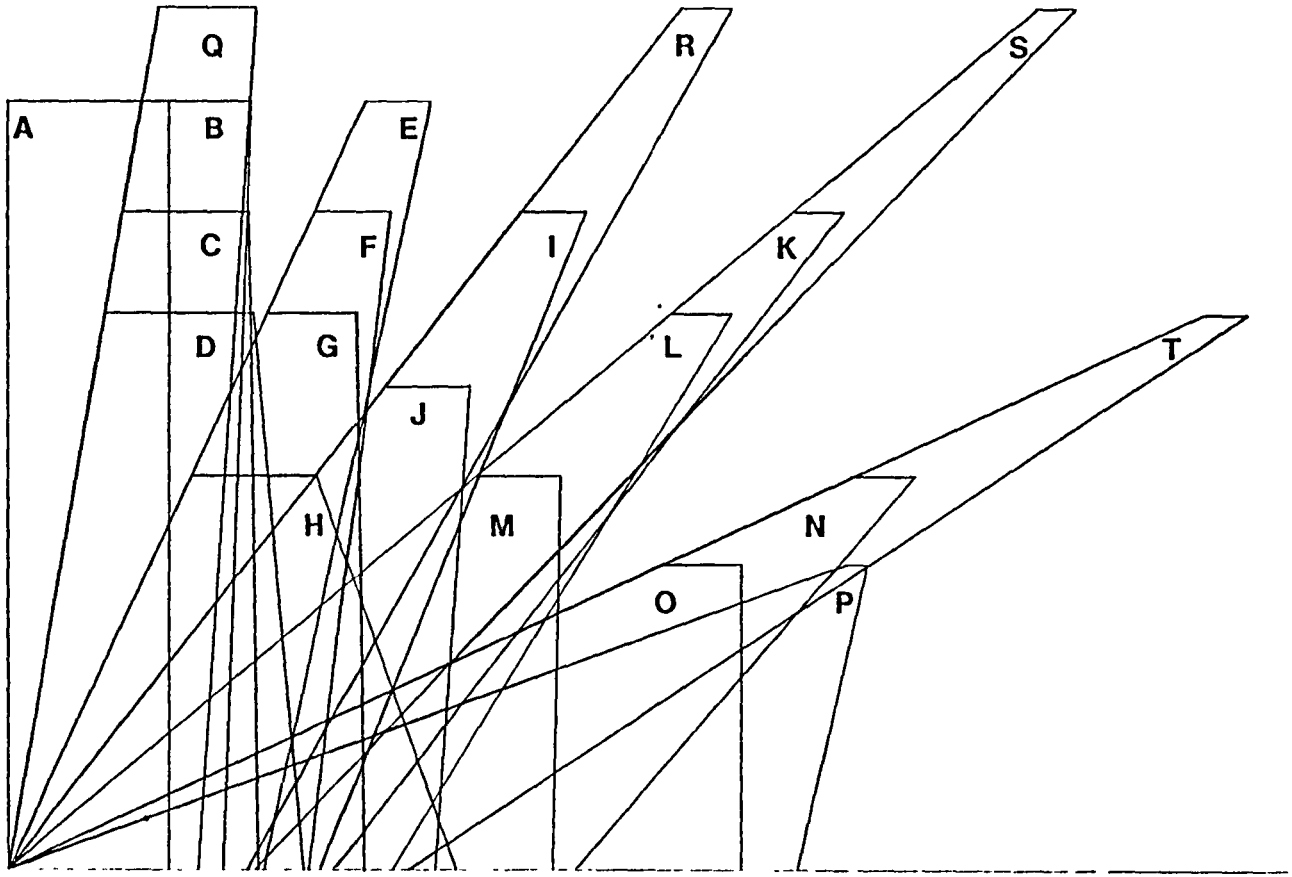

Figure 41. Complete matrix of wing planforms A through T aspect ratios: (O,P): 1.5, (H,M,N): 2.5, (J): 3.75, (D,G,L,T): 5.0, (C,F,I,K): 7.0, (A,B,E,): 9.0, (Q,R,S): 12.0.

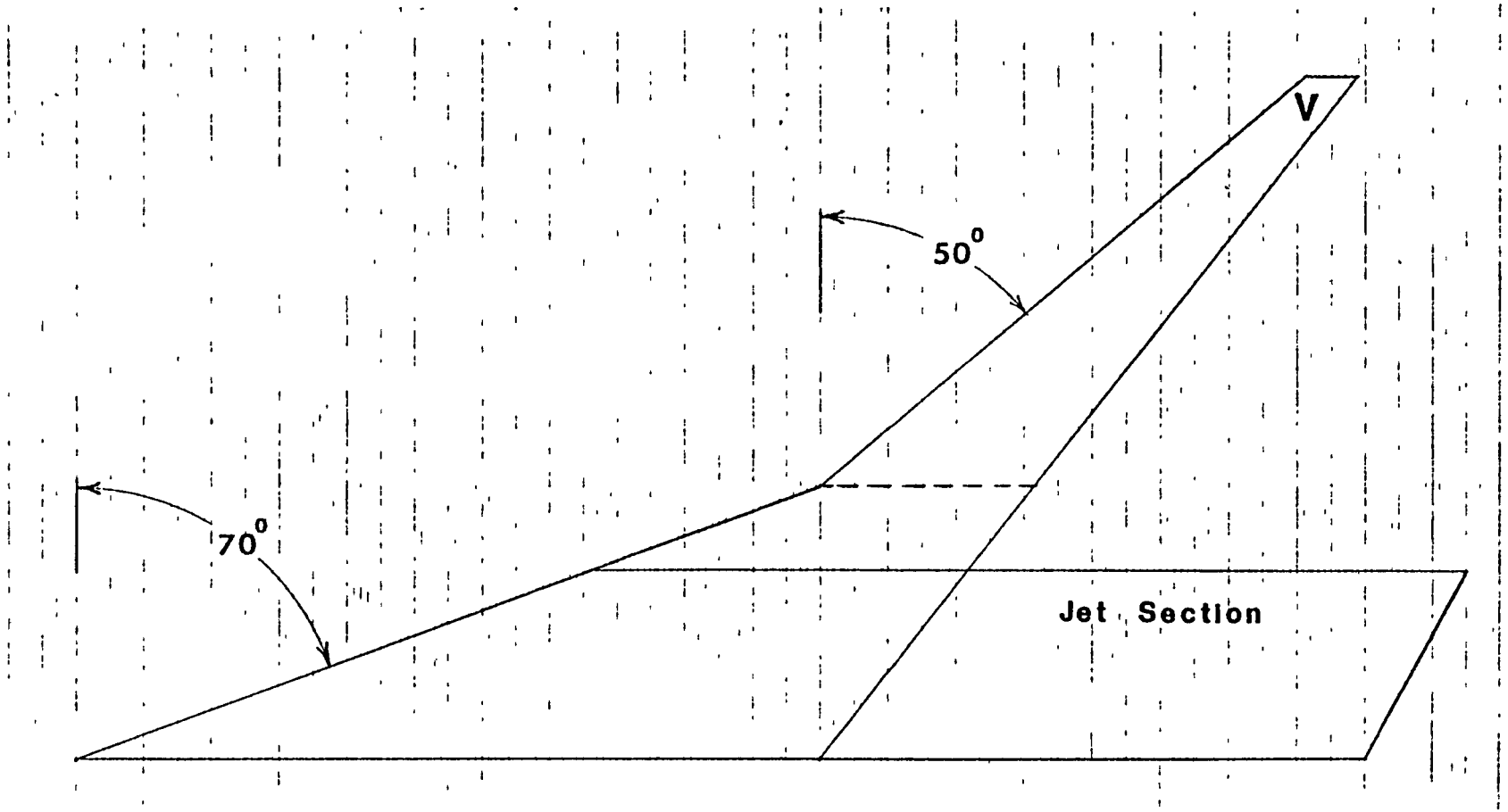

Figure 42. Wing V, AR = 5.0, λ = 1/15. $\Lambda_{LE} = 70^{o}$ inboard, $\Lambda_{LE} = 50^{o}$ outboard.

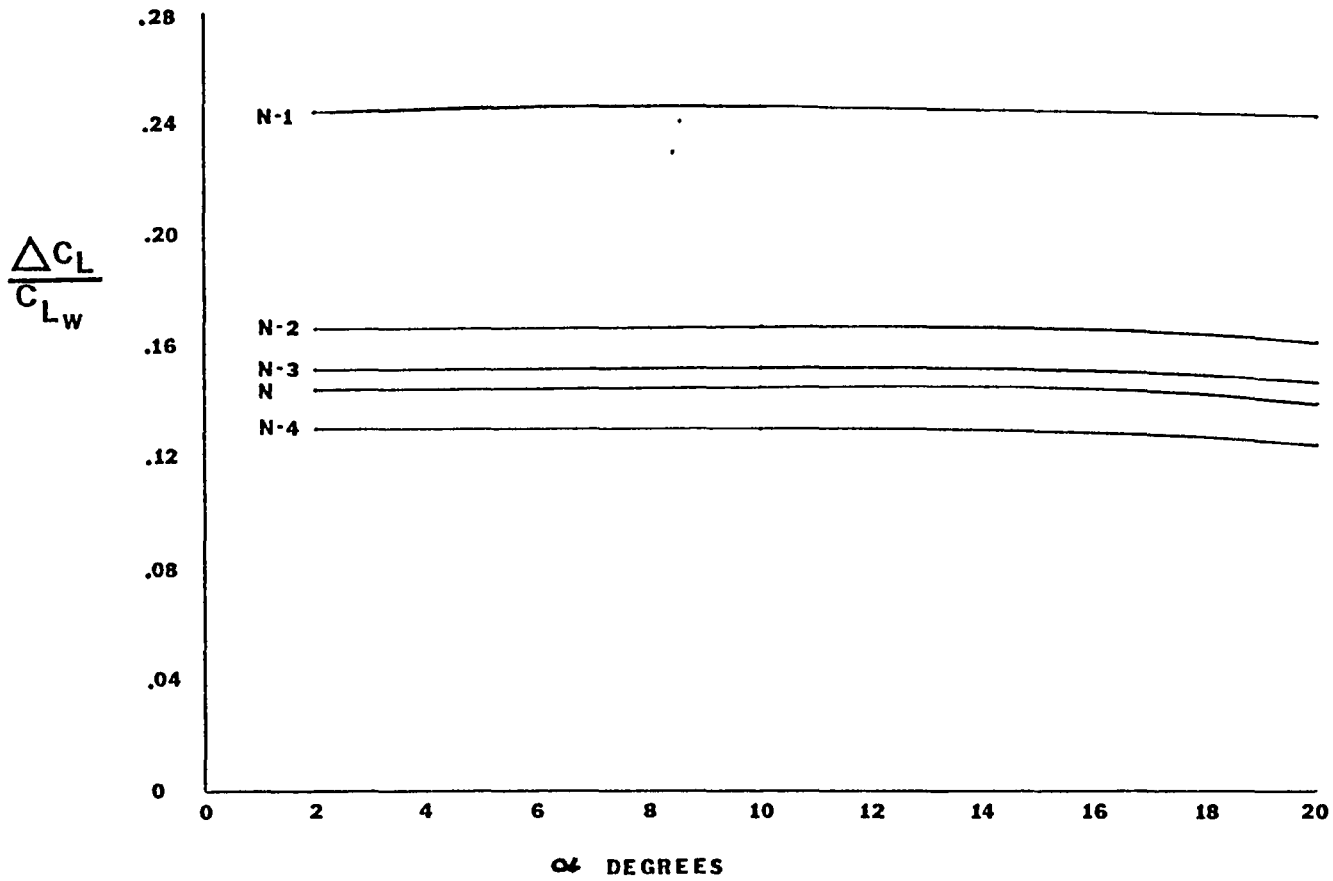

Figure 43. The effect of wing taper ratio on incremental lift production over a wide range of angles of attack.

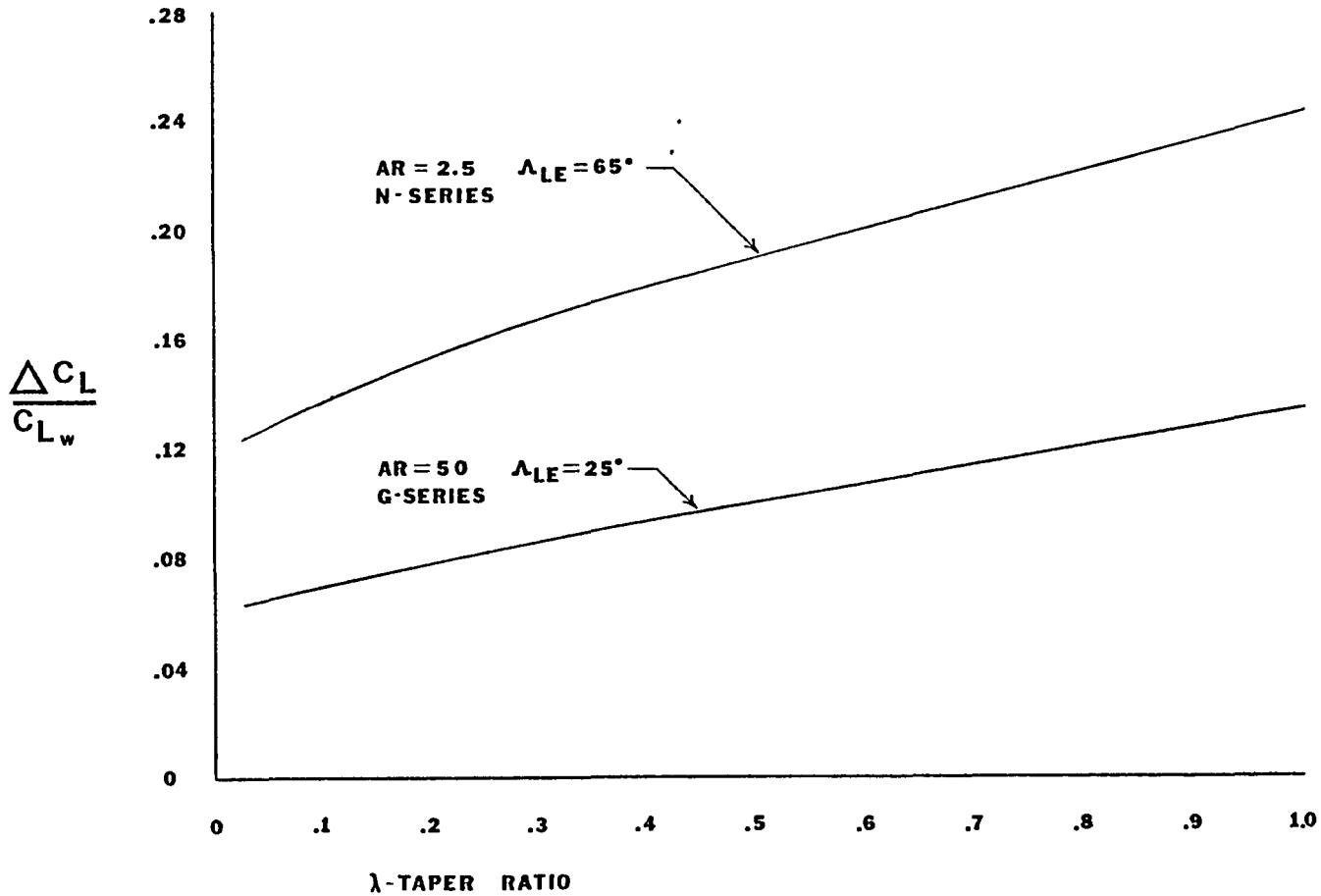

Figure 44. Effect of wing taper on the ratio of incremental/wing alone lift coefficients at $\alpha = 20^{o}$.

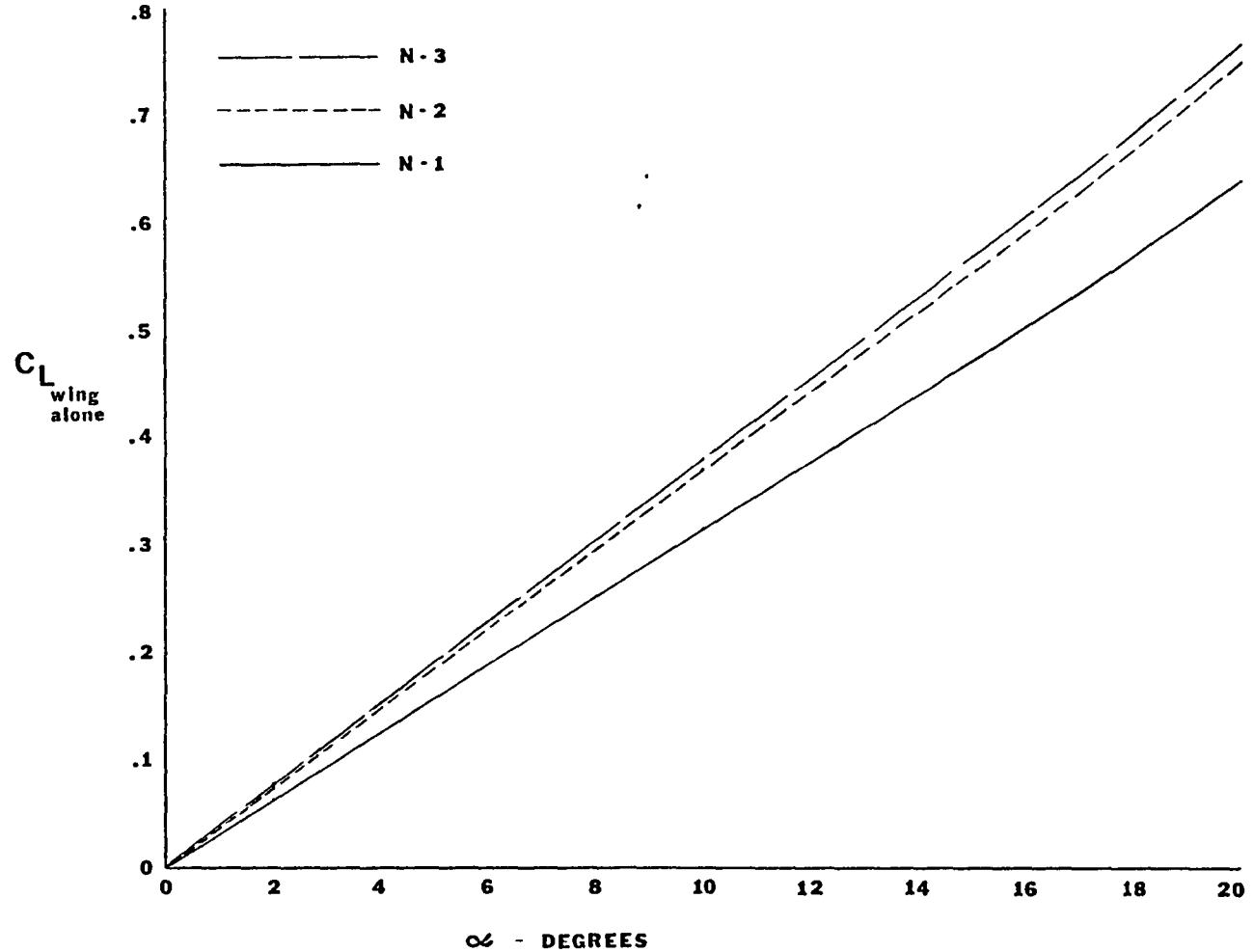

Figure 45. Effect of wing taper on wing lift-curve slopes with no blowing. Taper ratios: N-1 λ = 1.0, N-2 λ = 1/4, N-3 λ = 1/6.5.

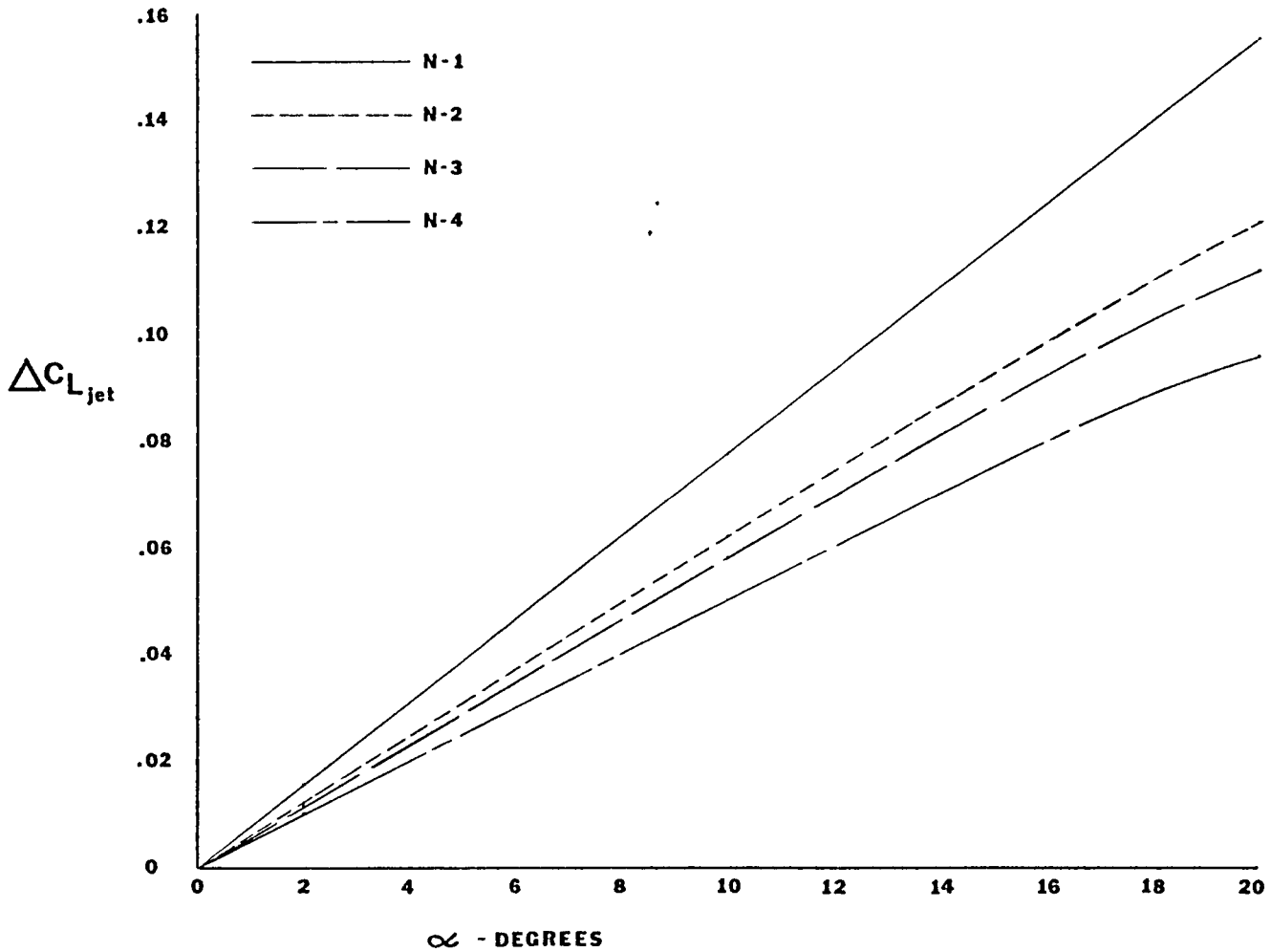

Figure 46. Effect of wing taper on incremental lift coefficients. Taper ratios. N-1 λ = 1 0, N-2 λ =1/4, N-3 λ = 1/6.5, N-4 λ = 1/36.

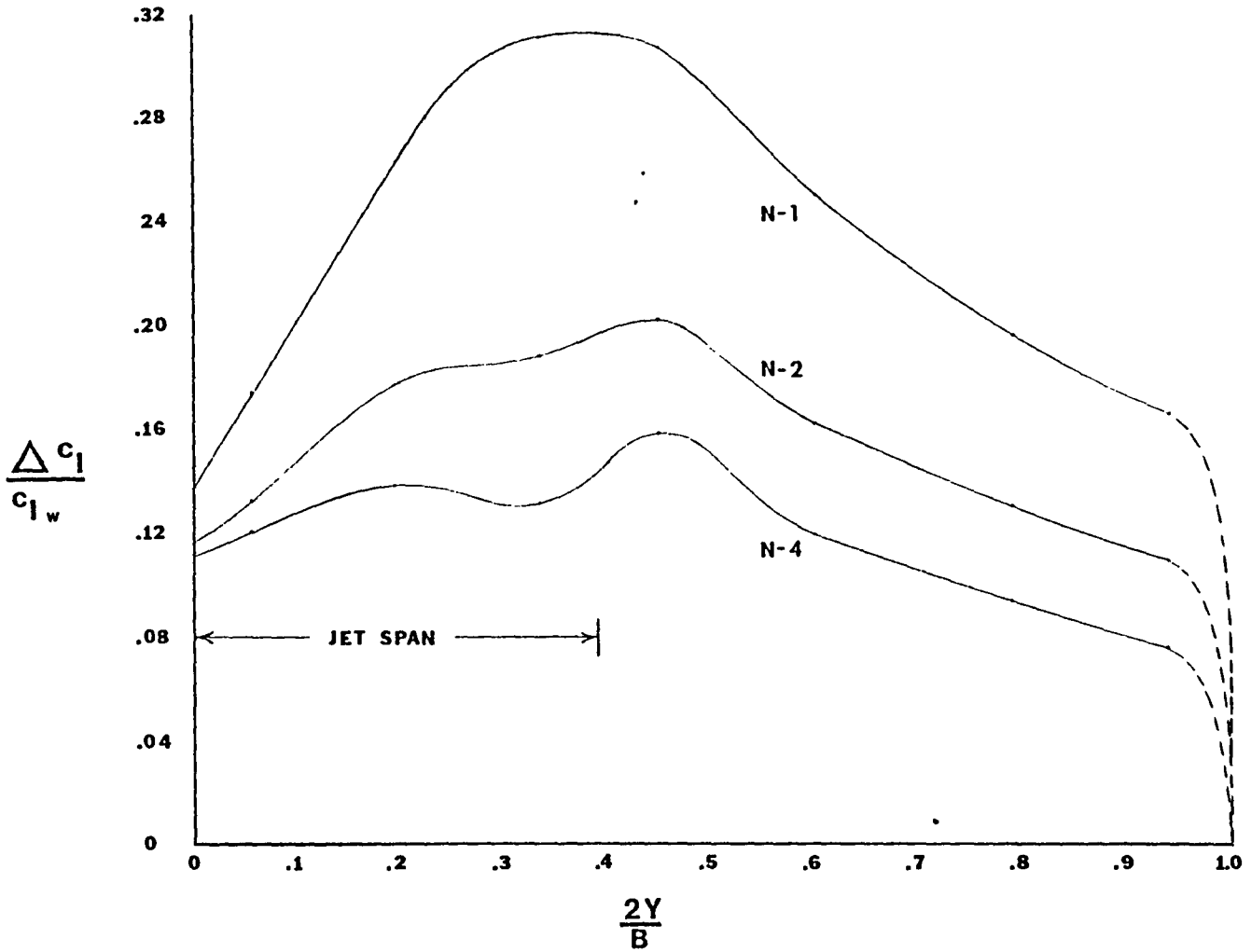

Figure 47 Effect of wing taper ratio on the spanwise distribution of incremental lift coefficient, normalized with wing alone lift coefficients, $\alpha = 20^0$.

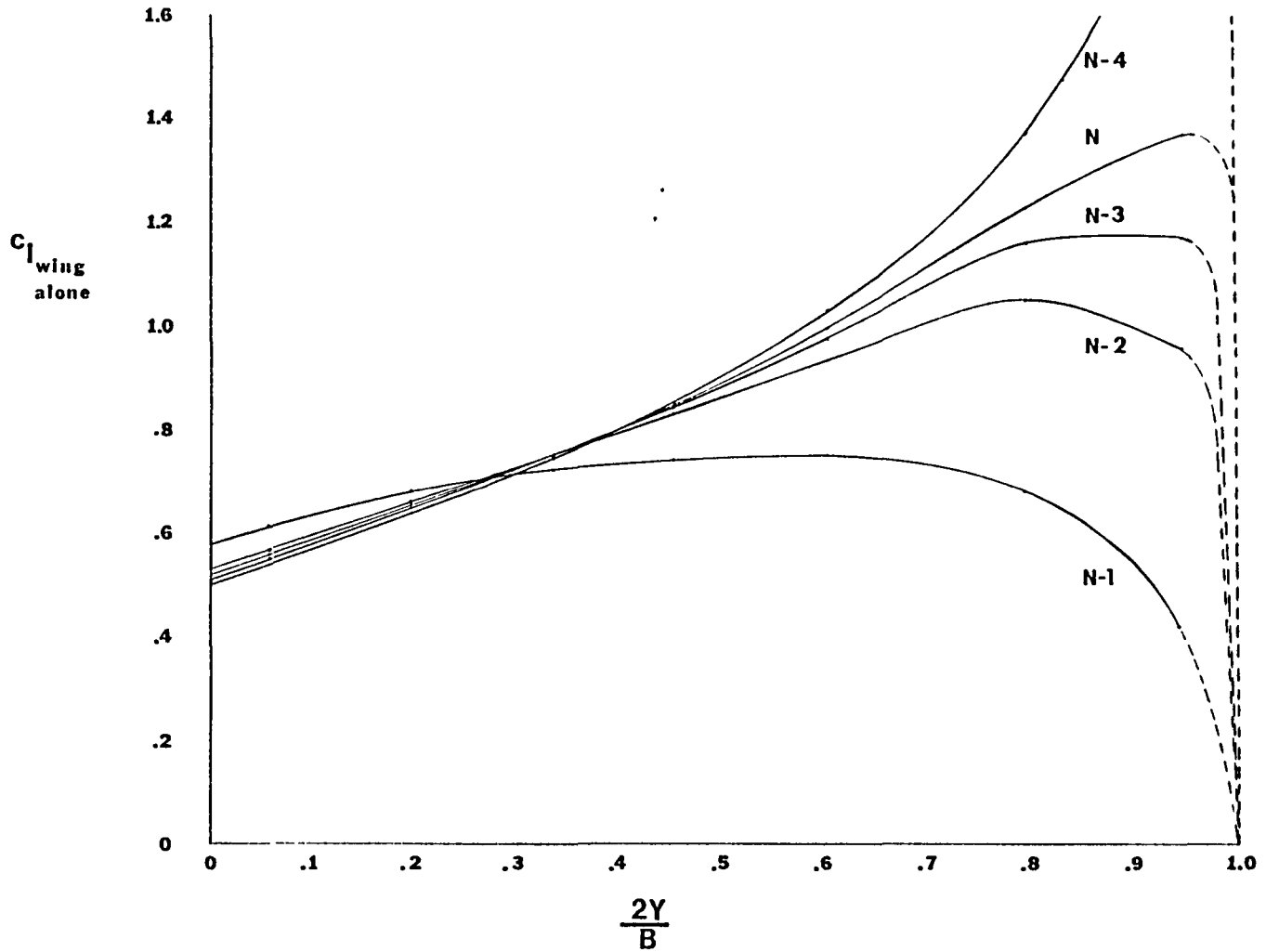

Figure 48. Effect of wing taper ratio on the spanwise distribution of lift coefficient with no blowing. $\alpha = 20^{0}$.

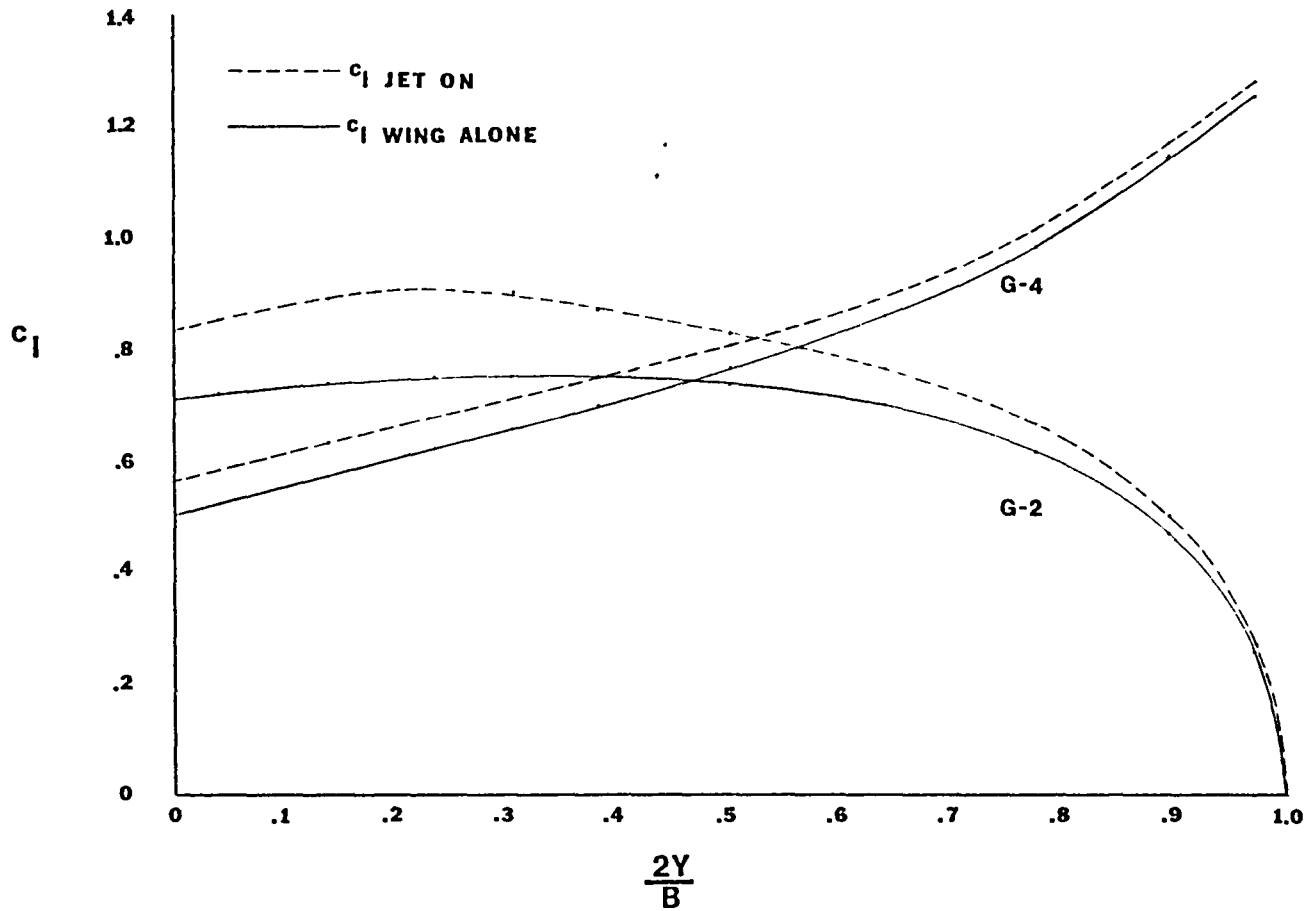

Figure 49. Comparison of the effects of a USB jet on the spanwise lift distributions of a tapered and untapered wing. $\alpha = 10^0$, G-2 $\lambda = 1.0$, G-4 $\lambda = 1/36$.

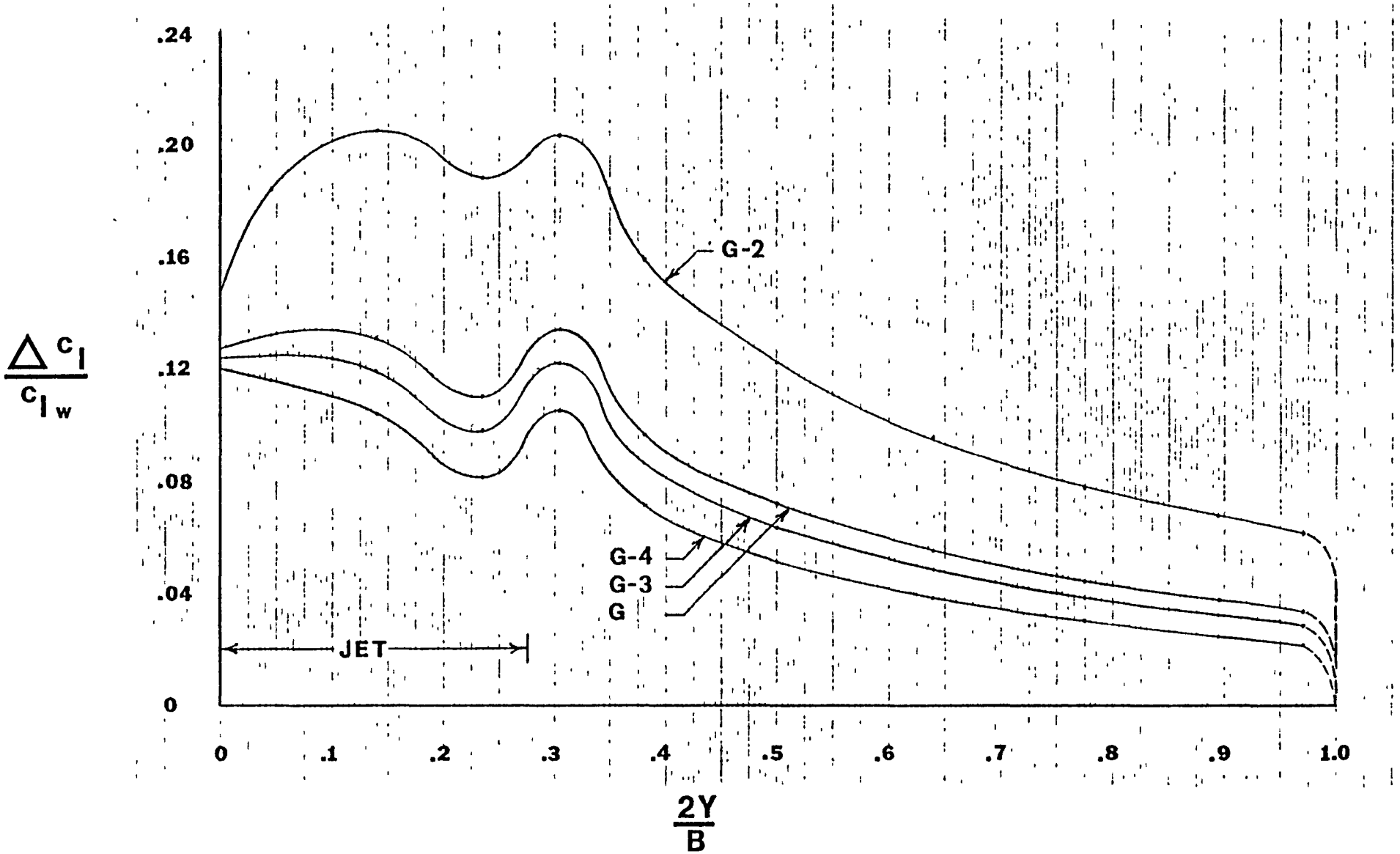

Figure 50. The effect of taper ratio on the spanwise distribution of incremental lift coefficient. $\alpha = 10^{o}$ taper ratios: G-2 λ = 1.0, G λ = 1/4, G-3 λ = 1/6.5, G-4 λ = 1/36.

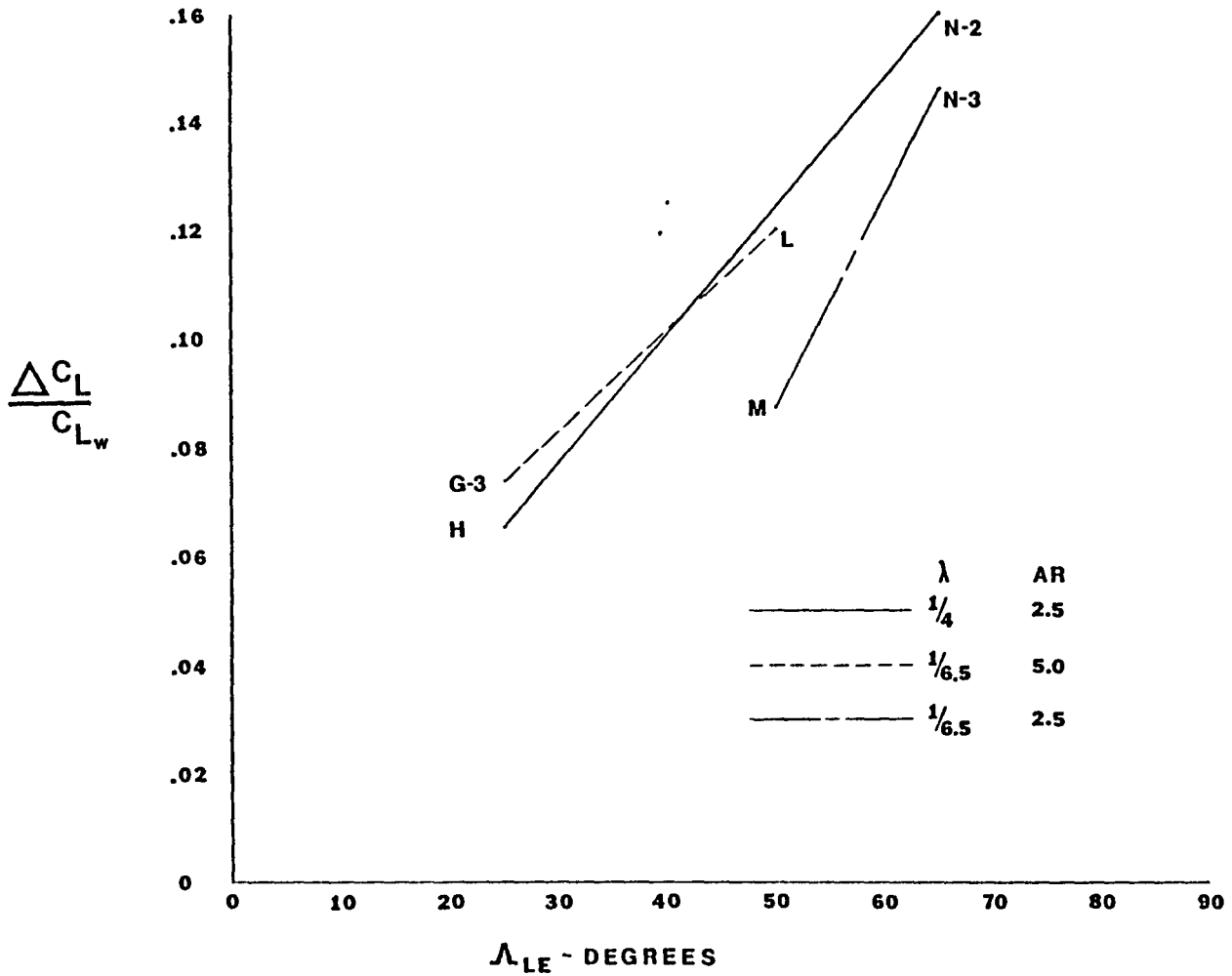

Figure 51. The effect of leading edge sweep angle on the ratio of incremental/wing alone lift coefficients. $\alpha = 20^{0}$.

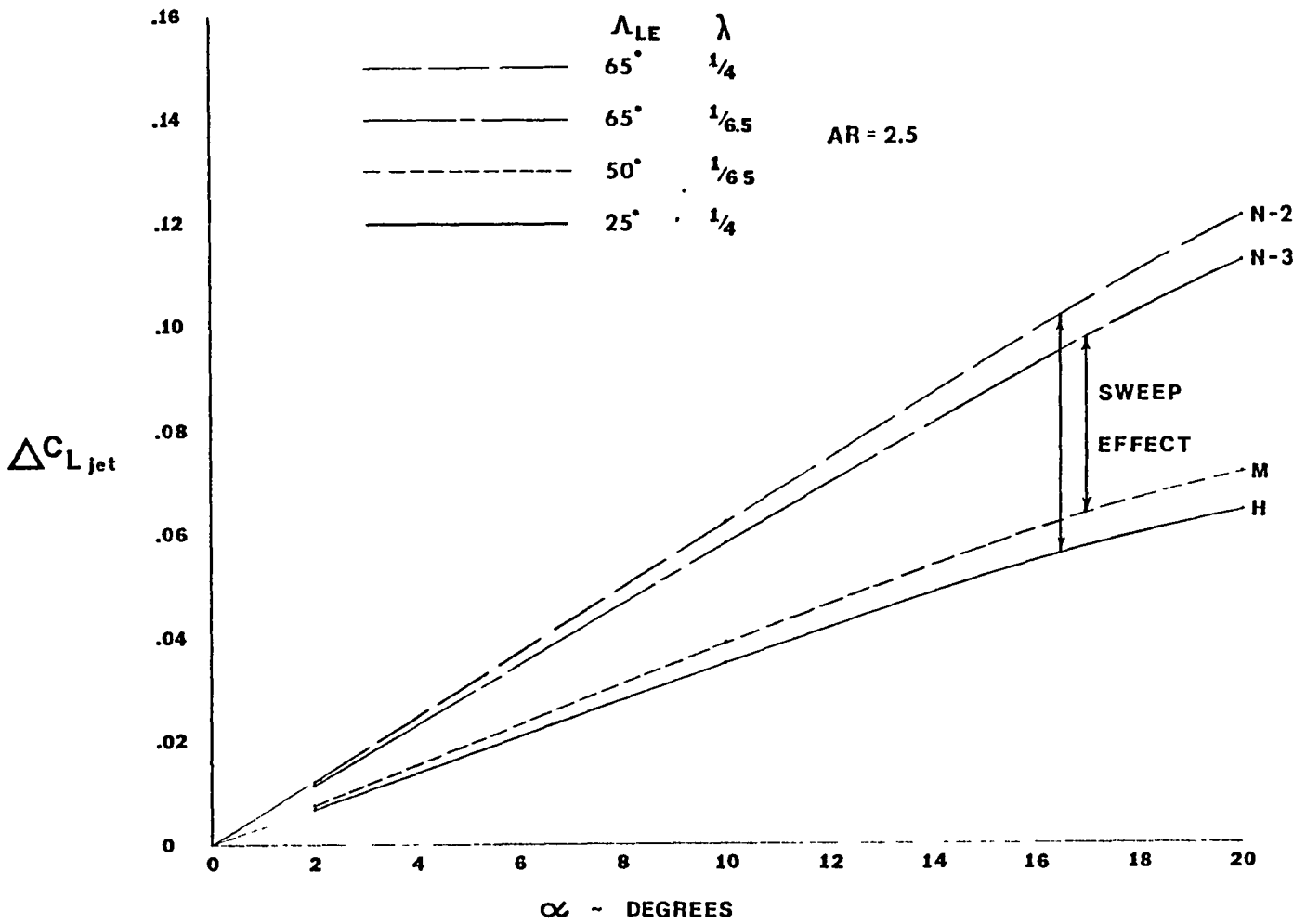

Figure 52. Effect of leading edge sweep angle on the incremental lift of two wing sets of equal taper ratio. AR = 2.5 for all wings.

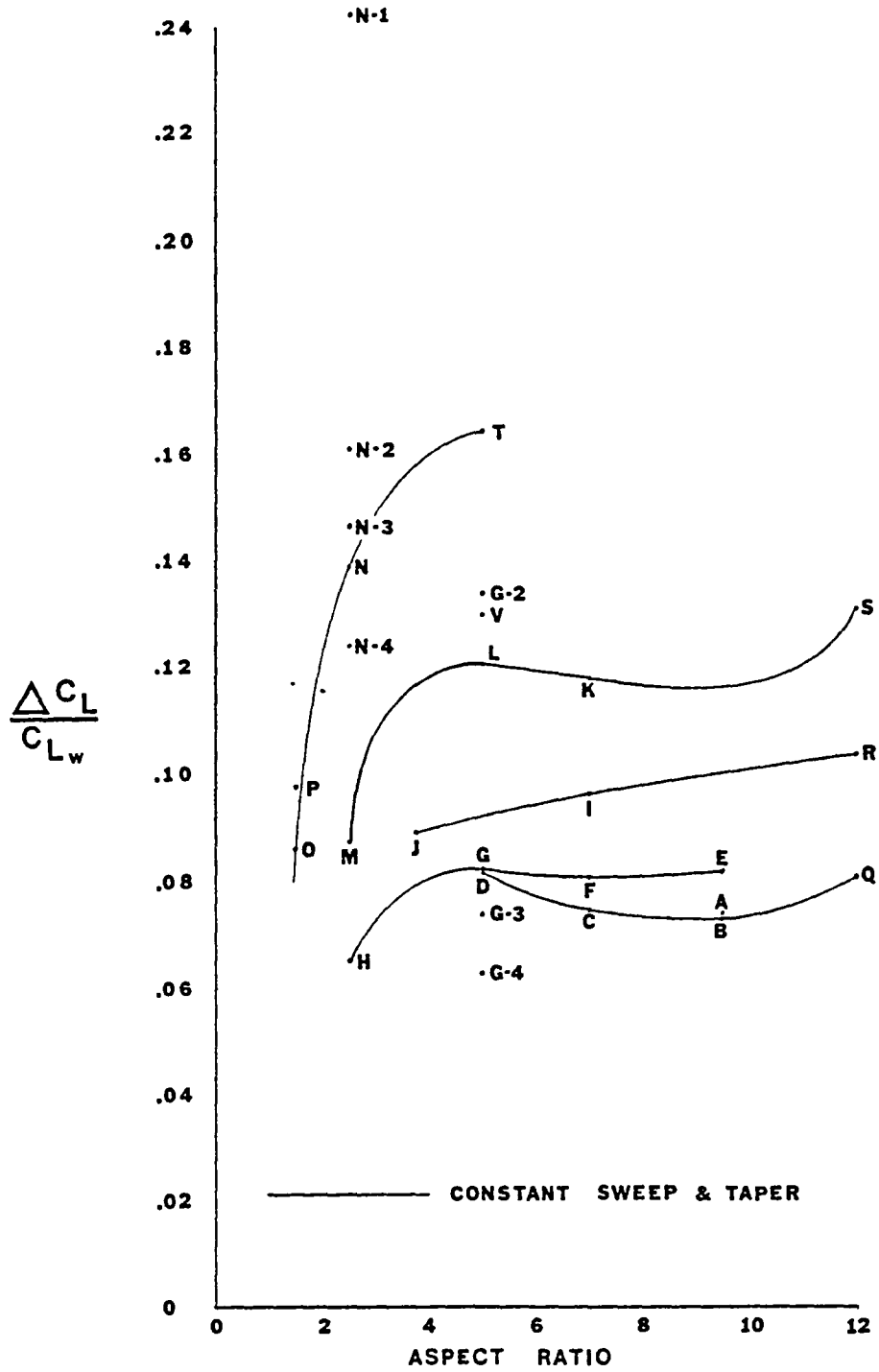

Figure 53. The ratio of incremental to wing alone lift coefficients as a function of wing aspect ratio.

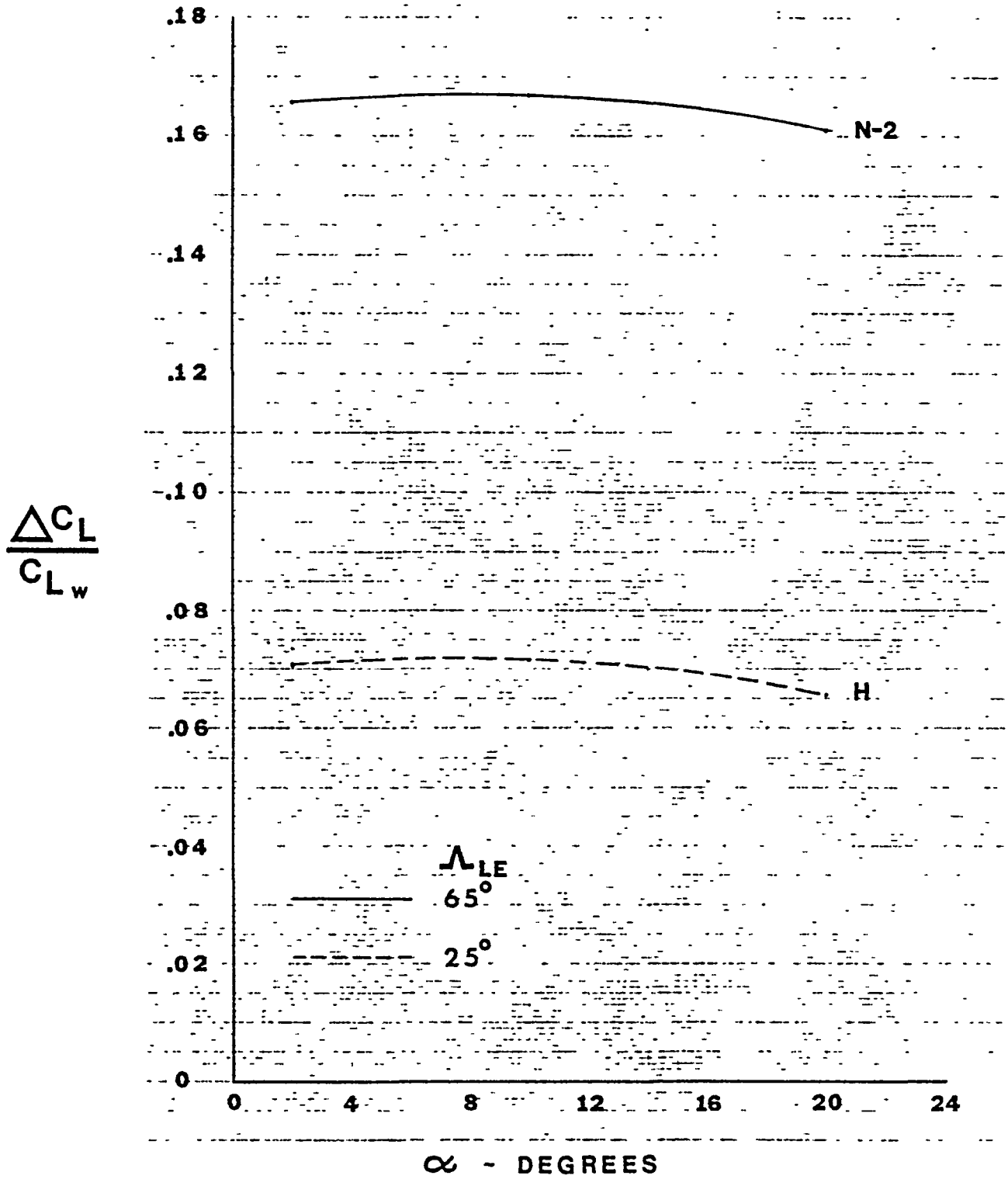

Figure 54. Effect of leading edge sweep on the ratio of incremental/wing alone lift coefficients. AR = 2.5, λ = .25.

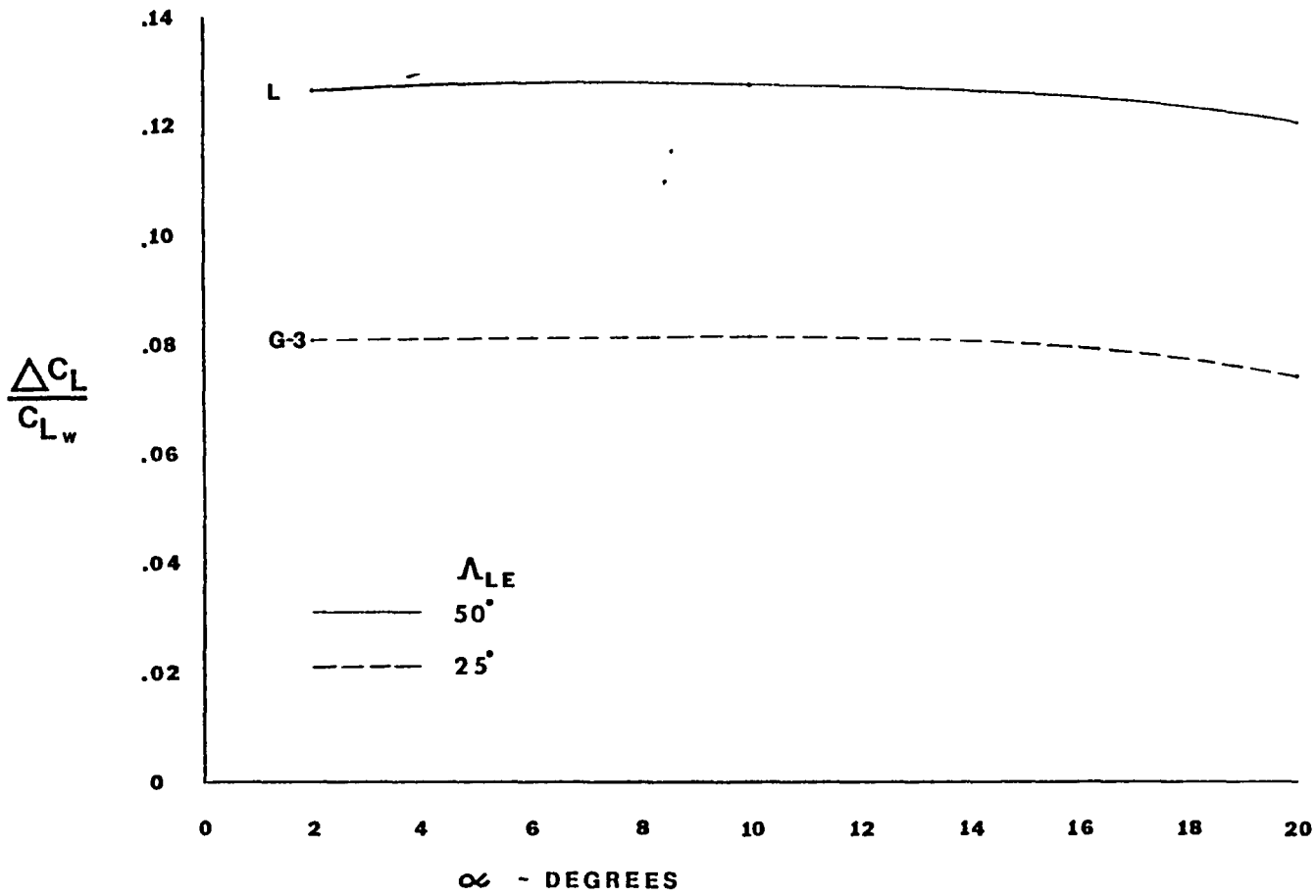

Figure 55. Effect of leading edge sweep on the ratio of incremental/wing alone lift coefficients. AR = 5.0, λ = 1/6.5.

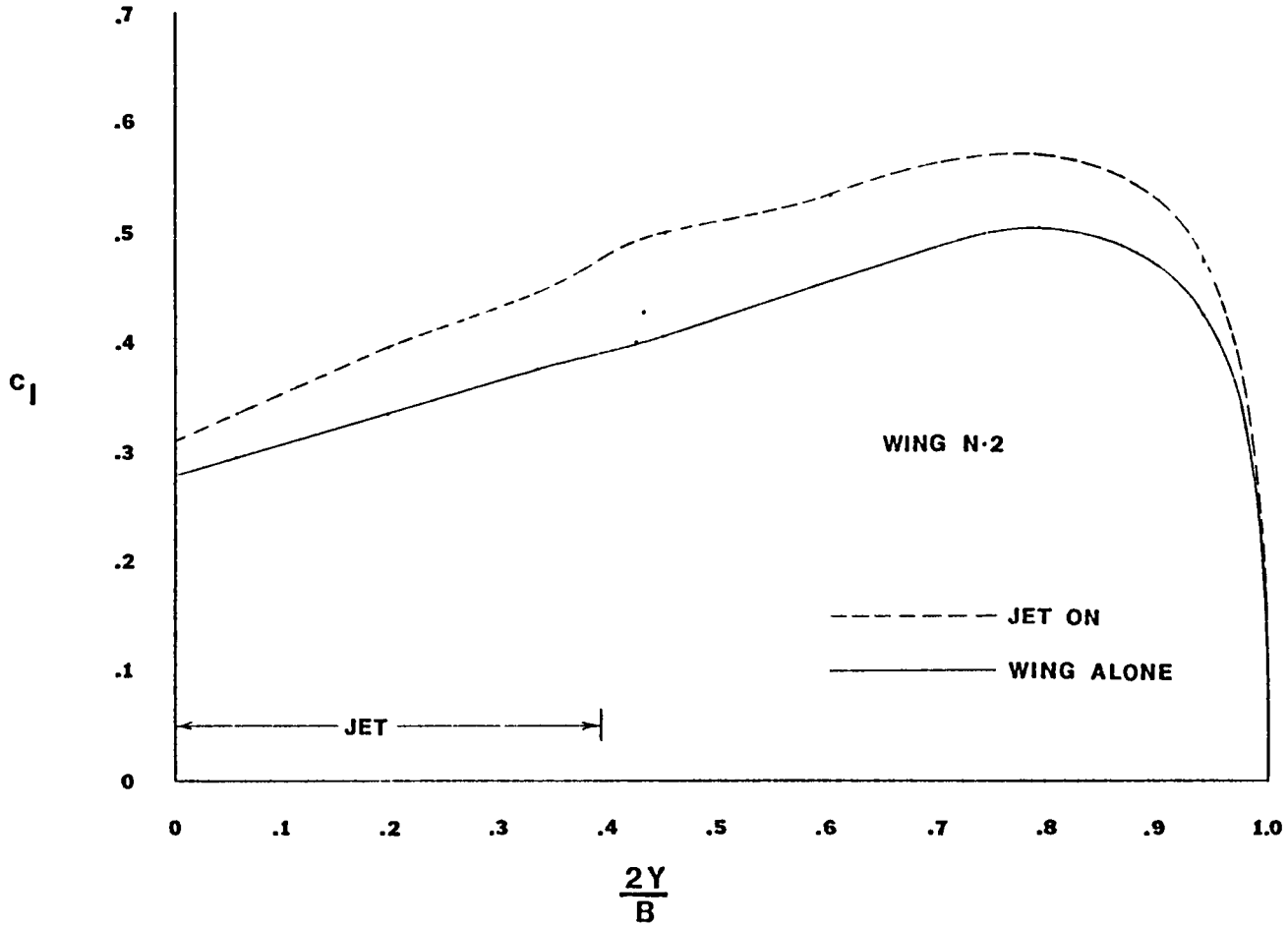

Figure 56. Effect of the USB jet on the spanwise distribution of lift coefficient for wing N-2. $\alpha = 10^{o}$ AR = 2.5, $\lambda = .25$, $\Lambda_{LE} = 65^{o}$.

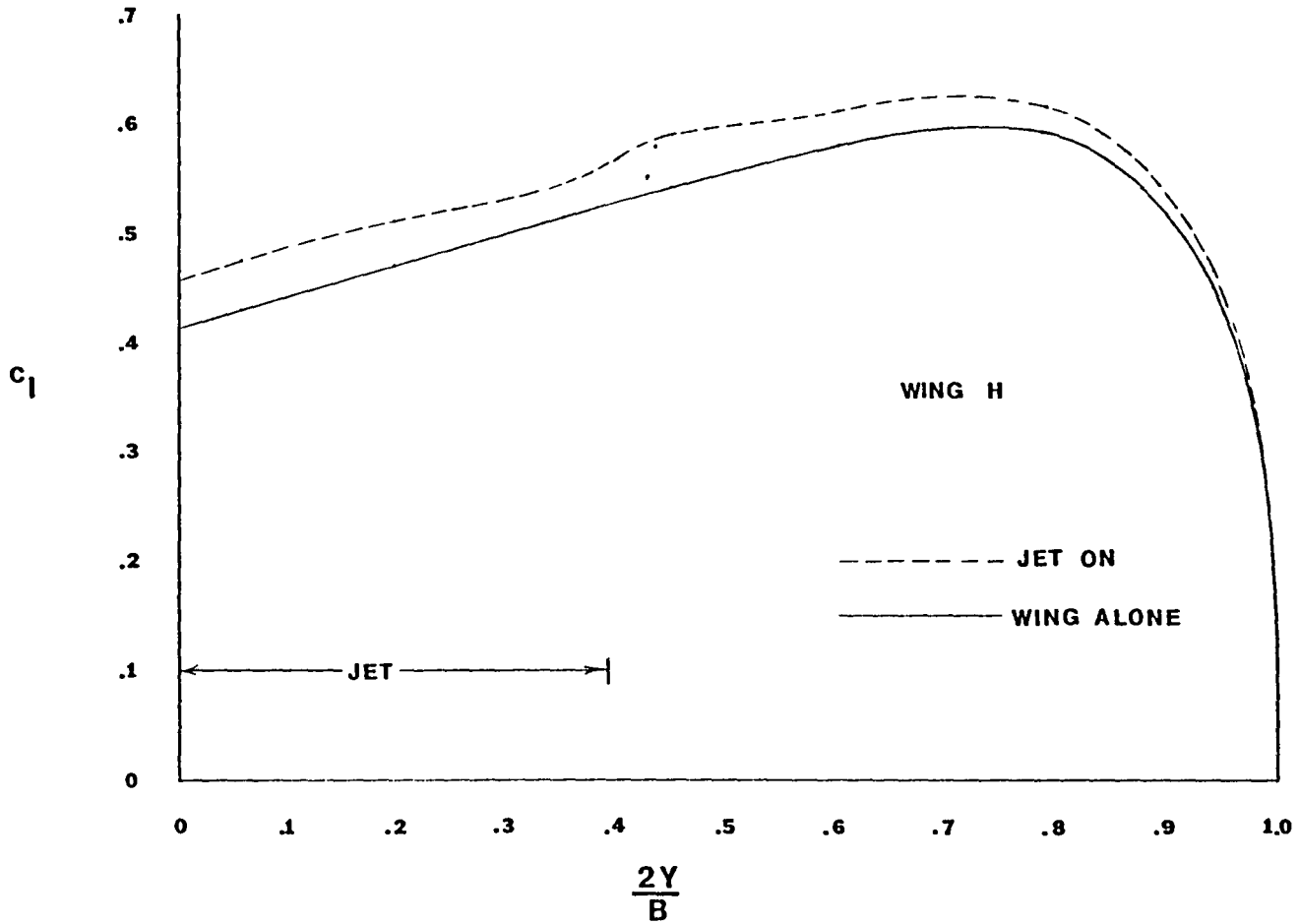

Figure 57. Effect of the USB jet on the spanwise distribution of lift coefficient for wing H. $\alpha = 10^{o}$, AR = 2.5, $\lambda = .25$, $\Lambda_{LE} = 25^{o}$.

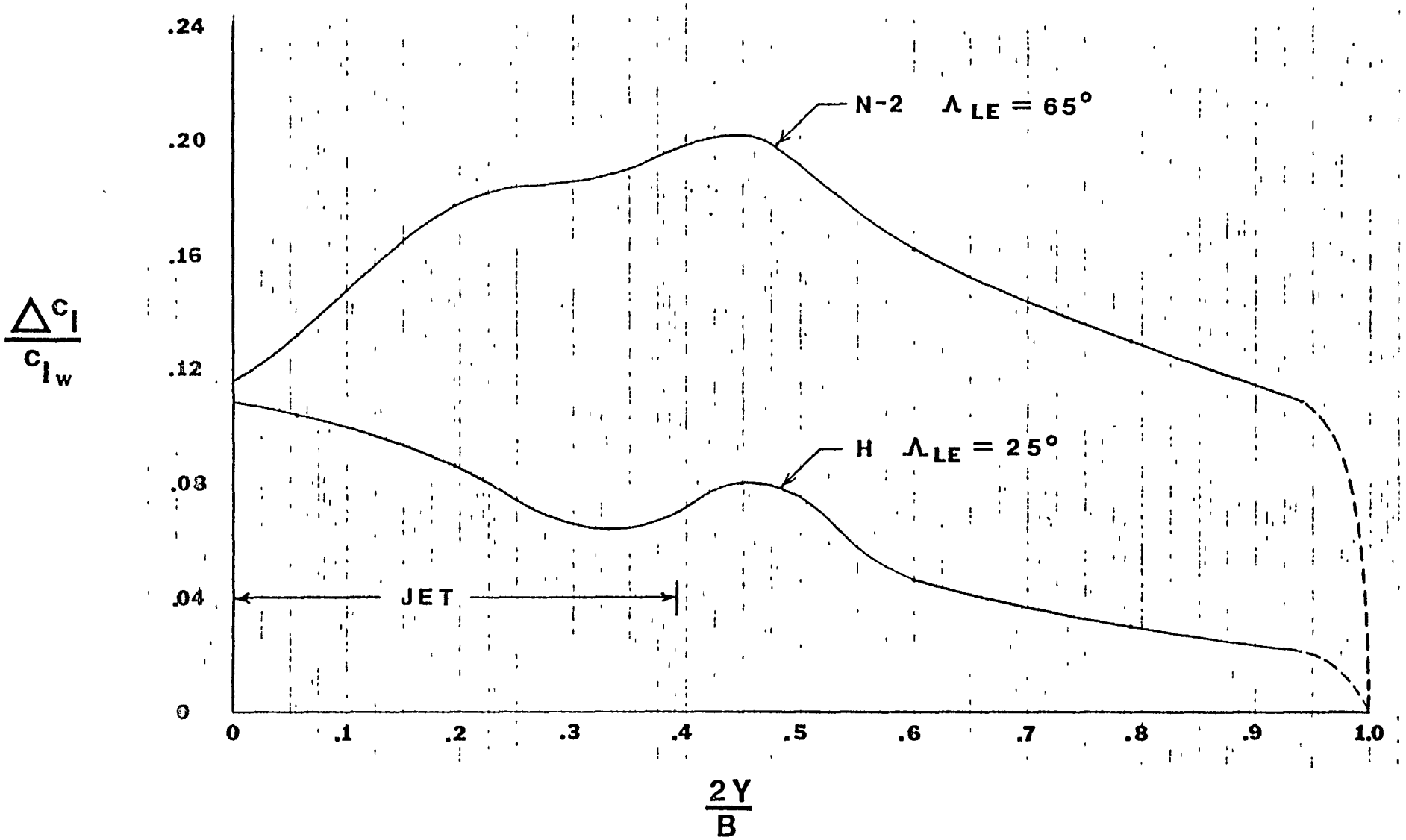

Figure 58. Effect of leading edge sweep on the spanwise distribution of incremental/wing alone lift coefficient ratio. $\alpha = 20^{o}$ AR = 2.5, λ = .25.

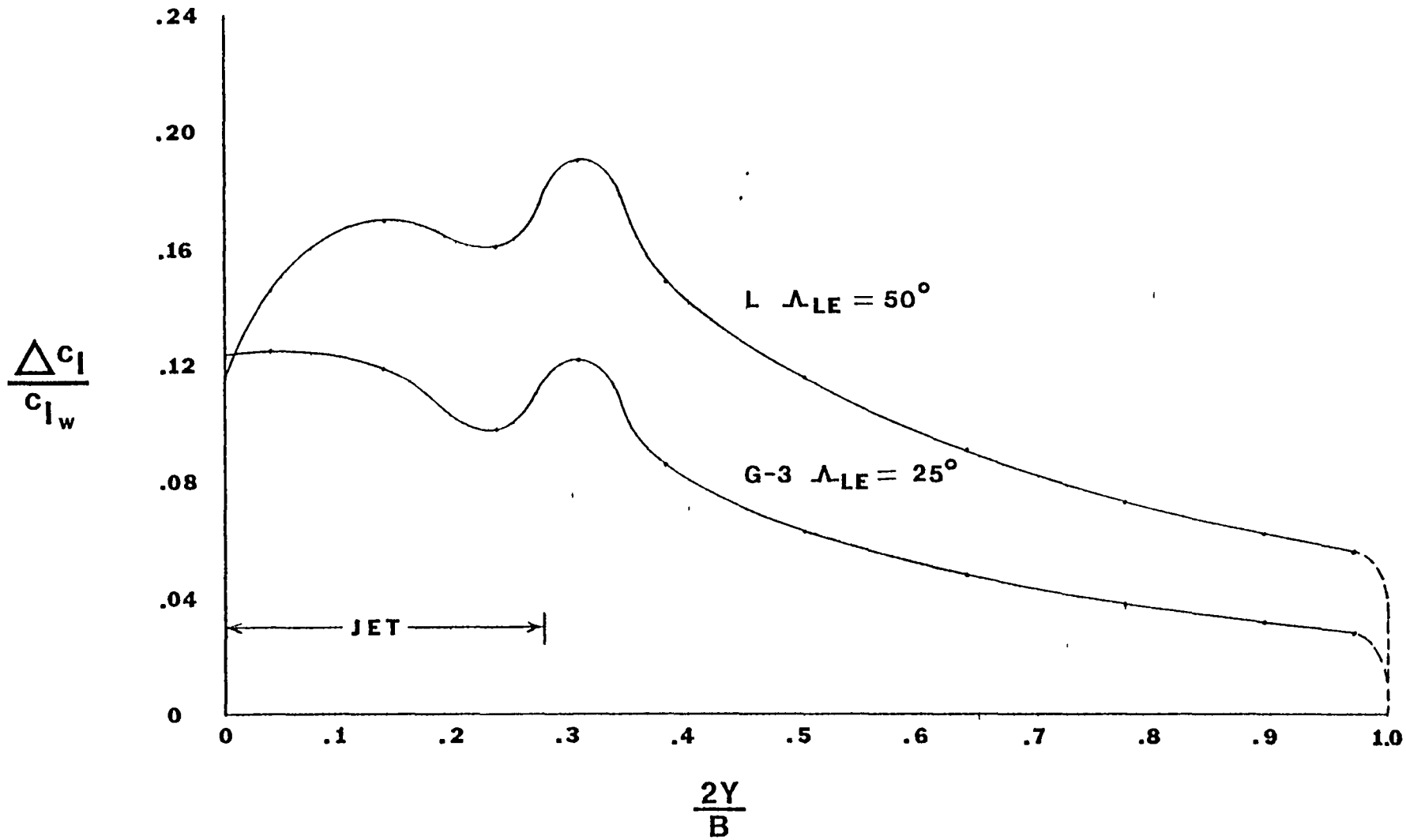

Figure 59. Effect of leading edge sweep on the spanwise distribution of incremental/wing alone lift coefficient ratio. $\alpha = 10^{o}$, AR = 5.0, λ = 1/6.5.

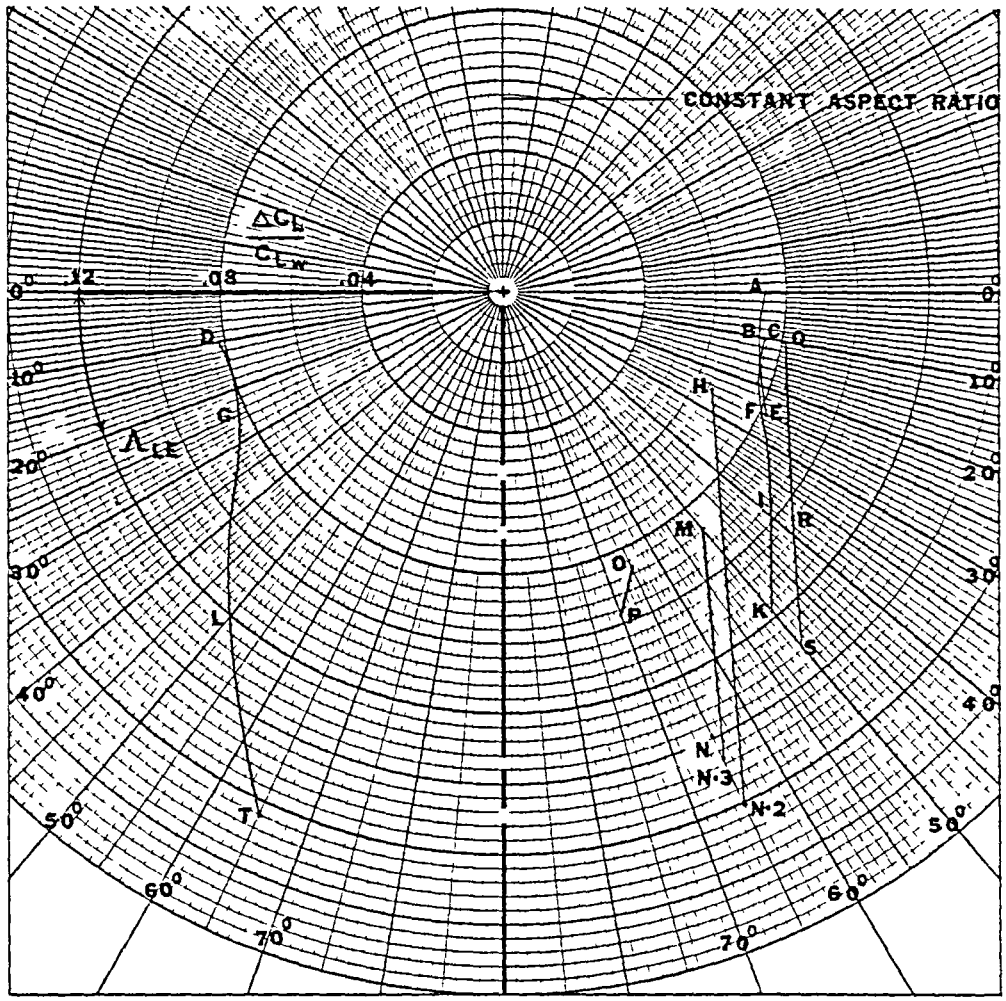

Figure 60. Polar plot using the ratio of incremental to wing alone lift coefficients at $\alpha = 20^{\circ}$ as the radial coordinate. Angular coordinate is the leading edge sweep angle of each wing. Curves shown are wings of constant aspect ratio.

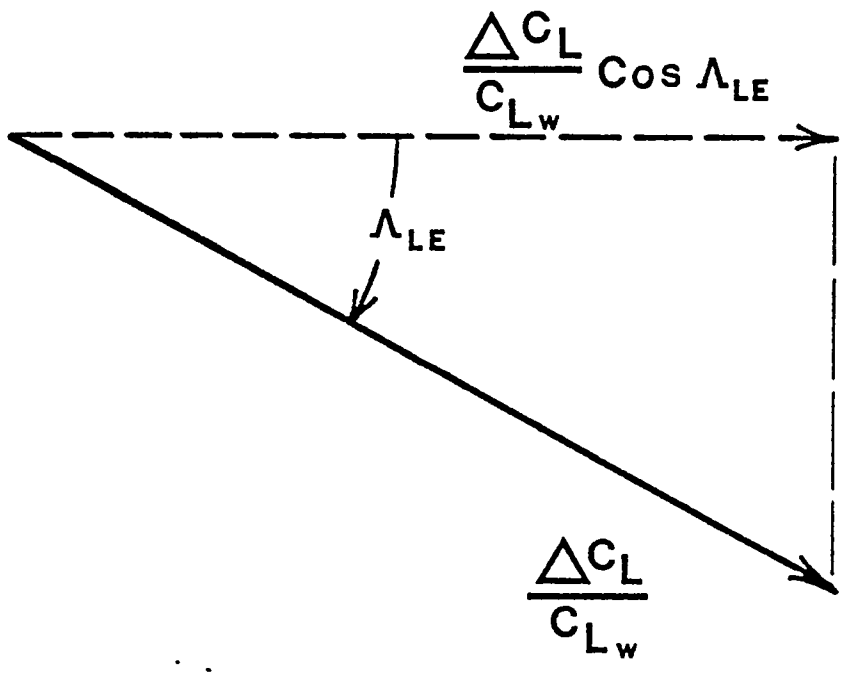

For a given aspect ratio:

$$\frac{\Delta C_L}{C_{L_w}} \text{ Cos } \Lambda_{LE} = \text{Constant}$$

Figure 61. Explanation of the trends seen in Figure 60 for wings with equal aspect ratios.

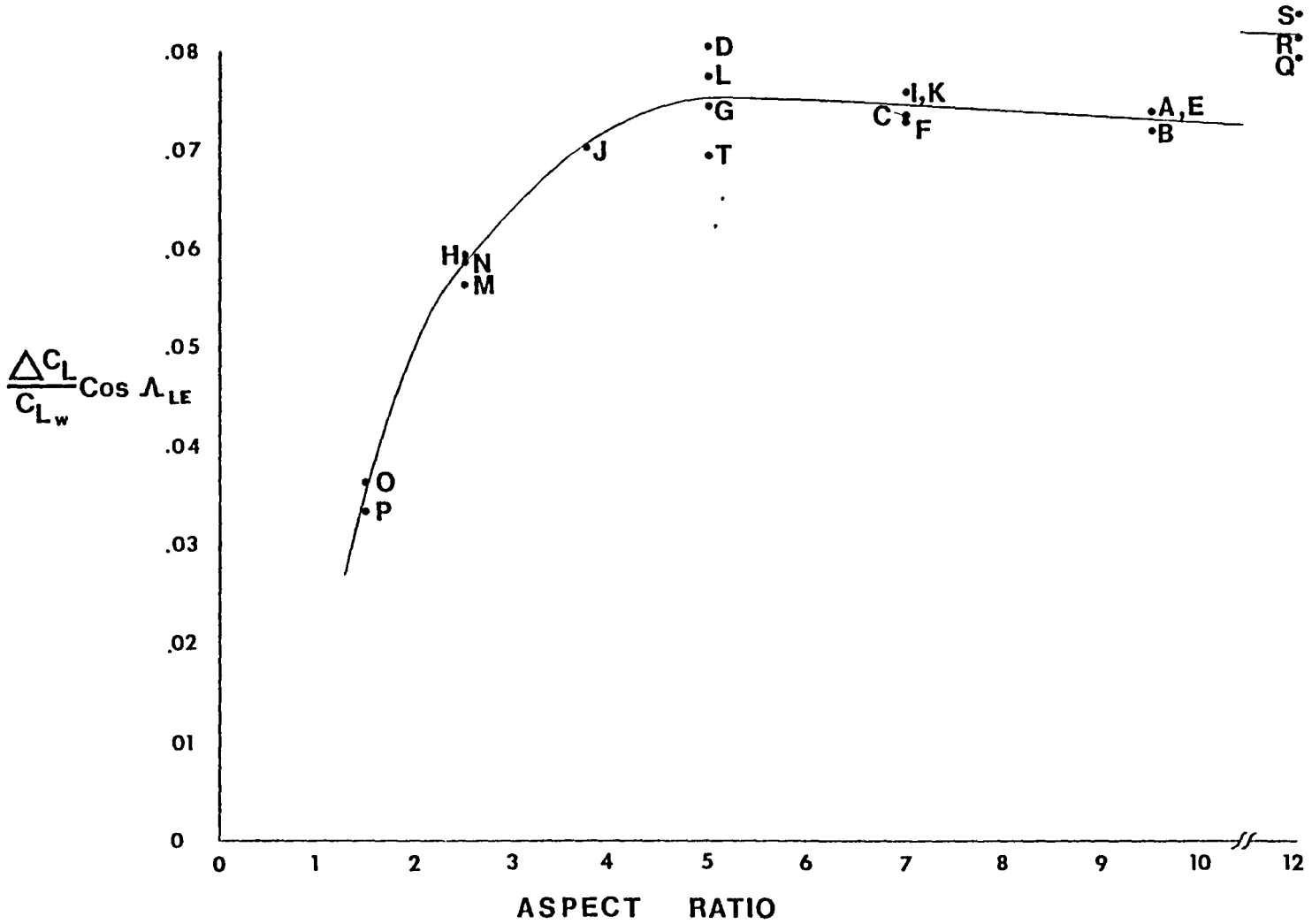

Figure 62. Variation of (the ratio of incremental/wing$_o$alone lift multiplied by the cosine of the leading edge sweep angle) with aspect ratio. $\alpha = 20^o$

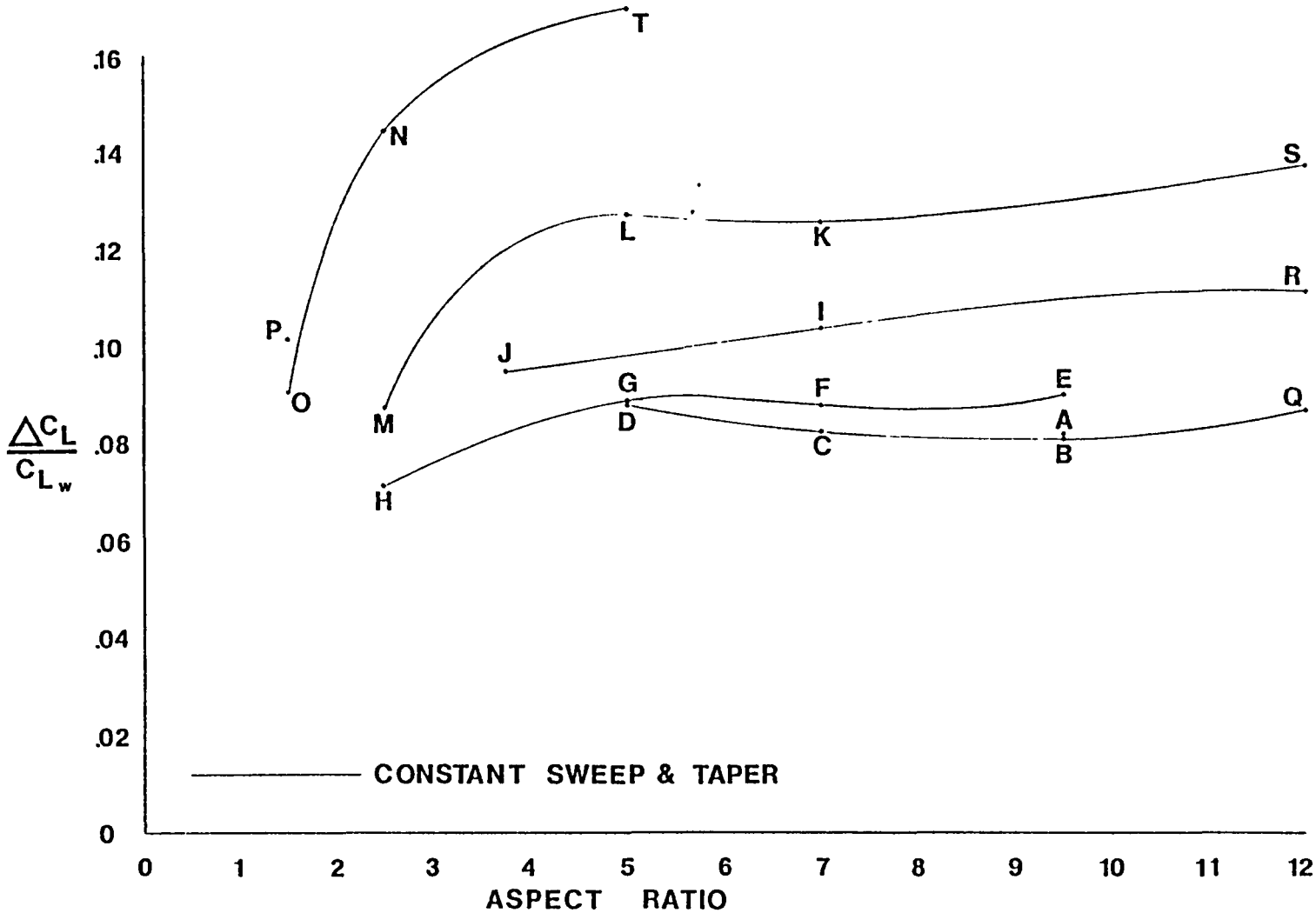

Figure 63. Variation of the ratio of incremental/wing alone lift coefficients with wing aspect ratio. $\alpha = 10^{o}$.

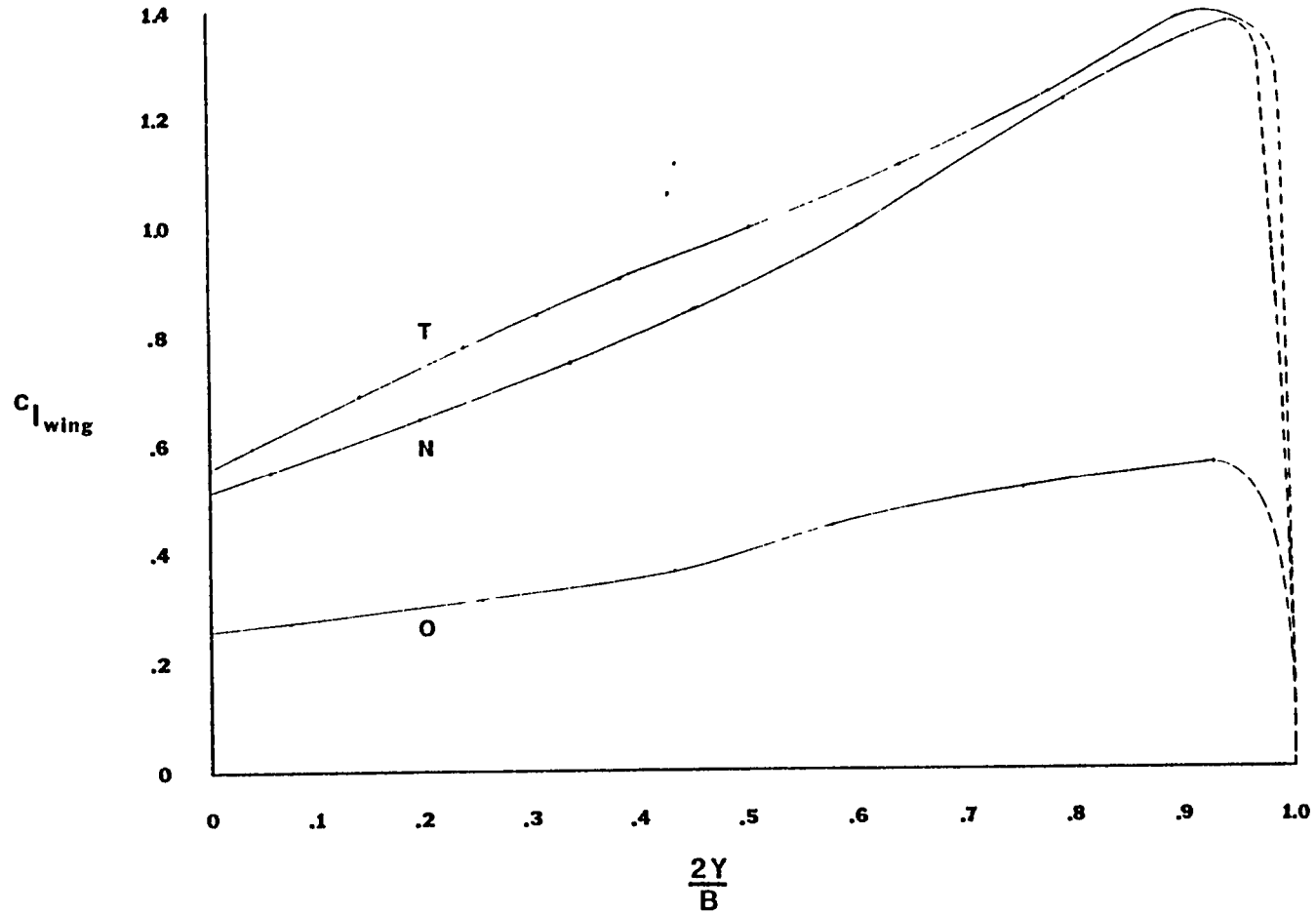

Figure 64. The effect of wing aspect ratio on the spanwise distribution of lift coefficient with no blowing. $\alpha = 20°$, $\Lambda_{LE} = 65°$, $\lambda = 1/9.214$ aspect ratios. O = 1.5, N = 2.5, T = 5.0.

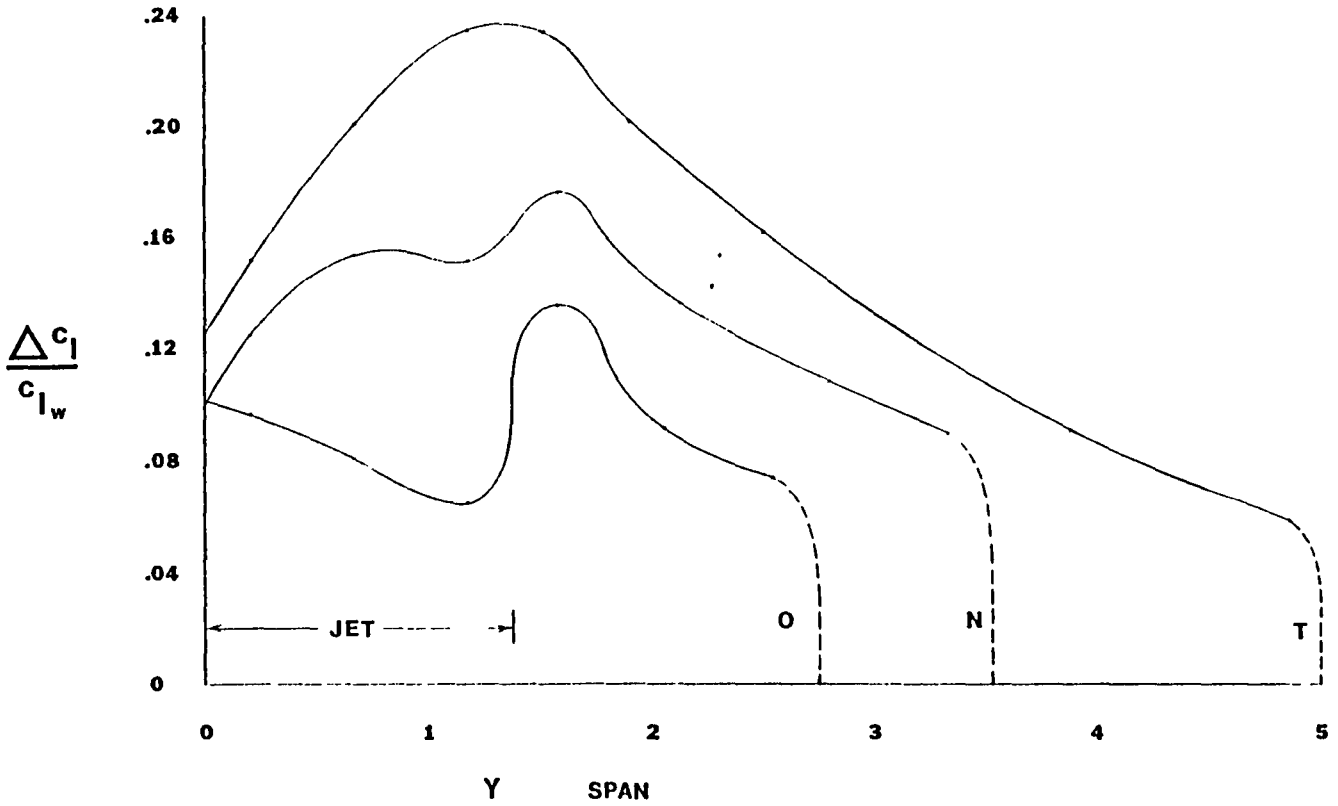

Figure 65. The effect of wing aspect ratio on the spanwise distribution of incremental lift. $\alpha = 20°$, $\Lambda_{LE} = 65°$ $\lambda = 1/9.214$ aspect ratios: O = 1.5, N = 2.5, T = 5.0.

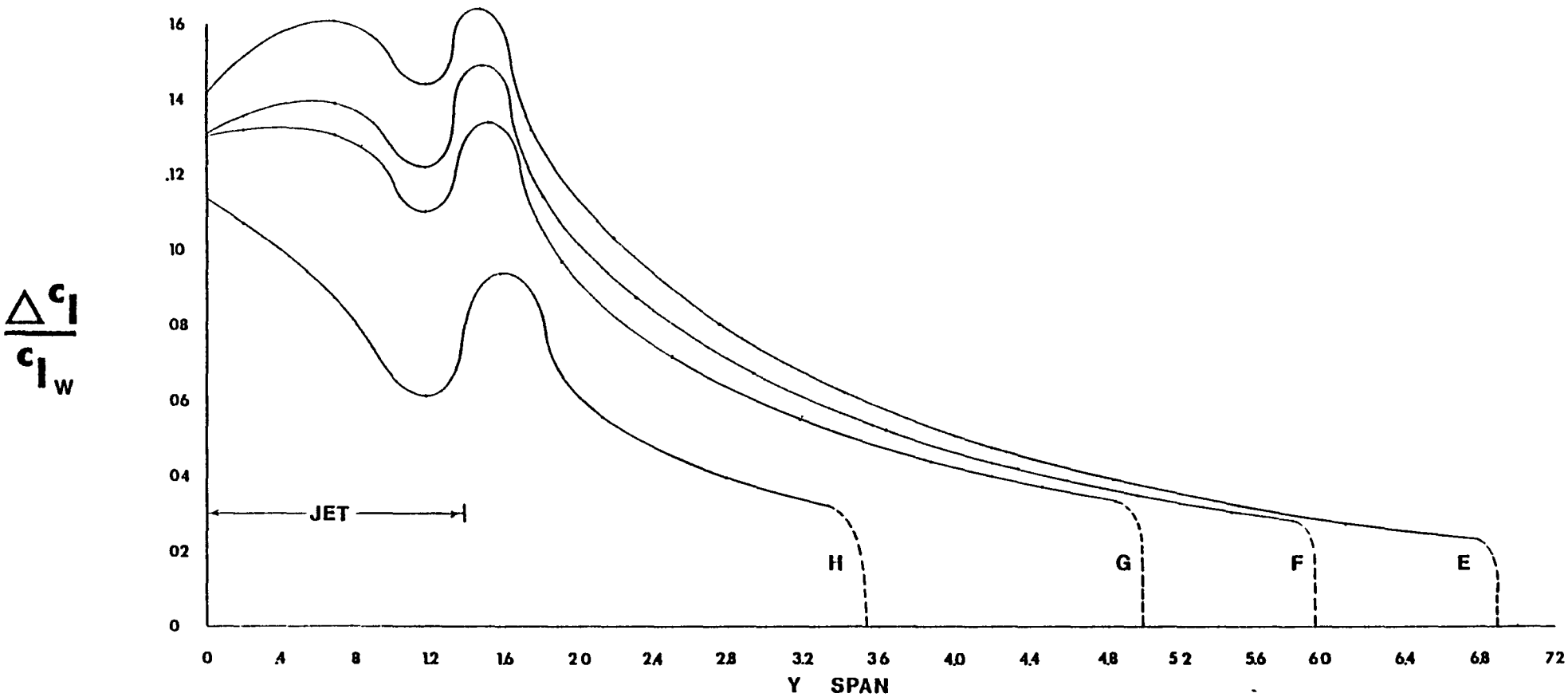

Figure 66 The effect of wing aspect ratio on the spanwise distribution of incremental lift. $\alpha = 10°$, $\Lambda_{\frac{1}{4}} = 25°$, $\lambda = .25$, aspect ratios E = 9 5, F = 7.0, G = 5 0, H = 2 5

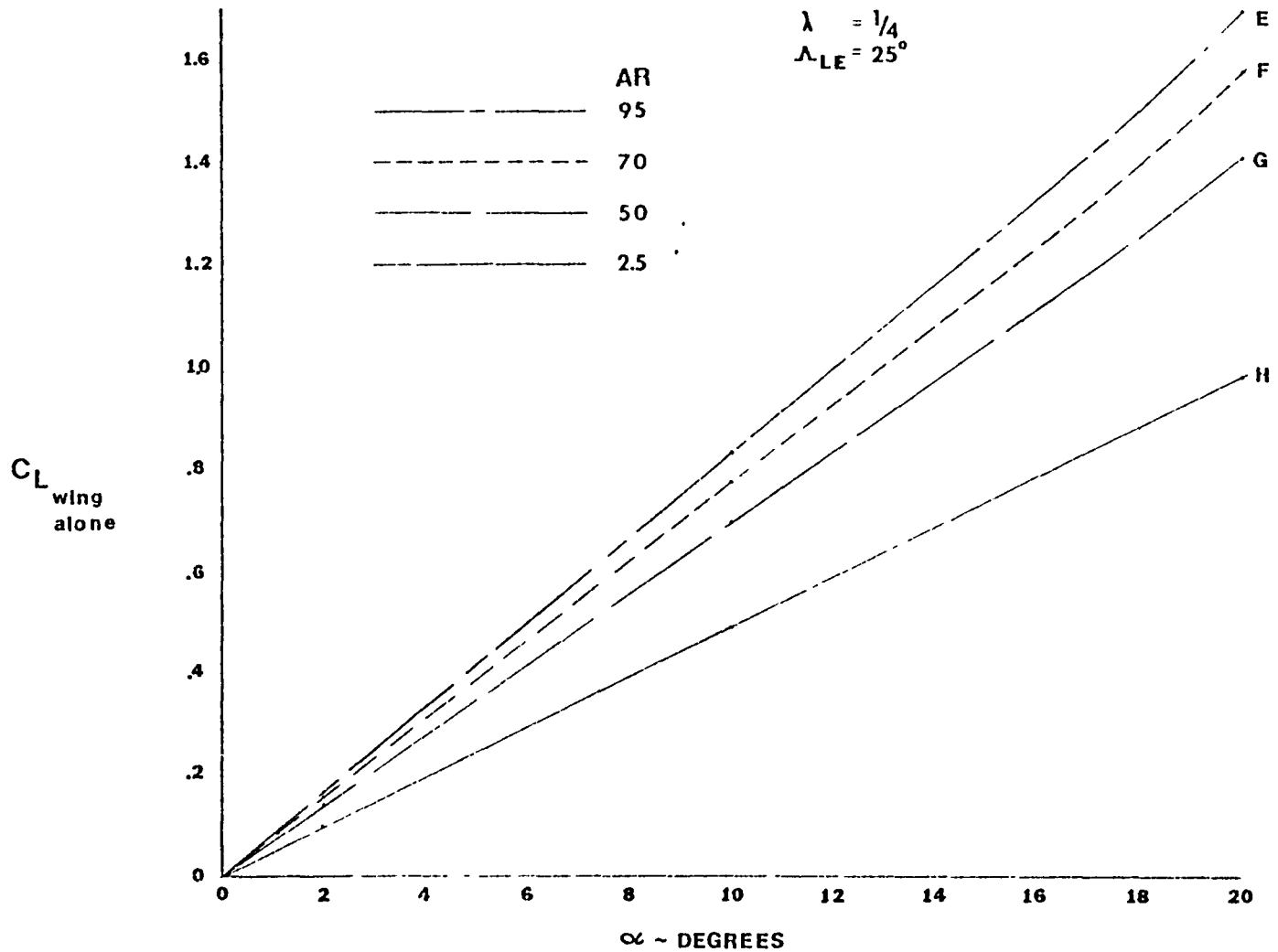

Figure 67. The effect of wing aspect ratio on the liftcurve slope of wings with no blowing $\Lambda_{LE} = 25°$, $\lambda = .25$, aspect ratios: E = 9.5, F = 7.0, G = 5.0, H = 2.5.

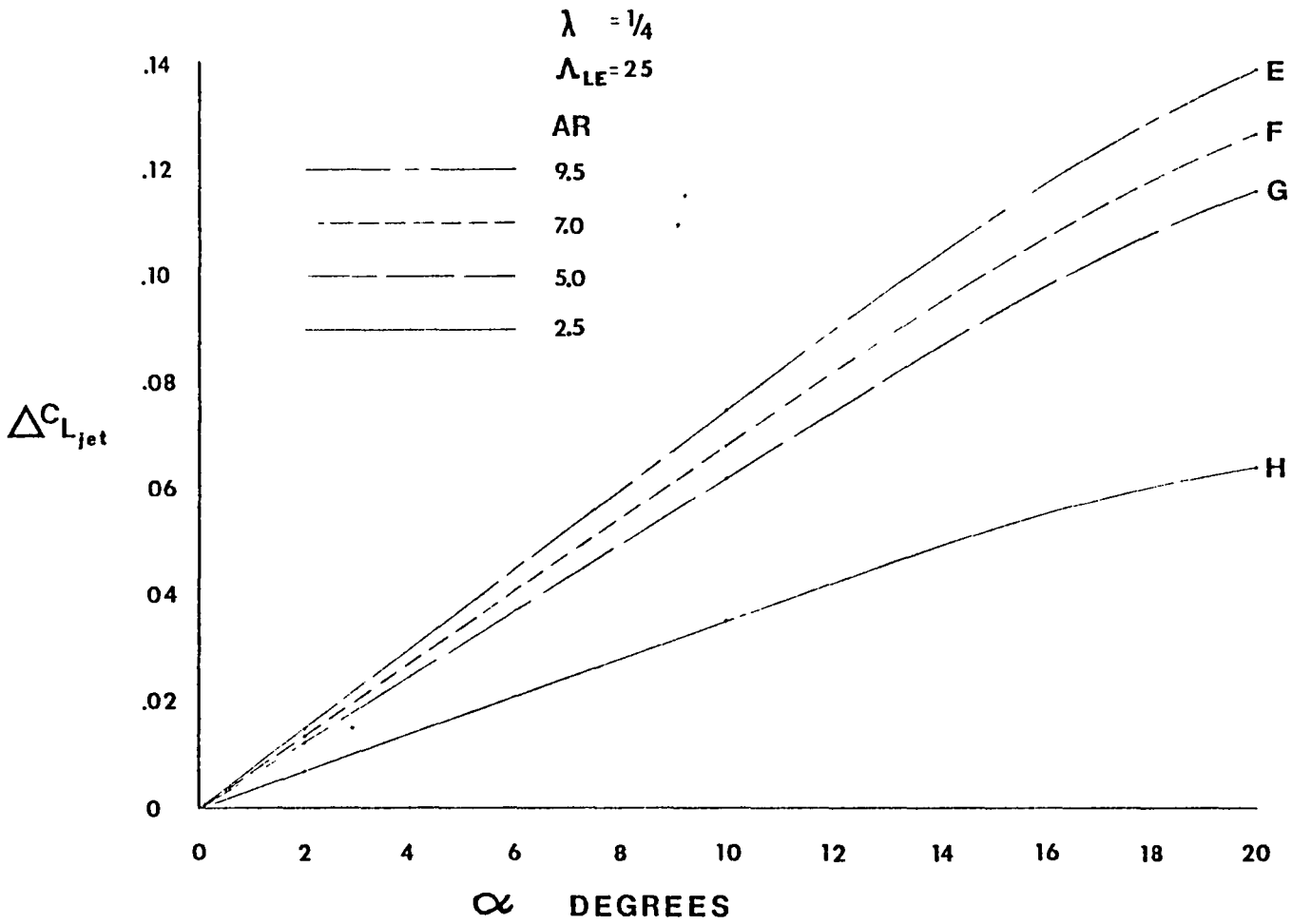

Figure 68. The effect of wing aspect ratio on the incremental lift due to blowing. $\Lambda_{LE} = 25°$, $\lambda = .25$.

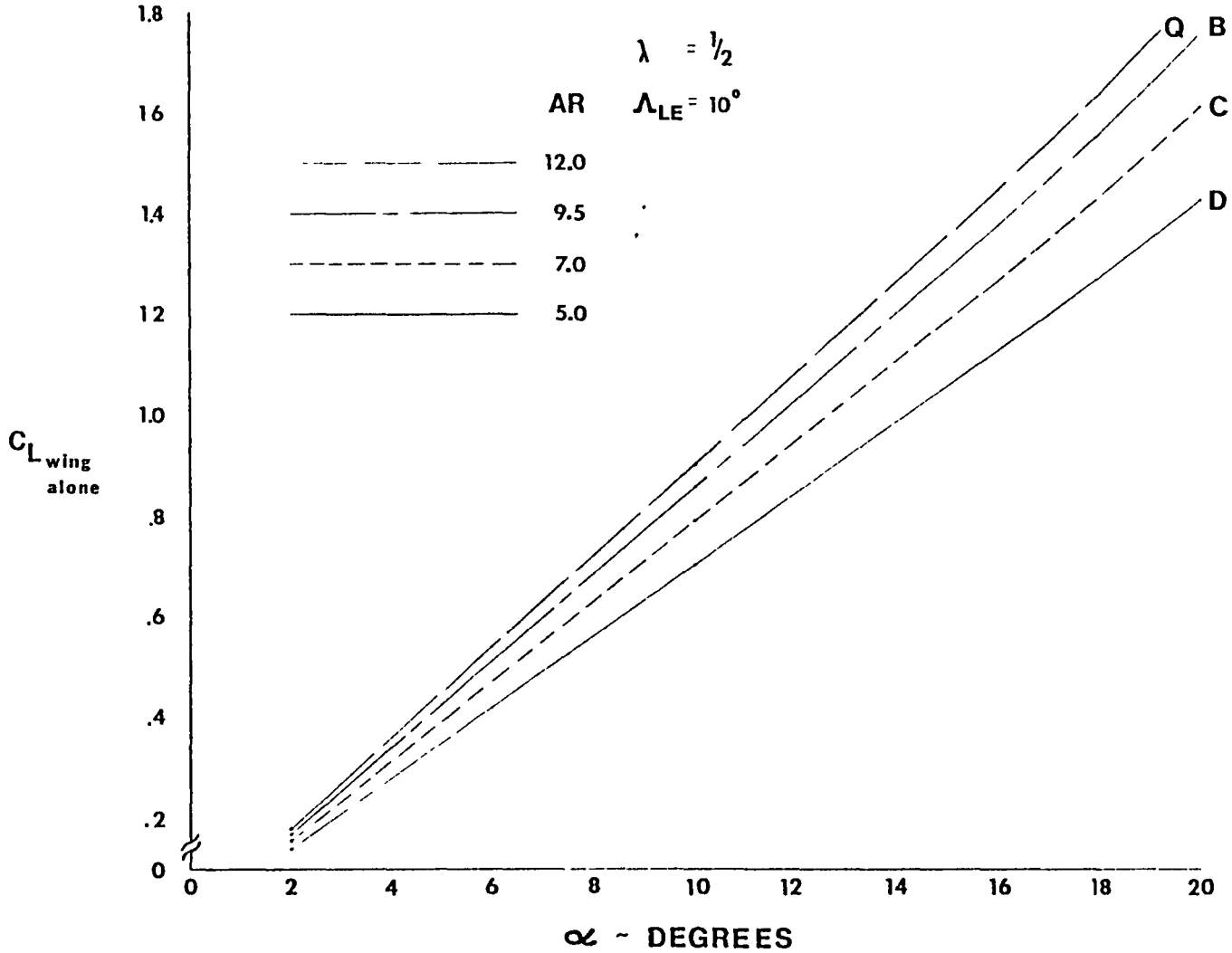

Figure 69. The effect of wing aspect ratio on the lift-curve slope of wings with no blowing $\Lambda_{LE} = 10°$, $\lambda = .5$.

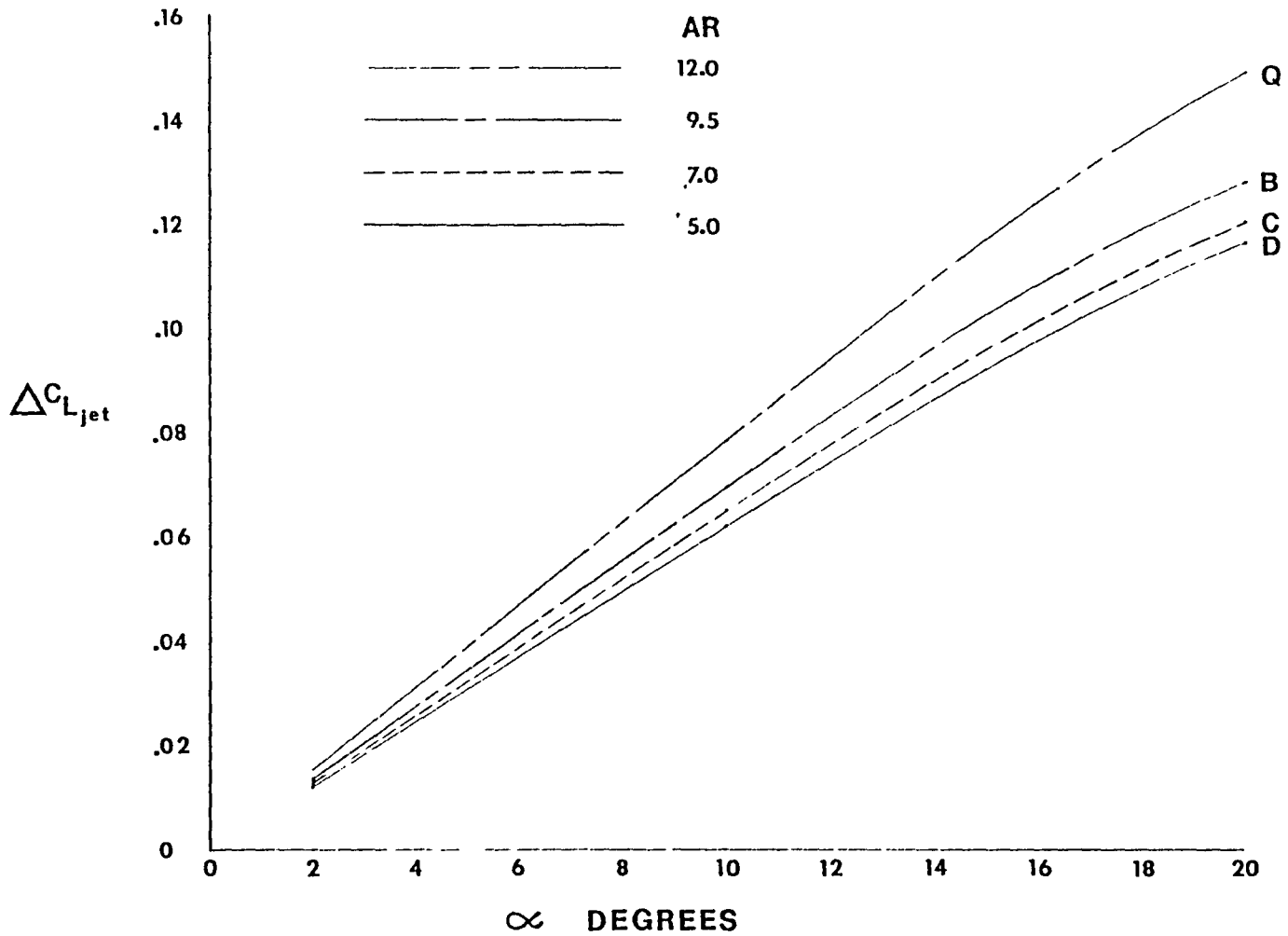

Figure 70. Incremental lift induced by a USB jet on wings of varying aspect ratio. $\Lambda_{LE} = 10°$, $\lambda = .5$.

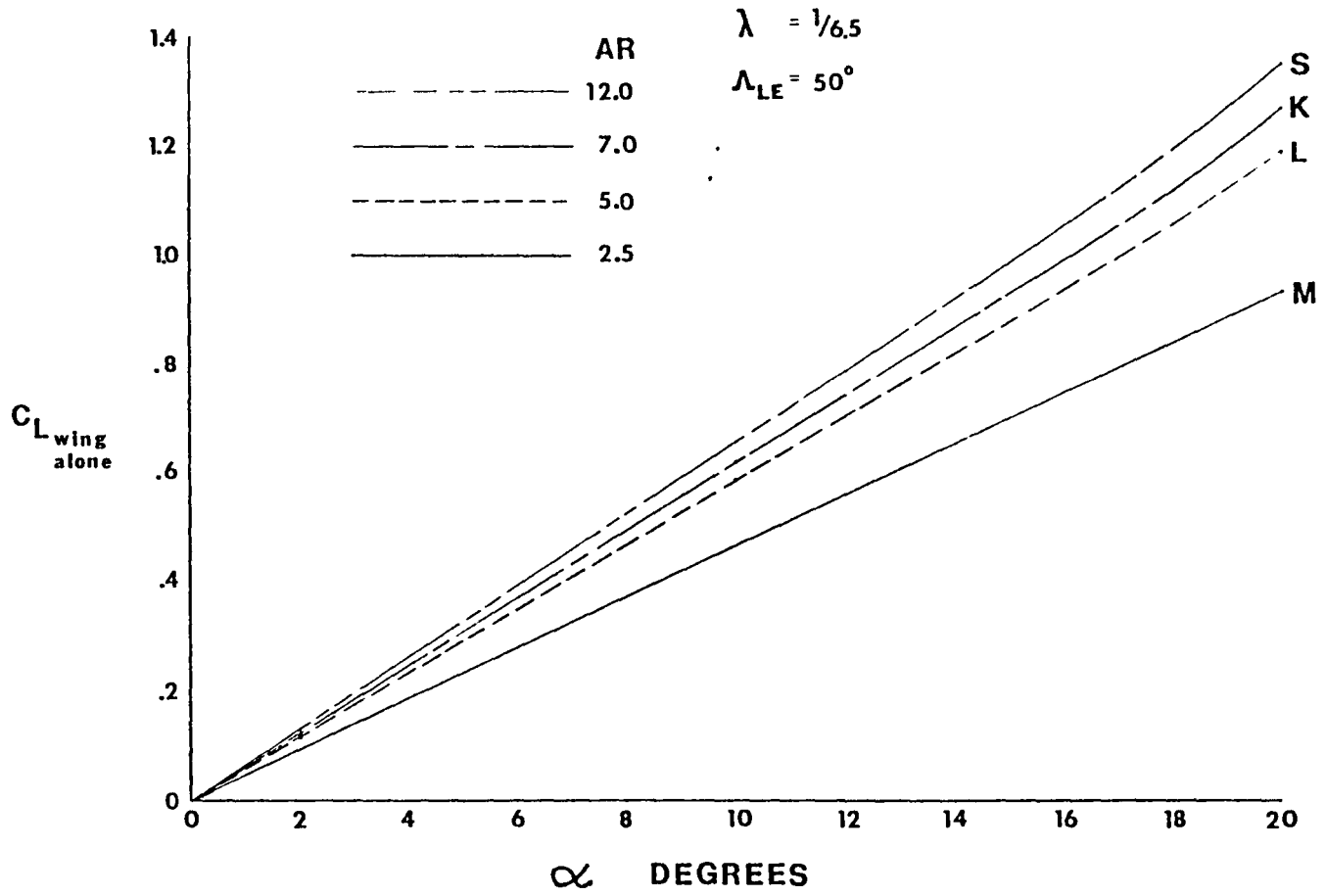

Figure 71. Effect of wing aspect ratio on the lift-curve slope of wings with no blowing. Λ_{LE} = 50°, λ = 1/6.5.

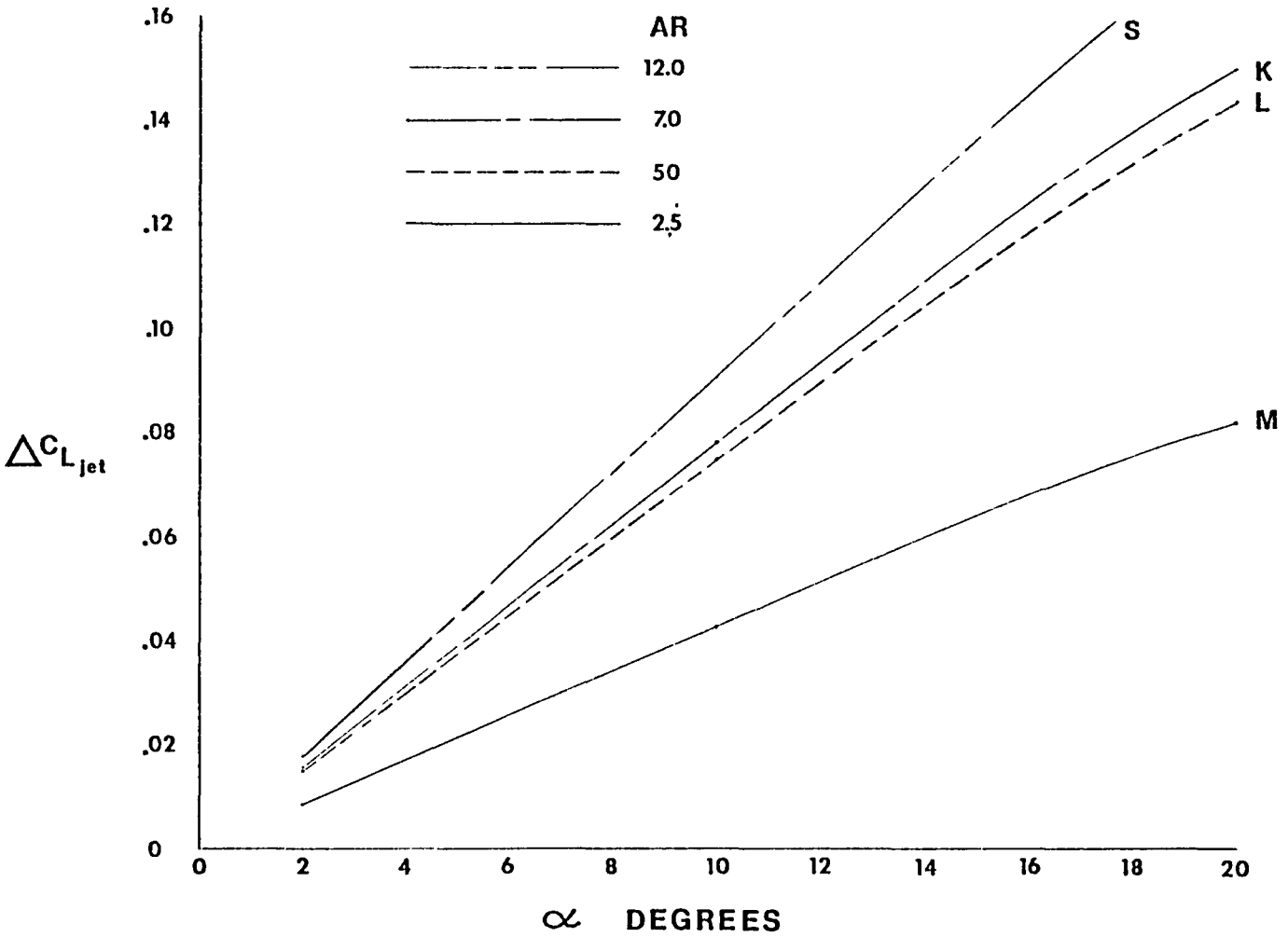

Figure 72. Incremental lift induced by a USB jet on wings of varying aspect ratio $\Lambda_{LE} = 50°$, $\lambda = 1/6.5$.

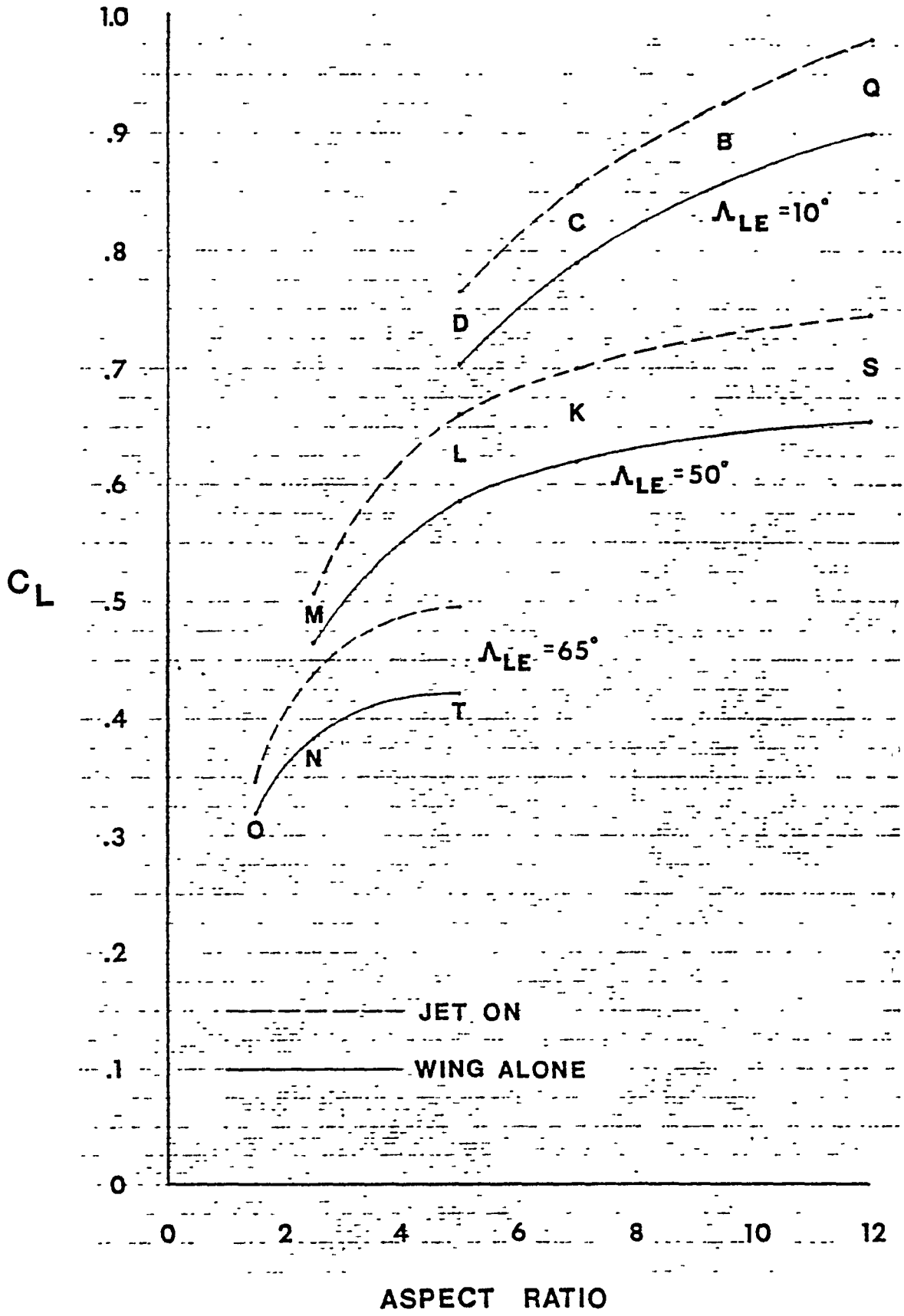

Figure 73. Effect of aspect ratio on the lift with the jet and with the wing alone, for three wing sets with equal sweep and taper. $\alpha = 10°$

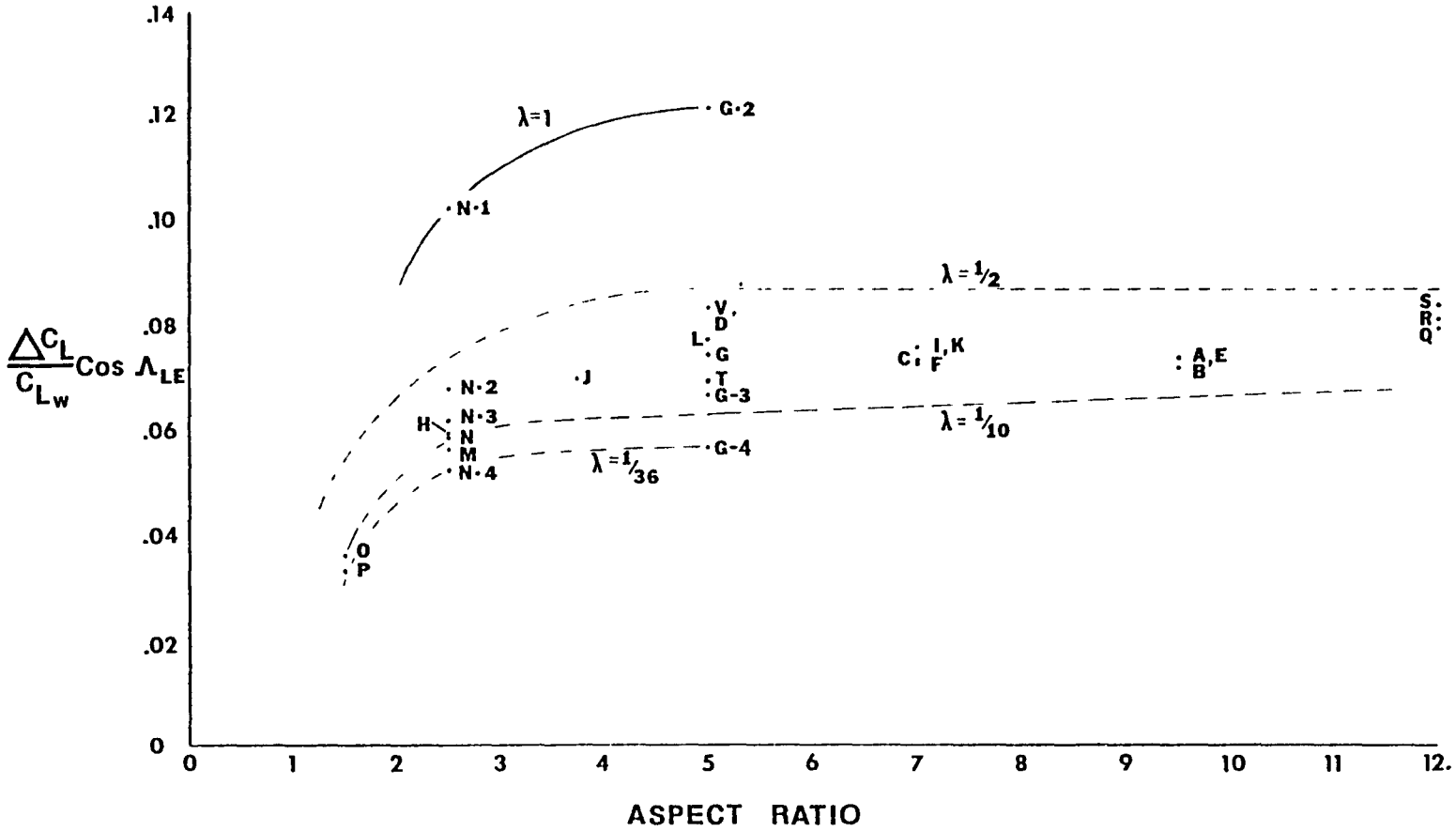

Figure 74. Variation of the parameter $(\Delta C_L/C_{LW})(\cos\Lambda_{LE})$ with wing aspect ratio for all of the wings. $\alpha = 20°$, $C_u = 2.0$.

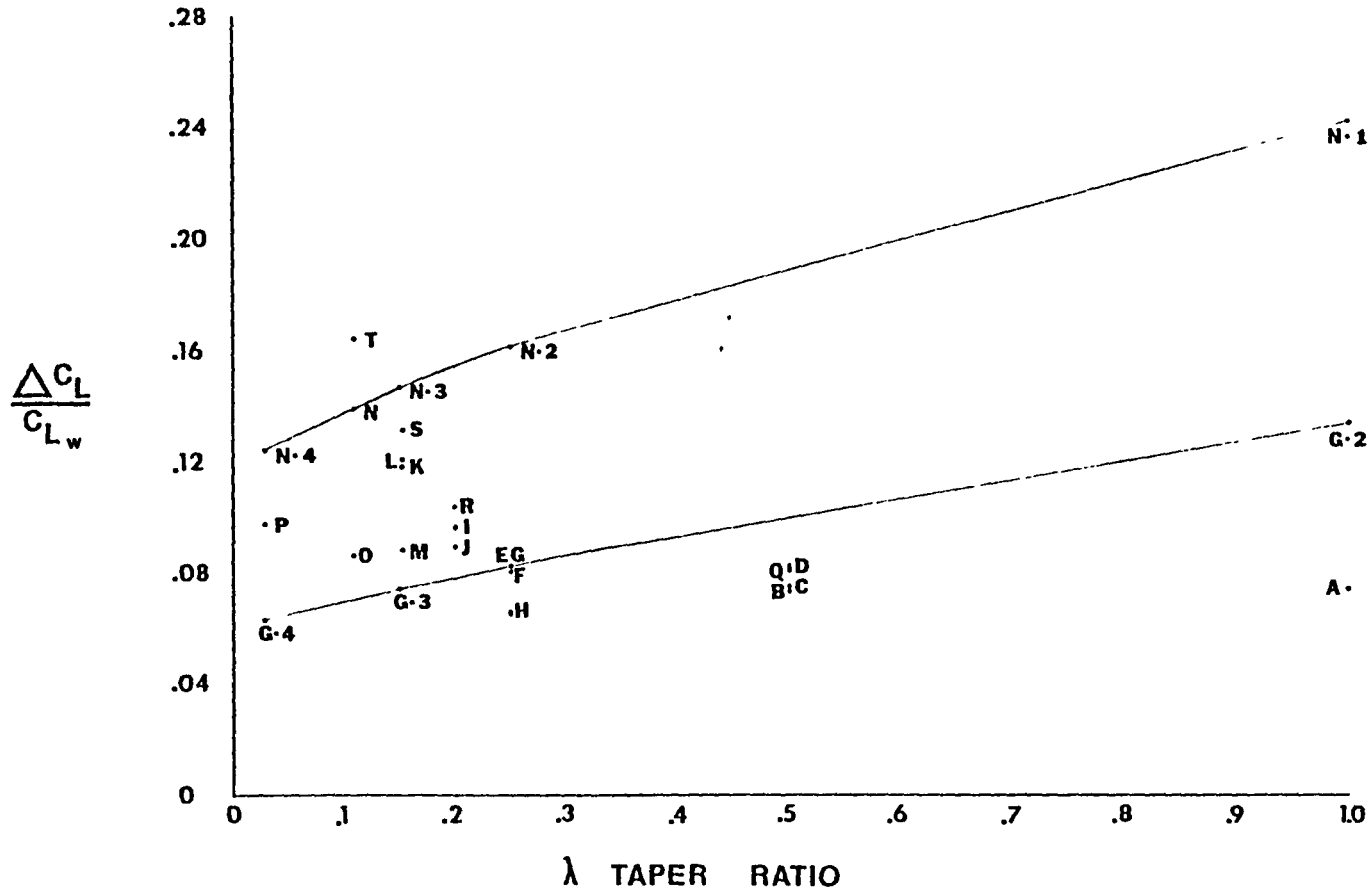

Figure 75. Plot of the ratio of incremental/wing alone lift coefficients as a function of the taper ratio of each wing. $\alpha = 20°$.

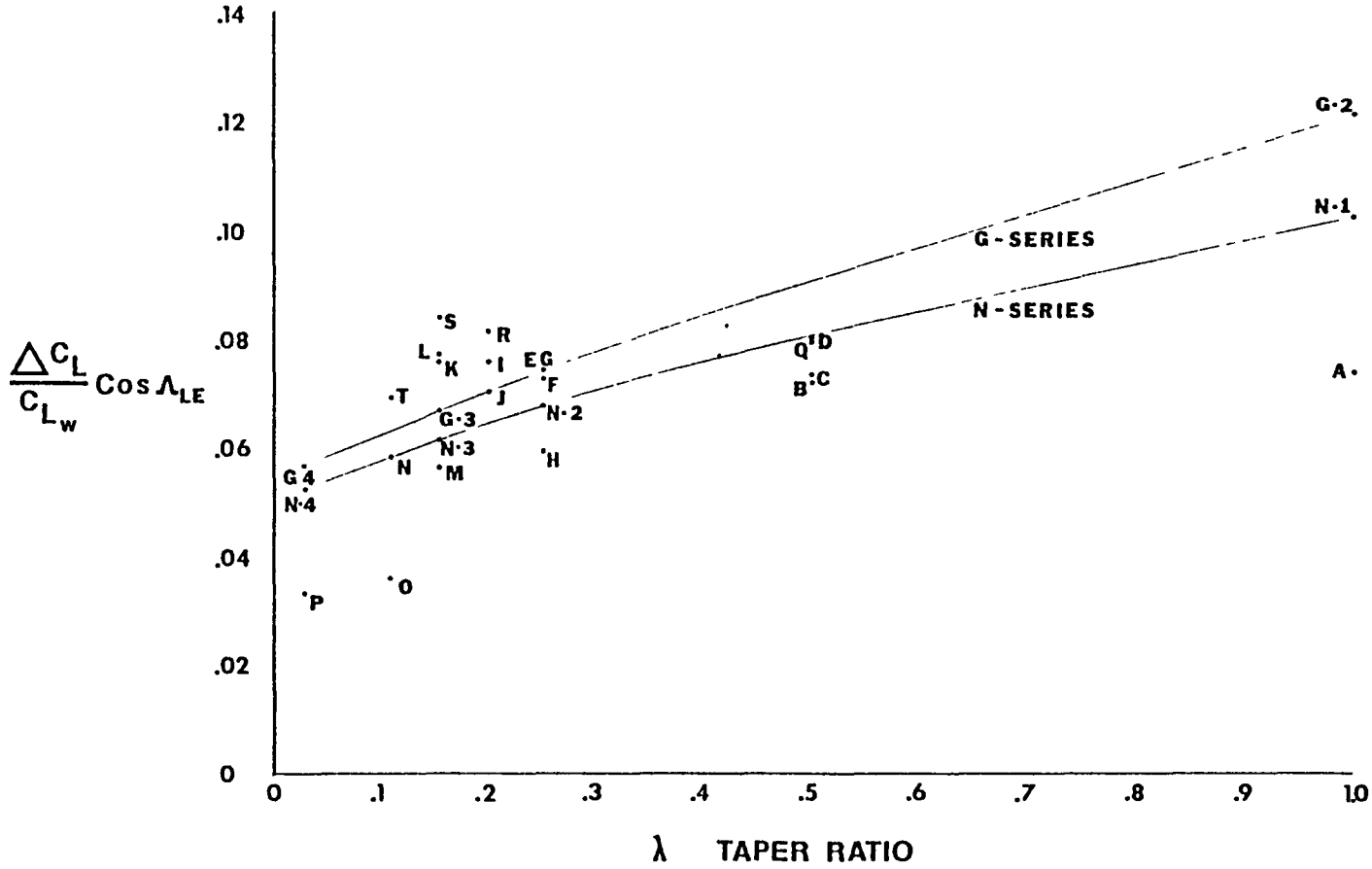

Figure 76. Variation of the parameter $(\Delta C_L/C_{L_W})(\cos\Lambda_{LL})$ with wing taper ratio. α = 20°.

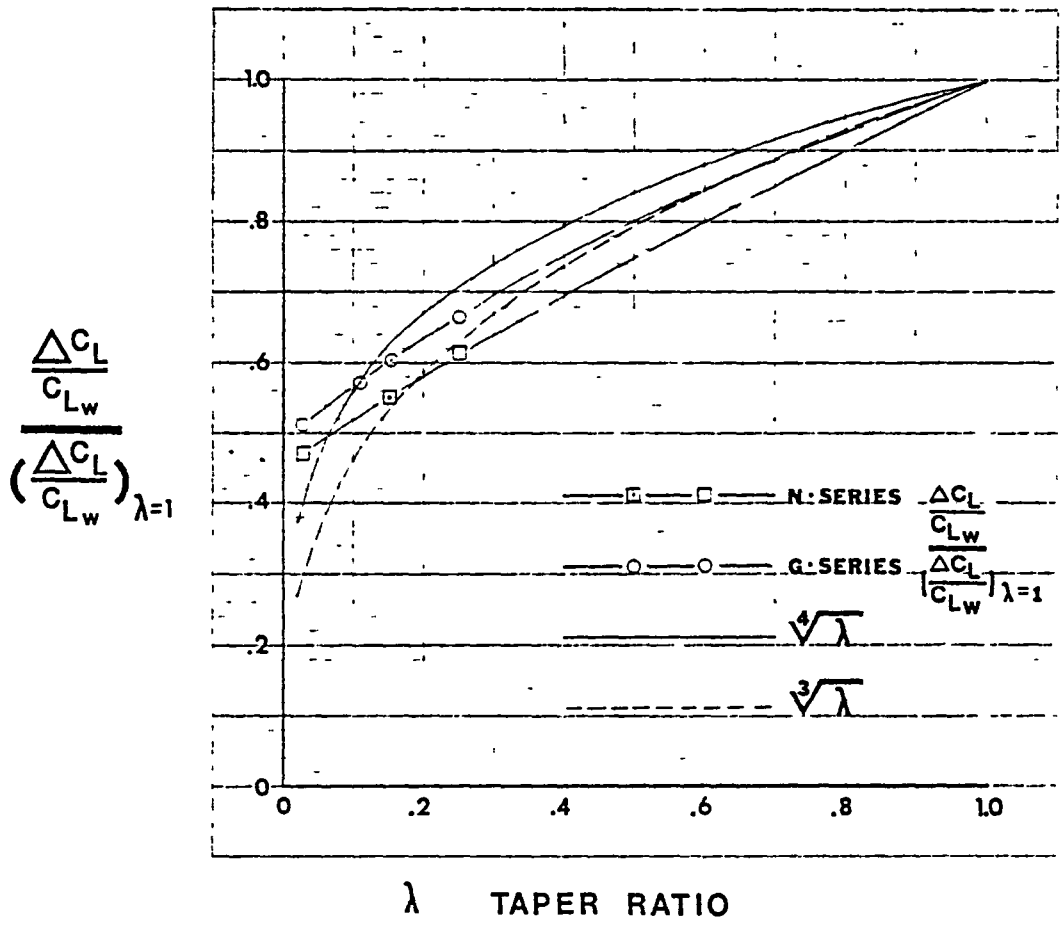

Figure 77. The ratio of incremental/wing alone lift coefficients of tapered wings, normalized with the ratio produced by an untapered wing. Also the third and fourth roots of taper ratio plotted as a function of taper ratio.

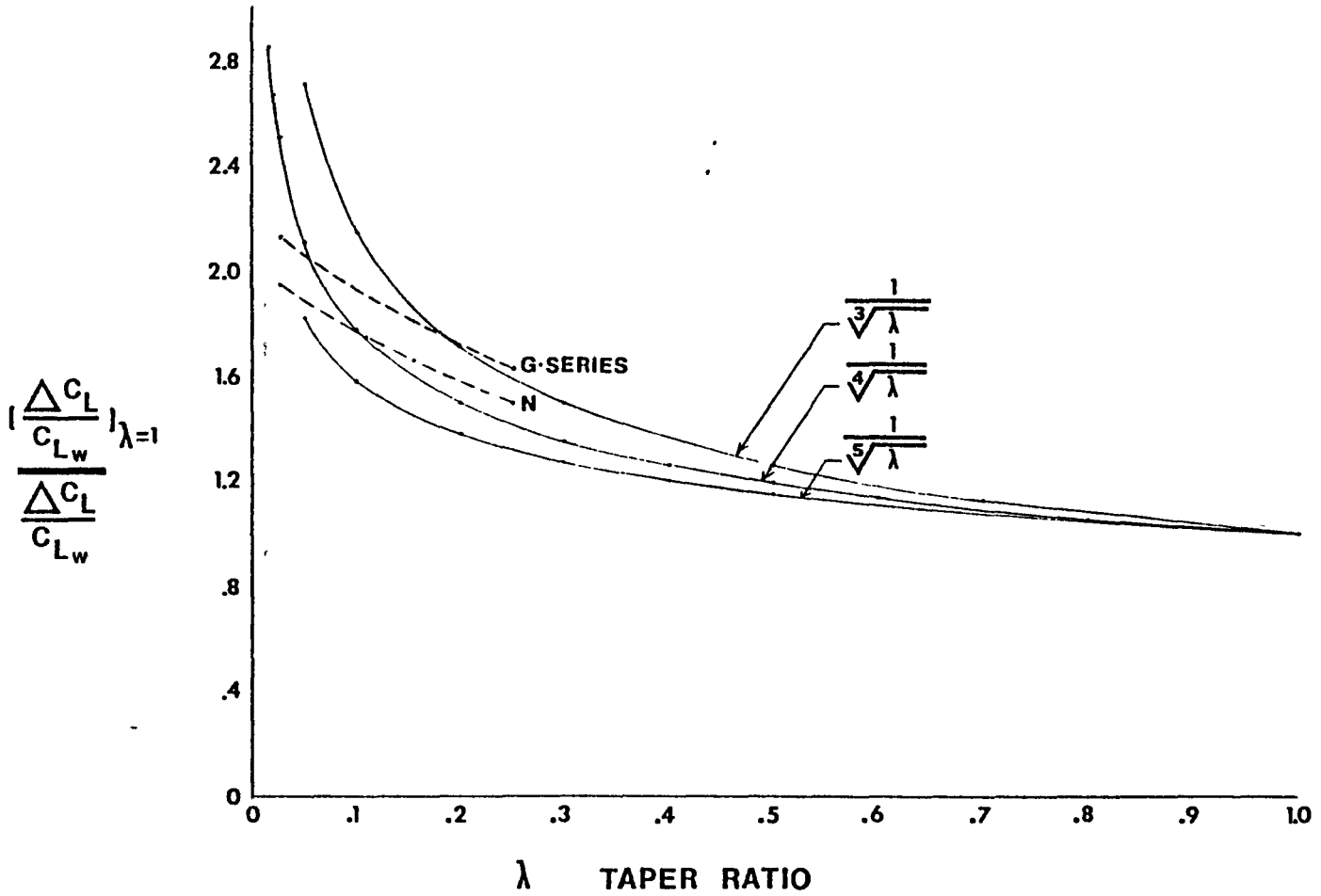

Figure 78. Plot of the inverse functions of figure 77 as a function of taper ratio.

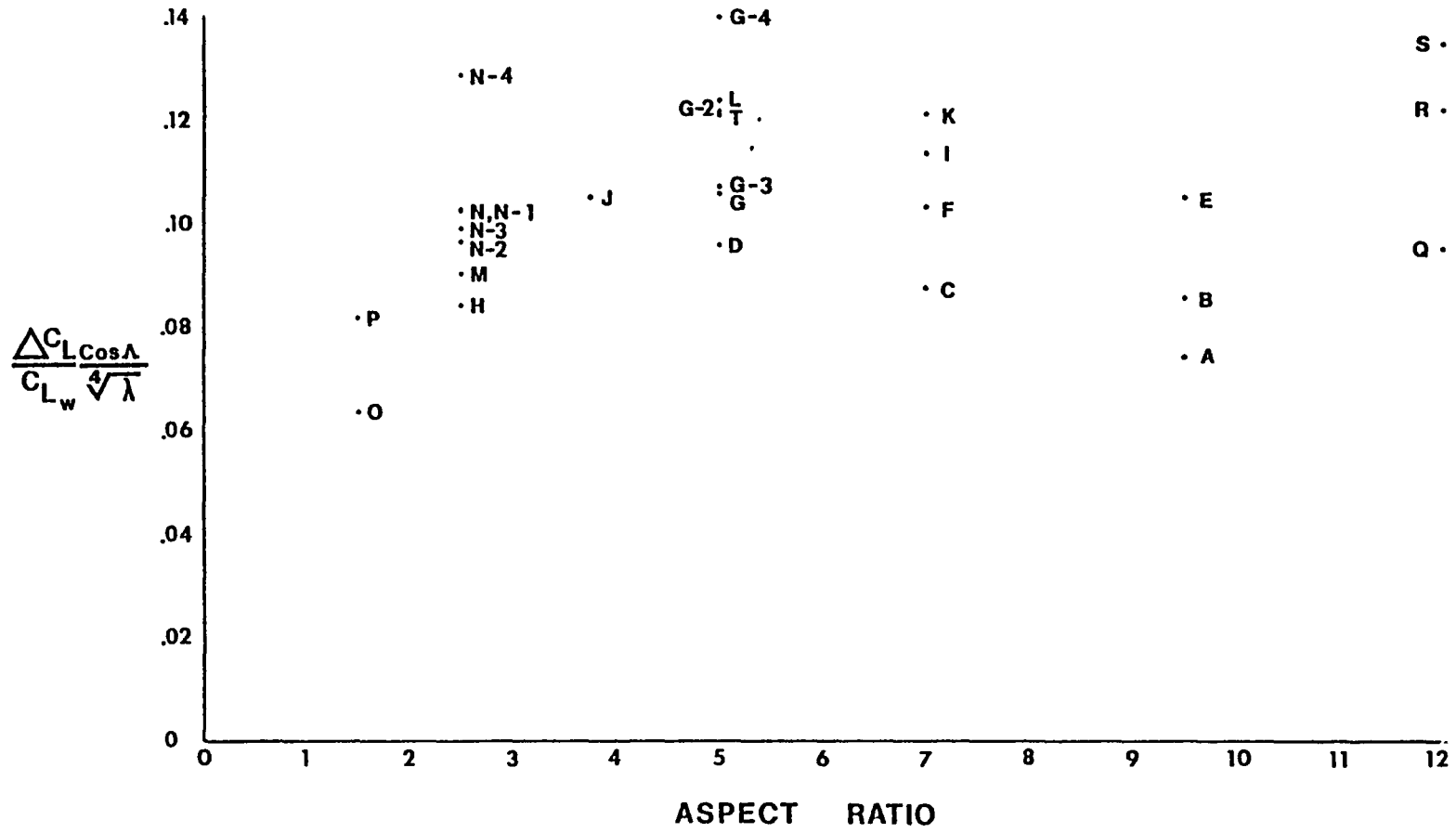

Figure 79. Plot of the function $(\Delta C_L/C_{L_W})(\cos\Lambda_{LE}/\lambda^{1/4})$ as a function of wing aspect ratio.

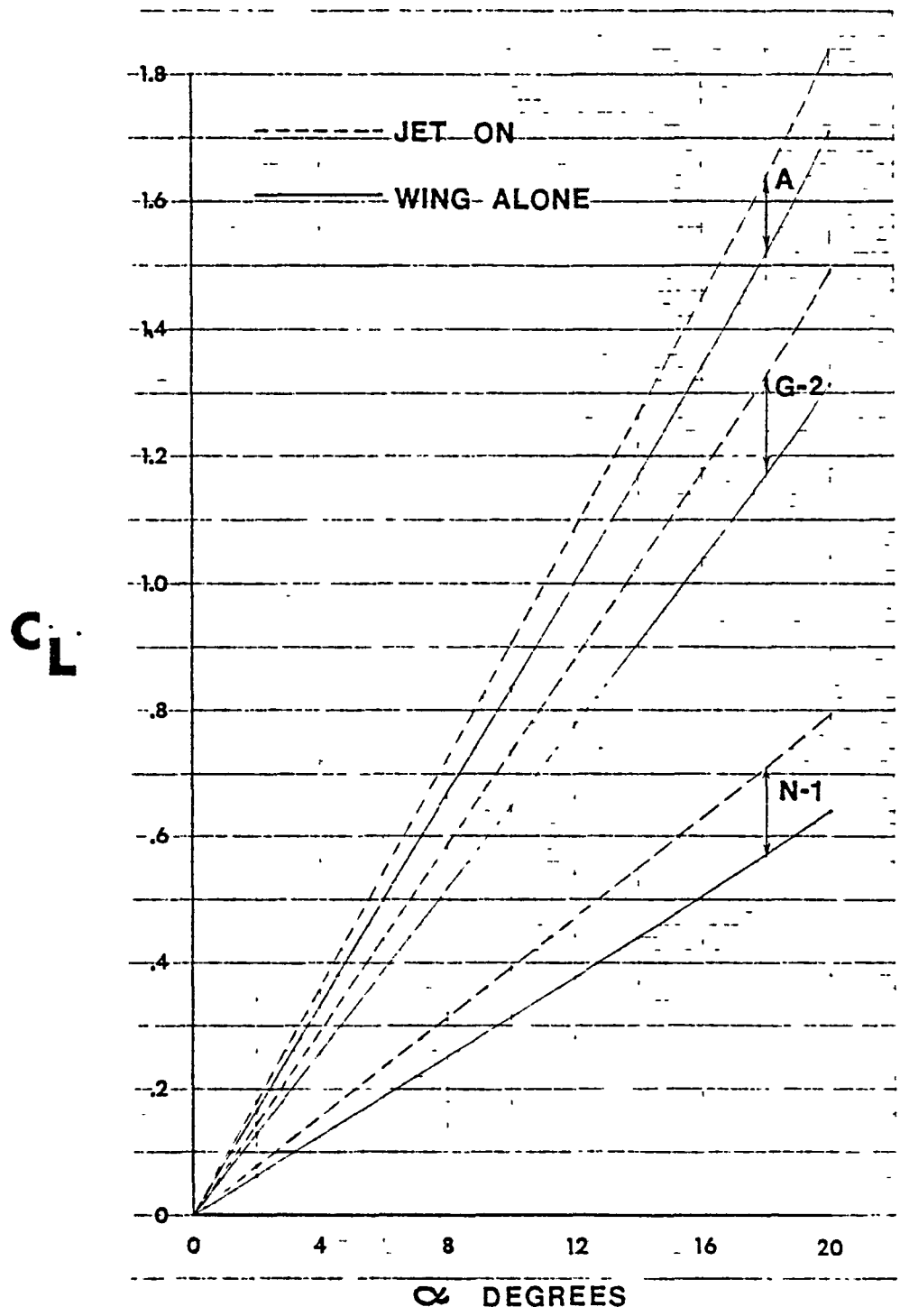

Figure 80. Effect of the USB jet on the lift-curve slopes of three untapered wings. A: $\Lambda_{LE} = 0^{\circ}$, AR = 9.5, G-2: $\Lambda_{LE} = 25^{\circ}$, AR = 5.0, N-1: $\Lambda_{LE} = 65^{\circ}$, AR = 2.5.

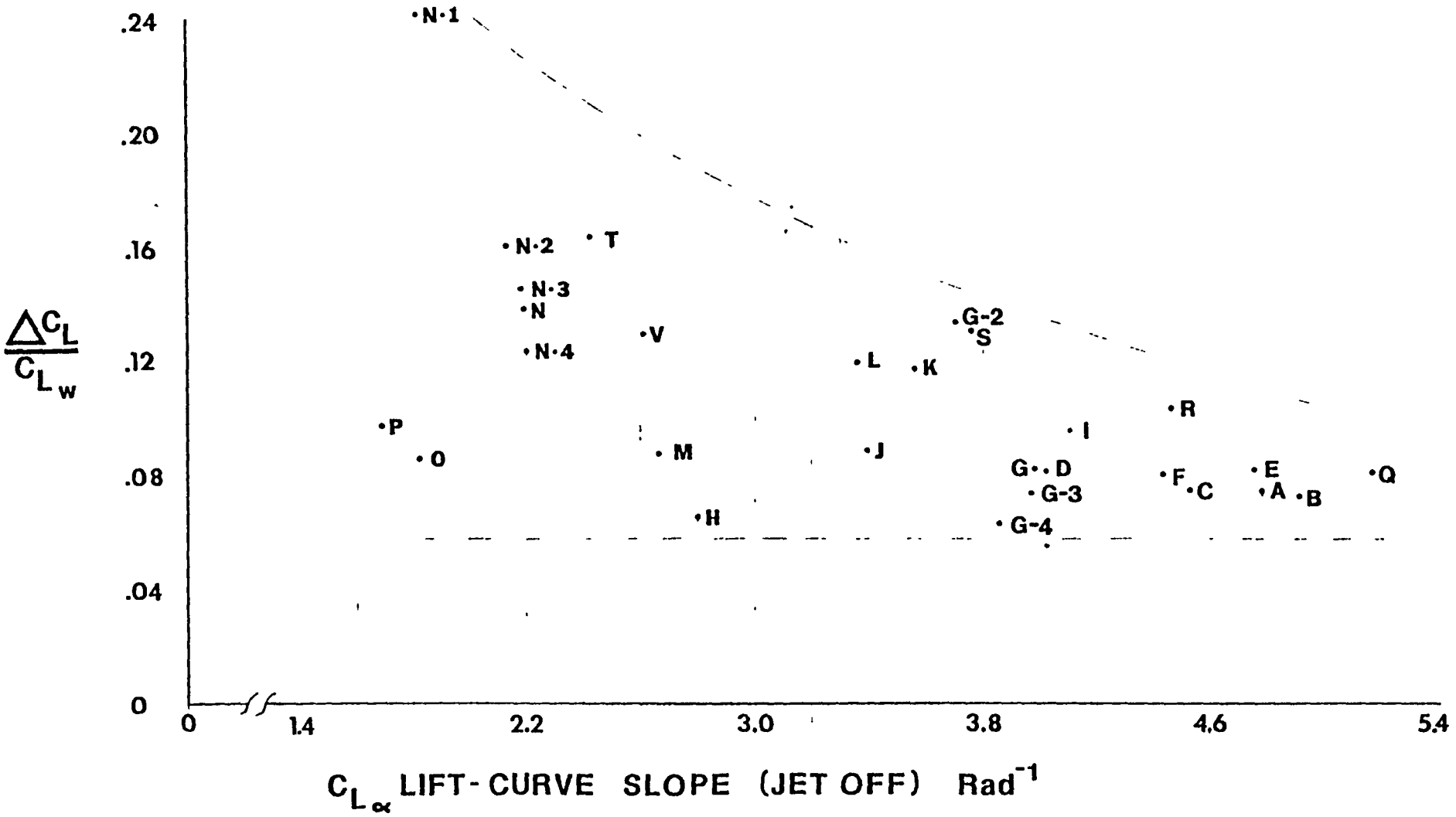

Figure 81. The ratio of incremental/wing alone, lift coefficients plotted as a function of wing lift curve slope without blowing.

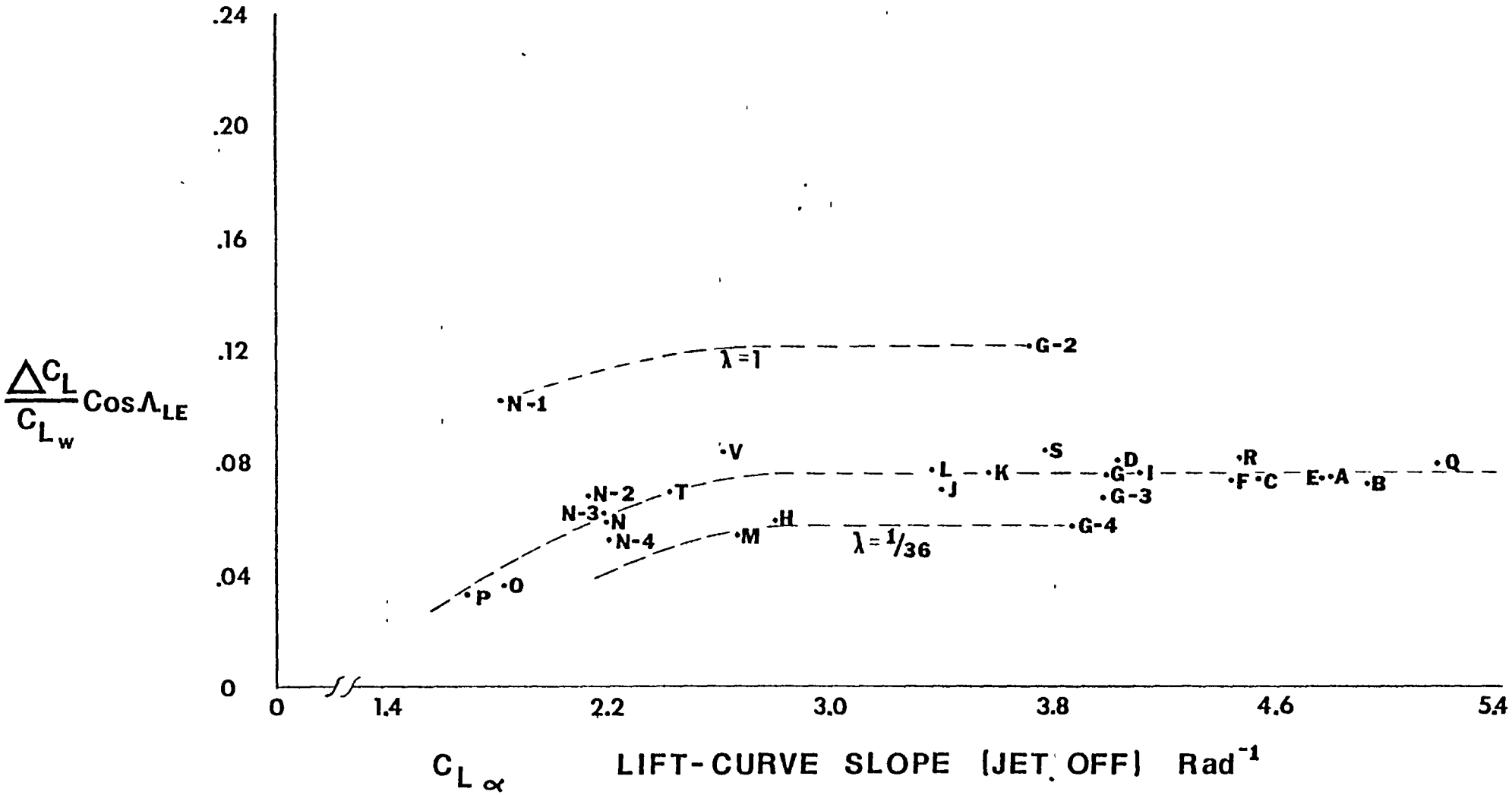

Figure 82. Plot of the parameter $(\Delta C_L/C_{LW})(\cos\Lambda_{LE})$ as a function of wing lift-curve slope withoug blowing.

3. CONCLUSIONS

3.1 Conclusions for the Analysis of the Induced Drag of an OWB Configuration

1. Certain OWB Configurations can generate more circulation lift than the wing alone with a net reduction in total induced drag.

2. This drag reduction associated with a lift gain is possible because the jet flow enhances the leading edge thrust of the wing as well as the pressure distribution. Net reductions in induced drag are achieved when the incremental change in leading edge thrust is larger than the incremental increase in pressure drag.

3. Two separate mechanisms exist through which the jet influences the wing flow field. These are jet entrainment and so-called wing-jet interaction. Jet entrainment is the dominant influence for OWB configurations in which the jet is far above the wing and does not wash it. (The high-aft configuration). For OWB configurations in which the jet is close enough to wash the wing surface (low-aft configuration), the wing-jet interaction becomes much more important and cannot be ignored.

4. As a OWB jet is lowered down to the wing surface, the wing-jet interaction causes deterioration of all wing leading edge thrusts in the near field of the jet. Pressure drag increments are increased so overall drag reduction deteriorates.

5. The above conclusion makes high OWB configurations more attractive from a cruise drag point of view.

3.2 Conclusions for the Analysis of Planform Effects on USB Lift Augmentation

1. The predicted incremental lift due to the upper surface blowing jet was found to be a constant percentage of the wing alone lift over a wide range of angles of attack, 2^{o} to 20^{o}. Although this ratio, $\Delta C_L/C_{L_W}$, is a constant for each planform examined, it varies widely between different planforms and is also sensitive to variations of the jet characteristics or power setting.

2. The taper ratio of a wing was found to be very important. Untapered wings were found to produce over 60% more additional lift with blowing than highly tapered wings with identical sweep and aspect ratio.

3. Analysis of sectional data revealed that the superior performance of the untapered wing was due to its more nearly elliptical distribution of lift coefficient along the span. Tapering of a wing shifted the crest of the wing alone lift distribution outboard, away from the jet, reducing the jet's influence upon wing lift.

4. Increasing the sweep angle of a wing permits much larger increments of additional lift, due to blowing, to be generated. When wings of identical taper and aspect ratio are compared, the more highly swept wing produces more additional lift due to the same blowing jet. This is because wing panels which are farther downstream from the jet are affected to a greater extent by wing-jet interaction. These outboard panels are also closer to the trailing jet section than the equivalent wing panels of an unswept wing.

5. It was discovered that the parameter: $(\Delta C_L/C_{L_W})\cos\Lambda_{LE}$ is a constant for wings with equal aspect ratios but widely varying sweep angles. It is applicable to USB configurations with identical jet characteristics and

thrust coefficient. Effects of twist or camber are not included.

6. Increasing wing aspect ratio beyond 5.0 resulted in only gradual increases in incremental lift. Increases in jet induced lift were in proportion to increases in wing alone lift and thus the ratio $\Delta C_L/C_{L_W}$ was constant for aspect ratio increases above 5. However, large improvements in incremental lift were achieved with aspect ratio increases made from 1.5 up to 5.0.

7. Plotting the ratio of incremental to wing alone lift coefficients as a function of the lift-curve slope for the wing alone reveals that for a given amount of blowing and jet geometry, there exists a minimum level of $\Delta C_L/C_{L_W}$ which all wings examined were capable of achieving. For this jet ($C_u = 2.0$), $(\Delta C_L/C_{L_W})_{MIN.} = .05$. Such a plot also shows that wings with small lift curve slopes to have the greatest potential for lift augmentation depending upon the planform geometry. As lift-curve slope for the wing alone is increased, the potential for lift augmentation goes down and is only a minimum for wings with lift-curve slopes approaching 2π.

8. Plotting of the parameter, $(\Delta C_L/C_{L_W})\cos\Lambda_{LE}$ as a function of the lift-curve slope for the wing alone produces a very consistent and narrow band of data for wings with wide variations of sweep, taper, and aspect ratio. The multiplying factor ($\cos\Lambda_{LE}$) drastically reduces the data scatter evident in plots of $\Delta C_L/C_{LW}$ vs C_{L_α}.

4. REFERENCES

1. Lan, C. E., Fillman, G. L, Fox, H., "Computer Program for Calculating Aerodynamic Characteristics of Upper-Surface-Blowing and Over-Wing-Blowing Configurations," NASA TMX-73987, Feb. 1977.
2. Lan, C. E., "A Theoretical Investigation of Over-Wing Blowing Aerodynamics," NASA CR-144969, March 1976.
3. Putnam, L. E., "Exploratory Investigation at Mach Numbers from 0.40 to 0.95 of the Effects of Jets Blown over a Wing," NASA TN D-7467, November 1973.
4. Putnam, L. E., "An Analytical Study of the Effects of Jets Located More Than One Jet Diameter Above a Wing at Subsonic Speeds," NASA TN D-7754, August 1974.
5. Lan, C. E., "Theoretical Aerodynamics of Over-Wing-Blowing Configurations," Journal of Aircraft, Vol. 14, No. 6, June 1977, pp. 517-518.
6. Lan, C. E., Campbell, J. F., Fillman, G. L., "Theoretical Prediction of Over-Wing-Blowing Aerodynamics," AIAA Paper 77-575, June 1977.
7. Reubush, David E., "An Investigation of Induced Drag Reduction Through Over-Wing-Blowing," AIAA Paper No. 77-884, July 1977.
8. Phelps, Arthur E., Letko, William , Henderson, Robert L.:"Low-Speed Wind Tunnel Investigation of a Semispan STOL Jet Transport Wing-Body with an Upper-Surface Blown Jet Flap," NASA TN D-7183, 1973.
9. Lan, C. E., Campbell, J. F., "Theoretical Aerodynamics of Upper-Surface-Blowing Jet-Wing Interaction," NASA TN D-7936, November 1975.
10. Lan, C. E., "Some Characteristics of Airfoil-Jet Interaction with Mach Number Nonuniformity," Journal of Aircraft, Vol. 11, August 1974, pp. 491-494.

11. Lan, C. E., Campbell, J. F., "A Wing-Jet Interaction Theory for USB Configurations," Journal of Aircraft, Vol. 13, No. 9, Sept 1976, pp. 718-726.

12. Hassell, James L., "Results of Static Tests of a 1/4 Scale Model of the Boeing YC-14 Powered Lift System," NASA SP-406 Powered Lift Aerodynamics and Acoustics, May 1976, pp. 45-62.

13. Skavdahl, H., Wang, T., Hirt, W. J., "Nozzle Development for the Upper Surface Blown Jet Flap," SAE Paper 740470, April 1974.

14. Campbell, J. F., "Augmentation of Vortex Lift by Spanwise Blowing," Journal of Aircraft, Vol. 13, No. 9, Sept. 1976, pp. 727-732.

1 Report No	2 Government Accession No	3 Recipient's Catalog No
NASA CR-158349		

4 Title and Subtitle	5 Report Date
ANALYSIS OF SOME AERODYNAMIC CHARACTERISTICS DUE TO WING-JET INTERACTION	July 1979
	6 Performing Organization Code
7 Author(s)	8 Performing Organization Report No
Greg L. Fillman and C. Edward Lan	CRINC-FRL-281-4
	10 Work Unit No
9 Performing Organization Name and Address	
The University of Kansas Center for Research, Inc. Lawrence, KS 66045	11 Contract or Grant No NSG-1139
	13 Type of Report and Period Covered
12 Sponsoring Agency Name and Address	Contractor Report
National Aeronautics and Space Administration Washington, DC 20546	14 Sponsoring Agency Code

15 Supplementary Notes

Langley Technical Monitor: Dr. James F. Campbell

16 Abstract

This study presents a theoretical analysis of some aerodynamic characteristics of upper-surface blowing (USB) and over-wing blowing (OWB) configurations. The reductions in induced drag due to over-wing blowing are achieved when the incremental increases in leading-edge thrust are larger than the incremental increases in pressure drag. The jet entrainment and the wing-jet interaction processes are both important to estimating jet effects. The effects of wing taper ratio and sweep angle were found to be especially important when considering the relative levels of incremental lift produced by a USB configuration.

17 Key Words (Suggested by Author(s))	18 Distribution Statement
Theoretical Wing-Jet Interaction Over Wing Blowing Upper Surface Blowing	Unclassified - Unlimited Star Category - 02

19 Security Classif (of this report)	20 Security Classif (of this page)	21 No of Pages	22 Price*
Unclassified	Unclassified	126	

* For sale by the National Technical Information Service, Springfield, Virginia 22161

End of Document